Feasibility Analysis of a Powered Lower-Limb Orthotic for the Mobility Impaired User

by

Wesley R. Eby

A thesis
presented to the University of Waterloo
in fulfillment of the
thesis requirement for the degree of
Master of Applied Science
in
Systems Design Engineering

Waterloo, Ontario, Canada, 2005

I hereby declare that I am the sole author of this thesis. This is a true copy of the thesis, including any required final revisions, as accepted by my examiners.

I understand that my thesis may be made electronically available to the public.

Abstract

Powered orthotic devices can be used to restore mobility to the impaired user, and may thereby assist them in daily living tasks. An investigation is performed herein to examine the feasibility of a powered lower-limb orthotic in assisting the sit-to-stand task by 50% of the required torque. Feasibility is considered via simulation.

A three-link sit-to-stand model, which is driven by kinematic data, is developed. Models of a Pneumatic Muscle Actuator and a DC motor are used to determine which of the two technologies can make a more appropriate contribution to the sit-to-stand task. Simulation revealed that both the Pneumatic Muscle Actuator and the DC motor are reasonable actuator choices, and neither limited the ability to achieve 50% torque assistance. The ability to assist the task was, however, limited by the ability to derive a control signal for the actuator from the user-orthotic interface. It was concluded that the user-orthotic interface requires further investigation. It was also found that while both actuator technologies are suitable for contributing 50% of the required torque, the Pneumatic Muscle Actuator is preferable due to its ability to scale to greater torques.

Acknowledgements

Thank you to my supervisor Dr. Eric Kubica. Your patience and gentle guidance are both appreciated. Your passion for the study of biomechatronics, and specifically the development of assistive technologies is inspiring. I would also like to acknowledge both the time and feedback of my readers Dr. David Wang and Dr. Carolyn MacGregor.

Dr. Patrick Cawley and Breg, Inc. were very generous in their donation of off-the-shelf knee braces. It is upon these braces that a prototype of the powered orthotic examined in this thesis will be built.

Finally, I would like to thank my friends and family for their kindness and support. I am blessed by each of you in countless ways.

Contents

List of Tables

List of Figures

Chapter 1

Introduction

Statistics Canada reports that 12.4% of Canadians living in households have an activity limitation. This rate increases with age, to the point where over 40% of those aged 75+ have some sort of mobility impairment [1]. This represents a significant financial cost to the health and continuing care systems. Moreover, mobility impairment can have a severe personal and financial cost to the individual.

The University of Chicago Hospitals suggests that disability causes family members to become co-managers in patient care, and involves modifying family roles. They acknowledge that the resulting "changes in living arrangements, childcare issues, and community re-entry can all pose new problems for the patient and family" [2]. Other research suggests that injury often causes families to utilize intra-family labour reallocation, borrow money, or sell belongings to cope with the cost of rehabilitation and to subsidize income that may be temporarily or permanently lost [3].

Clearly injury and disability, in which mobility impairment is included, is significant at both an institutional and personal level. The goal of the research presented in this thesis is to offset the cost of injury and disability by assisting the mobility impaired person. Specifically, the research explores the development of a powered lower-limb orthotic to help in the execution of daily living tasks.

The research is focused on assisting the Sit-to-Stand (STS) task. STS is a good task platform for the initial phases of orthotic modelling and design. While full gait augmentation is the penultimate goal of assistive technology development, gait includes many complexities that overwhelm the initial design. Modelling the

impact dynamics of foot contact and achieving dynamic lateral balance are two such examples [4,5,6,7]. The augmentation of STS reduces the complexity of the problem to the more essential issues of human-machine interface design, actuator selection, and actuator control.

Schultz et al. found that their elderly, impaired group selected a STS strategy that markedly reduced the required torque at the knees [8]. This indicates that either knee weakness or knee pain affect the mobility impaired person, the effects of which can be reduced during the STS task with orthotic augmentation.

The utility of a powered lower-limb orthotic, however, may only be as good as the ability of the user to interact with it. Wight found that a position controlled robot can in fact be augmented with a force controlled orthotic, and suggested that a force augmentation system could work with the human position controlled system [9]. Though the work by Jansen-Osmann et al. focused on children, they found that "the human motor system is inherently flexible enough to adapt to any novel force within the limits of the organism's biomechanics" [10]. Thus, it is reasonable to assume that a powered orthotic may augment a human task, within the bandwidth of human response.

A powered lower-limb orthotic is therefore modelled in order to assess its utility before being built. Though the orthotic is not yet implemented, two currently available actuator technologies are modelled and used in simulation in order to determine both the utility and the feasibility of the orthotic. The simulation is used to provide insight into the implementation of a technology to assist human locomotion.

An understanding of human biomechanics, robotics, and biofidelic robotic actuators is required in order to develop technologies to assist human locomotion. Therefore the relevant background research is provided in Chapter 2. While locomotor assistance is an emerging research area, some technologies do already exist. They are presented in Chapter 2.

Modelling is an important part of biomechanical research, as it provides researchers a method of accessing otherwise immeasurable forces and torques within the human system. A model of STS is developed to examine the torques involved in the task. A model of the powered orthotic is also developed, thus allowing a comparison of actuator technologies under the constraint of reasonable human dynamics.

Their modelling issues are examined in Chapter 3.

The STS model requires kinematic data as input. This is collected through a series of experiments, and presented in Chapter 4. In many ways modelling the Sit-to-Stand (STS) task is easier than modelling human gait. However, simplifications are still required. The validity of the STS model is examined in Chapter 4.

Conceptually, control of the powered lower-limb orthotic can be separated into two levels of control. There is the high level control from the human to the orthotic, where the issue of how to best provide augmentation is addressed. There is also the lower level control of the orthotic to ensure that the signal from the high level control is adequately actuated. Controller design is presented in Chapter 5.

Finally, in Chapter 6, the simulation results are presented. From the results, conclusions and recommendations are given in Chapter 7.

Chapter 2

Background

This chapter offers a summary and evaluation of the existing research in the area of assistive locomotion technologies. Two promising areas of assistive technologies are presented. Further discussion is then devoted to the options for the human-machine interface and to the actuator technologies for powered orthoses.

2.1 Assistive Locomotor Technologies

Research into assistive locomotor technologies, or mobility assist devices, is focused on providing people with mobility impairments an alternative to traditional aids such as wheelchairs, walkers, or canes. Mobility assist devices, as the name suggests, are used to increase the mobility of the user. The success of a device is measured first and primarily on its ability to increase the functional level of the user. That is: Does the device help the user perform daily-living tasks with improved ease? Functional Electrical Stimulation and Powered Orthoses are two assistive technologies currently being developed as alternative aids. They are examined here.

2.1.1 Functional Electrical Stimulation

One mobility assist technology currently under investigation is known as functional electrical stimulation (FES). Loeb and Richmond describe FES as "precisely controlled muscle contractions that produce specific movements required by the patient to perform a task" [11]. More accurately, they are artificially induced muscular

contractions.

Electrical stimulation of muscle is based on sound physiological principles, which are reviewed here. In the intact efferent pathways, a somatic motor neuron originating in the brain or central nervous system will innervate a group of muscle fibres. This is shown in Figure 2.1. The neuron and the fibres that it innervates are known as the motor unit. The motor unit forms the basic unit of contraction. An electro-chemical signal is transmitted down the neuron to the fibres of the motor unit that is to contract. The signal is continued down the fibres, causing an electro-chemo-mechanical response that results in the contraction of the muscle fibre. An externally applied voltage potential to the motor unit can trigger the same electro-chemo-mechanical response. Therefore, electrical stimulation can cause a muscle to contract. Given that a contraction can be induced artificially, the muscle can then be used as an actuator to improve patient function.

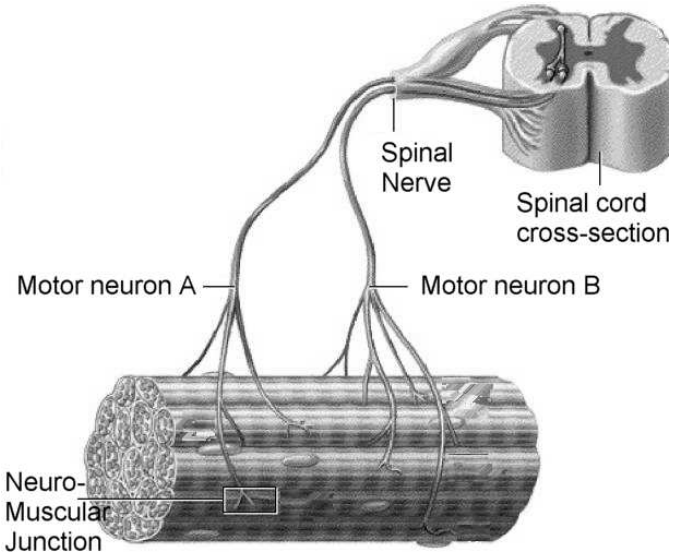

Figure 2.1: Muscle with two innervating motor units shown. (reprinted from [12])

Along with the functional benefits of FES, such as allowing a paraplegic to rise from a chair [13] or walk [14, 15], there are also therapeutic benefits to electrical stimulation. Electrical stimulation has been found to increase muscle bulk, increase flexibility of the joints, and increase blood flow. Increased flexibility is often accompanied by improved locomotion [14]. It is known that muscle atrophy due to disuse can lead to the development of pressure sores [16], commonly known as bed

sores. Electrical stimulation, through the pumping action of contracting skeletal muscle can increase blood flow to the muscle and lead to improved tissue health as determined by tissue oxygen levels [16].

Despite the functional and therapeutic effects of electrical stimulation, some subtlety of the physiological contraction of muscle is missed. The fibres of the motor unit belong to a single muscle, but are dispersed throughout the muscle. This is relevant since it means that normally the force is generated throughout the muscle. Additionally, a motor unit contracts in an all-or-none fashion. Thus, a different mechanism must be at work in modulating the force output of skeletal muscle.

Under normal control of the central nervous system, the force output of muscle is graded through the use of a standardized recruitment sequence. Smaller, fatigue-resistant motor units are recruited first. As the force requirement is increased the firing rate of these fibres is increased. The fibres are stimulated more frequently and produce a larger force. As the force requirement grows beyond the ability of the currently recruited fibres to generate a force, then larger and less fatigue-resistant motor units are recruited and their firing rates are increased. The functional implication is that fatigue of the muscle is mitigated, while the muscle is still able to meet the force requirements. Fatigue is also avoided in sustained contraction with asynchronous recruitment. In the asynchronous modality, the nervous system forces the motor units to take turns maintaining the tension. [17]

The contraction induced by an artificial electric field is quite different from a physiological contraction. Neither the electrodes used nor the control techniques available are capable of targeting individual muscle fibres the way a motor unit might. Instead, all the fibres within the generated electric field are stimulated concurrently and synchronously. The effect is poor limb control [18] and rapid muscle fatigue [18,19]. Additionally, it was found in [13] that electrically stimulated knee extensors can produce only up to one quarter of the force required to rise from sitting.

As advances are made in the area of functional electrical stimulation, the technology may eventually offer more to some users with mobility impairment. While there is great hope for this area of research, further advances must be made towards physiological muscular contraction. Even then, it should be recognized that FES is not intended for patients with neuropathologies, and it has only limited utility until

muscle bulk is regained. Furthermore, FES is essentially limited to patients with disrupted afferent, or sensory, pathways. The same electric potential that is used to stimulate the muscle also stimulates the touch receptors in the skin, causing pain in users with an intact afferent pathway [20, 21]. Therefore, while spinal-cord injured patients are typically candidates for FES, patients with an intact sensory system, such as those with hemiplegia, are not good candidates [21].

2.1.2 Powered Orthoses

The second approach to minimizing mobility impairment is the use of a powered exoskeleton, also known as a powered orthosis. The approach is straight-forward in principle, though it can be rather complex in implementation. An exoskeleton, as depicted in Figure 2.2, is strapped to the patient. Actuators attached to the orthosis are used to move the limbs of the wearer.

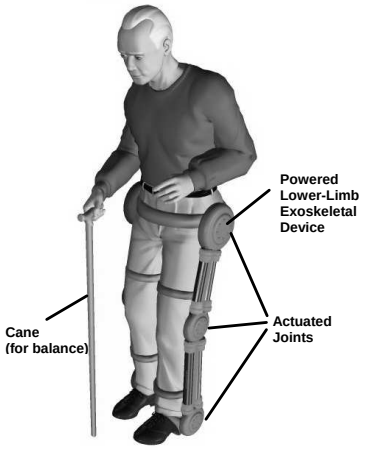

Figure 2.2: Conceptual rendering of an exoskeletal device to assist the mobility impaired. (reprinted from [9])

2.1.2.1 Candidates for a Powered Orthosis

A powered orthosis can be worn by patients with normal function, minor or severe muscle atrophy, or muscle paralysis. People who are not candidates for FES may still be good candidates for a powered orthotic. While no published research was

found where a powered orthotic was adapted for an amputee, it would certainly be a possibility. Potentially, the technology could be adapted into a powered prosthetic to drive joints with a distal amputation. The work presented here, however, will focus solely on powered orthoses.

2.1.2.2 Classification of Powered Orthoses

Exoskeleton applications may be categorized into power amplification, telerobotics, and haptics. The application alluded to above falls under the heading of power amplification. In a power amplifier mode, the human provides a control signal and possibly some power, while the orthotic device provides additional power to perform the task. Exoskeleton devices may also perform as the master device of force-reflecting master-slave system. If a virtual slave interacts with a virtual environment, as with computer-based training of surgeons, then the master exoskeletal system may be categorized as a haptic device. For further information on the classification of exoskeletal systems, see [22]. While research into powered orthoses for mobility assistance is limited, there is related research being performed in the areas of telerobotics and haptic interfaces. Relevant research from the areas of power amplification, telerobotics, and haptic interfaces is used throughout the rest of this chapter to develop a comprehensive view of the research to date.

2.1.2.3 Function of Powered Orthoses

Powered orthoses have the capacity to serve many purposes. Some of the first powered orthoses were designed to augment human performance. Devices presented in [22,23,24] were designed to provide the user with the ability to perform tasks that require super-human strength. Powered exoskeletons, more so than robots, keep the human in control and allow adaptation to the task requirements.

The Defense Advanced Research Project Agency (DARPA), a United States Department of Defense Agency, has recognized the ability of humans to adapt to tasks, but also understands the limited strength of their personnel. For this reason, DARPA has created the Exoskeletons for Human Performance Augmentation project. Their mission, as outlined in [25], is to "develop devices and machines that will increase the speed, strength, and endurance of soldiers in combat environments".

While human enhancement research may be able to offer some insight into how to provide mobility assistance, the nature of the two problems are fundamentally different. Human enhancement exoskeletons require that the user have normal strength and range of motion capabilities, with the exoskeleton augmenting that strength. A person with a mobility impairment, in comparison, has difficulty making unencumbered movements. Their impairment may preclude them from manipulating the exoskeletal device.

Research into powered orthoses that are meant to serve in a functional or therapeutic role for the person with a mobility impairment has only recently been emphasized. A powered ankle orthotic has been developed to assist in walking [26]. Johnson et al. developed a device for use in a clinical setting to help improve the range of motion, strength, and balance of patients [27]. Yobotics has developed an exoskeletal device that claims to allow the wearer to perform deep-knee bends almost indefinitely [28]. On the other hand, due to the nature of its construction, the Yobotics device does not allow the user to sit while wearing the device, which represents a significant disadvantage.

While current devices offer some advantages, the powered orthotic device of the future should offer people with mobility-impairments previously unheard-of freedom. In order for the research to be useful, two major hurdles must be overcome. First, a method of obtaining a control signal from the human user must be developed. The final human-machine interface will inevitably take on a much different form than those used in current human augmentation exoskeletons. Secondly, an actuator technology capable of providing the required power to the exoskeleton must be selected. Fortunately, this area of the research is substantially similar to that of actuator selection for human augmentation exoskeletons.

2.2 Human-Machine Interface for Powered Orthoses

The human-machine interface (HMI) is perhaps the most complex problem of mobility assistance. Ideally the HMI would be intuitive, follow gross motor movements, and allow fine motor balance. An intuitive interface lends itself not only to ease-of-use, but also to safety and a quick response to stimulus. The ability to track gross

motor movements essentially allows the user to plan their path, with the exoskeleton assisting the movement. Furthermore, the interface should be sensitive enough to user demands to ensure that balance is maintained. This last point, however, has largely been ignored due to the complexities of sensing and actuating restorative balance forces. Supportive aids such as a cane or a walker have been used in most research to date. Given the current knowledge base of mobility assist interfaces, the use of supportive aids seem to be a reasonable compromise. The interfaces that have been investigated in previous research and that contribute to the knowledge base are examined here.

2.2.1 Joystick Interface

Perhaps the easiest interface to envision is a joystick control for the exoskeletal device. A joystick has the benefit of working equally well for human performance augmentation, for users with muscle atrophy, and for users with paralysis. However, joystick control is not an intuitive interface, particularly with multiple degree-of-freedom systems. While joystick control does put the human in the loop, it does not incorporate reflexive balance control. Therefore, restorative balance forces may only be a conscious, and inevitably delayed, version of reflex control. For this reason, joysticks have not found wide-spread favour for exoskeleton HMI.

The standout research in joystick control comes from the Armstrong Laboratory of the Wright-Patterson Air Force Base. A design, presented in [27], maps finger movements to control of the lower-limb orthosis and is shown in Figure 2.3 below. Essentially the fingers are used to walk the legs. The design allows individual control of each joint, and is somewhat more intuitive than most joysticks. The results of user testing, however, have not been presented. Therefore, it remains to be seen if this technology will meet the expectations of the designers and the needs of the intended users.

This area of research, ultimately, may be the only viable human-in-loop option for users suffering from paraplegia, since they cannot generate the control signals needed for the interfaces of Section 2.2.2 and 2.2.3. However, the joystick interface does not inherently include the human feedback mechanisms necessary for balance. Due to this disadvantage, for the user with some limb control, there are other options that merit consideration.

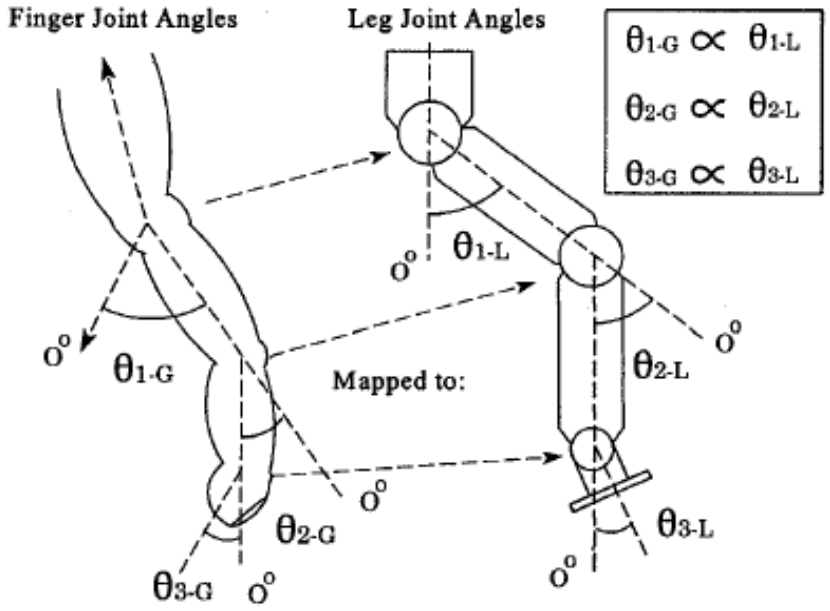

Figure 2.3: Mapping of finger position to desired leg position. (reprinted from [27])

2.2.2 Position and Force Control of Powered Orthoses

Human performance augmentation exoskeletons, as described in [22], are usually designed as full body suits. Their purpose is to allow the user to lift a large external load. These devices are master-slave systems. As the inner master suit is moved by the wearer, the outer performance enhancing slave moves as well. First generation suits typically used position control, while there has been a progression towards force control in the new suits. Note that caution must be applied when interpreting the terms position and force control. These terms are used to describe the HMI, and do not necessarily dictate an actuator implementation.

Recently, an augmented space suit using force sensing at the joints was presented [23]. Unfortunately, since the wearer of the space suit must still be able to exert normal forces at the joint, this technology, as with its position and force control predecessors, offers little insight into HMI for mobility assistance.

A power assist for nurses, presented in [24], while utilizing force control, could offer some promise in the area of mobility assistance. The suit uses force sensors located over the muscles to determine muscle stiffness. Muscles become stiffer, or harder, as they exert more force. Then, conceptually at least, muscle stiffness may

be used as a rough indication of the force the muscle is exerting. Stiffness, however, does not change drastically for changing exertion. Even with a very sensitive force sensor, there is too much variability in muscle contraction for the technique to offer much information to the controller.

Position and force control of powered orthoses is appealing due to the simplicity of the sensors and the ease of which the device may be put on and taken off. It is a reasonable option for users with some mobility, particularly due to its simplicity and wearability. On the other hand, the technology discussed in Section 2.2.3 provides more advanced information about user intention.

2.2.3 EMG Interface for Powered Orthoses

Electromyography (EMG) force estimation techniques are based on the same underlying physiology as functional electrical stimulation, as described in Section 2.1.1. Rather than attempting to emulate the voltage associated with muscular contraction, as is done with electrical stimulation, the myosignals are measured and processed to estimate force. Myosignal based control is the newest generation of exoskeleton HMI, and has a lot of potential.

2.2.3.1 Advantages of an EMG Interface

Myosignal interfaces are useful for a variety of reasons. First, EMG is a measurement, albeit noisy, of the actual signal being sent to the muscle by the central nervous system of the user. Therefore, EMG provides more information than the other interfaces. Unlike position and force control, it also does not suffer from the electro-chemo-mechanical delay associated with converting the myosignal into a muscular contraction [22]. Second, the interface is intuitive, as it measures the signals of the neuromuscular system, and incorporates the reflexive and balance features of the human system. Third, as long as the myosignal can be measured, there is no requirement that the user actually be able to move. A myosignal-based interface has been used successfully in [22] for human performance augmentation. The exoskeletal device, developed by Rosen et al., is used to assist flexion of the elbow. Using EMG as a control signal, the operator manipulated an external weight but felt only a scaled version of the external load being lifted. Promising preliminary

results were obtained in [26] for mobility assistance, where a powered ankle orthotic was developed, though complete results are yet to be published.

2.2.3.2 EMG-force Estimation

The processing of the myosignals must be understood in order to appreciate the limitations of EMG-based force estimation. The voltage that is measured is the result of a spatial and temporal interference pattern from activated motor units near the sensing electrode. The signal must be amplified, as it is quite small. In fact, the signal is so small that high skin impedance, movement artifact of the electrode over the skin or the skin over the muscle, and cable motion artifact can all affect the signal. As shown in Figure 2.4, the amplified signal is usually rectified and smoothed. If the rectified signal is smoothed with an appropriate filter, then the resulting linear envelope will have approximately the same profile as the force produced by the muscle in isometric conditions. See [29] for more details.

Muscle is known to have mass-spring-damper characteristics [30]. The second-order low-pass filter, being the electrical equivalent of the mass-spring-damper system, is able to smooth the rectified EMG appropriately. A second-order low-pass filter with a reasonable cutoff frequency will introduce the electro-chemo-mechanical phase lag seen in muscle, and generate a good isometric force profile.

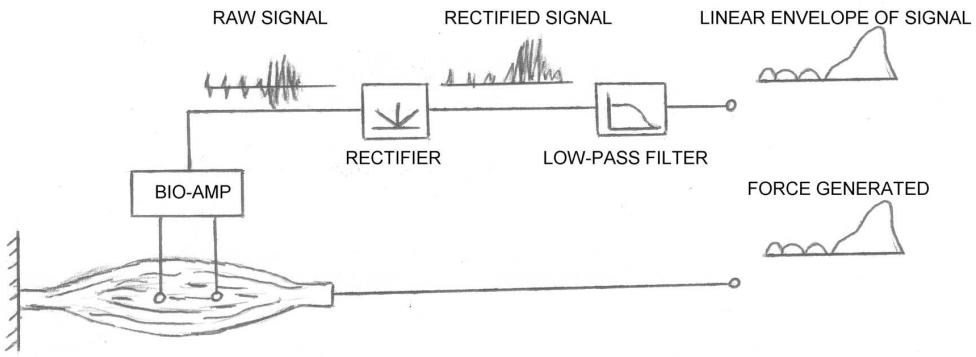

Figure 2.4: Processing of EMG signal to estimate muscle force

If force and the linear envelope EMG are calibrated, then, in the isometric case, it is possible to estimate the force from the amplitude of the linear envelope. It is

known, however, that there are two major factors that modulate the force output for a given activation pattern. Before explaining the modulators, the contractile mechanism of muscle should first be understood.

Muscle is made of two proteins that slide past each other to cause contraction of the muscle. This theory of contraction is known as the sliding filament theory. Myosin is a thick filament of intertwined proteins with heads at each end of the filament. Actin is a thin filament with docking stations for the myosin heads. When a myosin head is docked to the actin, a crossbridge is said to be formed. The interaction of actin and myosin is shown in Figure 2.5. With the crossbridge formed, the myosin head can ratchet and propel itself along, thereby contracting the muscle. The more crossbridges that are formed the more force the muscle can generate. Refer to [17] for more information on muscular physiology and its implications.

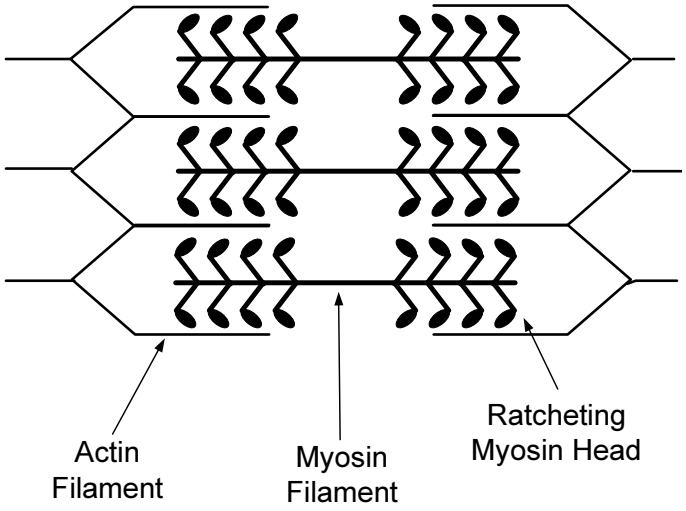

Figure 2.5: Contractile mechanism of muscle

The first force modulator is the length of the muscle. The force-length relationship of muscle is well documented [17,31,32,33,34]. The empirical results, which are presented in Figure 2.6, agree well with the current understanding of the contractile mechanism in muscle. The active component represents the force that is generated by the contractile mechanism. At shorter lengths, all the myosin heads are engaged, but the myosin fibre pushes against the end of the actin matrix, so less than maximal force is generated. At slightly longer lengths, around the resting length L_0, all the myosin heads are engaged and are free of interference. This is where the most force

can be generated. As the muscle lengthens past this point, fewer myosin heads are engaged with the actin, and force producing capabilities of the muscle are reduced.

The passive component of the force-length relationship represents the change in length of the passive tissue in the muscle as the muscular tissue is loaded with an external force. Note that the force of passive tissue does not increase indefinitely. Rather, the force placed on the passive tissue is limited by the ability of that tissue to withstand tearing.

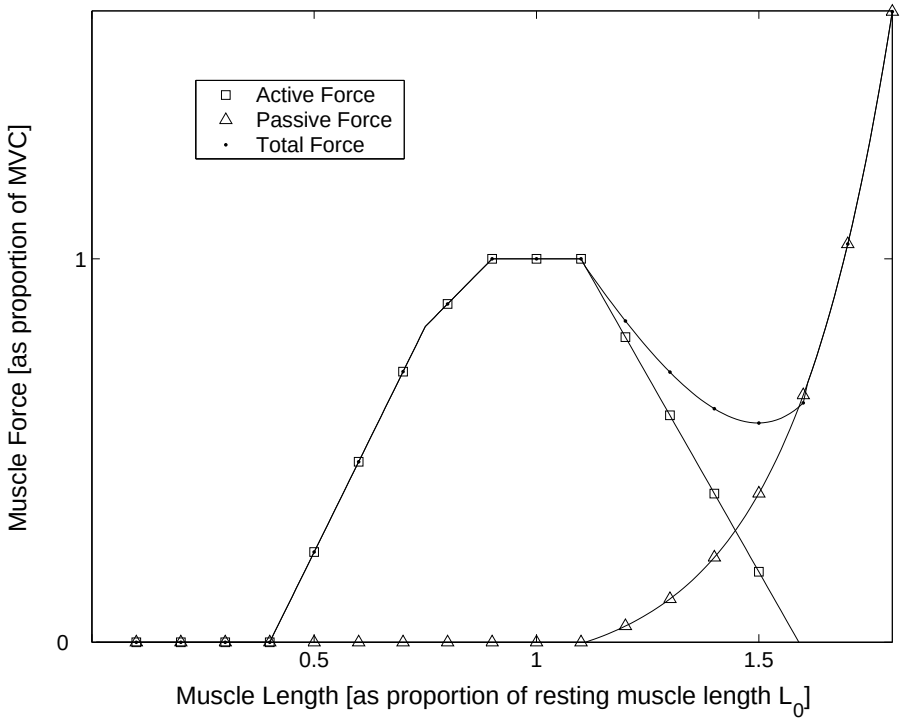

Figure 2.6: Force-length modulator in EMG-force relationship

The second modulator of the EMG-force relationship is the velocity of contraction. The force-velocity effect is also well documented [17, 31, 32, 33]. As is shown in Figure 2.7, the tension decreases for a given activation as the velocity (v) of shortening increases. This is due to the fact that to shorten at greater velocities, fewer crossbridges can be simultaneously formed. For $v = 0$, the isometric case, a force of 100% Maximum Voluntary Contraction (MVC) is obtained. The force exerted during active lengthening is actually greater than MVC. Unlike shortening, the force producing capabilities of the muscle are not dependant on the ratcheting

of the myosin heads over the actin, but rather the ability of the myosin heads to remain engaged with the actin. The myosin can remain engaged under higher tension than it can generate through the racheting mechanism.

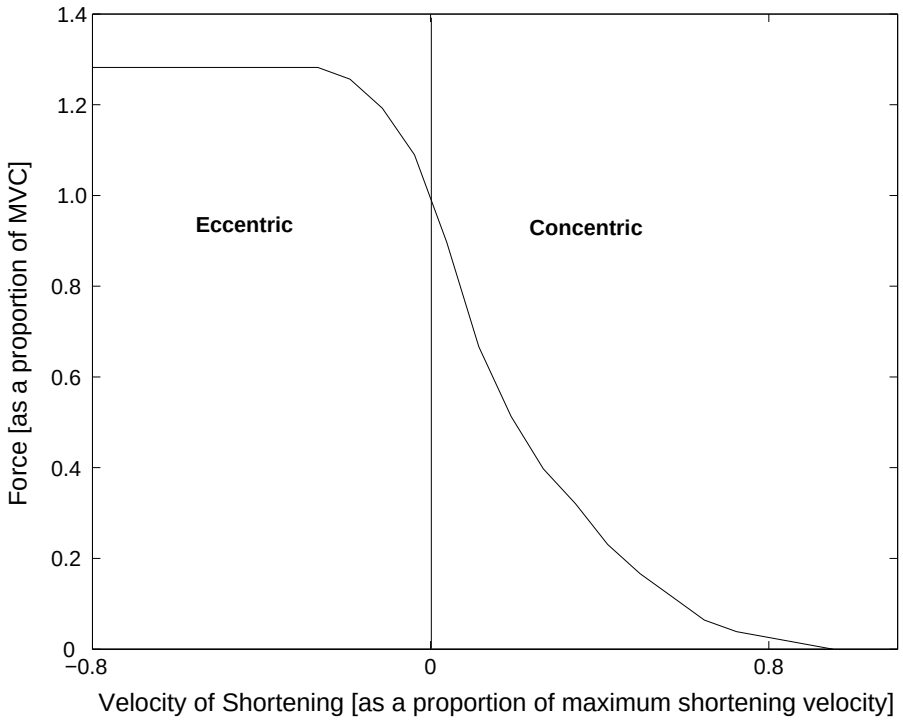

Figure 2.7: Force-velocity modulator in EMG-force relationship

In [31], the relationship between force and EMG amplitude, in the presence of the modulators, is expressed as

$$F_m = G[(EMG/EMG_m)(P_o)(\Omega)(\delta) + F_{pec}] \tag{2.1}$$

where,
F_m: Muscle Force (N)
G: Gain
EMG: Linear envelope of EMG amplitude (unitless)
EMG_m: Linear envelope of MVC EMG amplitude (unitless)
P_o: Maximum isometric force (N)
Ω: Coefficient for velocity modulation

δ: Coefficient for active length modulation
F_{pec}: Force due to passive elasticity (N)

The equation relating force to EMG amplitude is deceptively simple. While researchers have been successful in measuring either the modulating effect of the length or of the velocity, an understanding of the interaction between the two modulators has been elusive. The trickle-down of information from biomechanics research should eventually enable researchers in the area of powered orthoses to quite accurately estimate the forces that the user would like to produce in a given muscle. For now, EMG-force estimation will continue to assume a lack of interaction between the modulators.

2.2.3.3 Limitations of EMG Interfaces

Even if the interaction between the length and velocity modulators is minimal, other limitations remain in the estimation of force from EMG. First, there exists the large challenge of producing the modulator curves for each muscle that will be included in the force estimation model. It has also been demonstrated that, unlike Equation 2.1, a constant gain G is not appropriate for contractions under 40% MVC. Nonlinearities exist for forces below about 40% MVC, making mathematical modelling more difficult [35, 36]. It was hypothesized in [36] that the EMG-force relationship might be different for single-joint and multi-joint actions. It was found that the relationship was the same for isometric knee extension (single-joint: knee) and isometric leg press (multi-joint: knee, hip). The results, as Alkner et al. [36] point out, are only applicable to the isometric case. For dynamic actions such as walking or rising from a chair, there has been no evidence collected to either support or refute the hypothesis.

Along with the technical difficulties of estimating force from EMG for a given muscle, there exists other challenges for use in a powered orthotic interface. There are a few factors that make it difficult to determine the net torque at the knee. For example, there are four muscles that form the quadriceps group, and generate an extensor torque. There are three muscles that form the hamstrings group, and generate a flexor torque. There are many other muscles that cross the knee and are used for stabilization. Many of the muscles are not accessible with surface EMG. Therefore, they cannot be included in the muscle model and fidelity is lost.

Since muscles are only capable of exerting a tension, a revolute joint must be actuated by antagonistic muscle groups. The agonist muscle produces a tension to actuate the limb while the antagonist muscle exerts a tension to control the movement. The joint becomes more stable as the antagonist muscle contracts. The contraction of the antagonist muscle is known as a cocontraction since the antagonist contracts along with the agonist muscle. It is known that as the torque requirements at the knee increase, the antagonist muscles contract more strongly as well. The co-contraction is used to stabilize the knee, but few papers have attempted to quantify the effects of cocontraction.

Finally, in order to convert the force produced by a muscle into a torque at the knee, a detailed understanding of the knee anatomy is required. In order to find the origin and insertion points of muscle, its line of action, and the relevant moment arms, in-vivo imaging techniques must be used. It may not be reasonable to analyze each user. Thus, at the cost of accuracy, an anthropometric table could be used.

From the perspective of the user, the most severe limitation of an EMG interface is likely the need to apply and calibrate several electrodes every time the device is used. Since myosignals set up a spatial interference pattern, moving the electrode even slightly can have a significant impact on the measured signal [30]. Therefore, with every application of the electrode, a recalibration is required. The ease of applying and removing the orthotic is compromised by an EMG interface, and useability is affected.

Carlo De Luca, a leading researcher in the area of surface electromyography summarized the challenge of EMG/force estimation well when he stated that:

> One of the most frustrating, or appealing (depending on your perspective), aspects of the surface EMG signal is that when rectified and sufficiently smoothed, its amplitude is qualitatively related to the amount of torque (or force) measured about a joint, but more often than not, an accurate quantitative relationship is elusive. [37]

2.3 Actuator Technologies

The selection of an actuator technology will affect the design of the powered orthosis. While the orthosis may be designed to allow a variety of human-machine interfaces,

the bracing must be designed from the beginning to accommodate the actuator. In selecting an actuator, the torque, bandwidth, power-to-weight ratio, and physical configuration should be considered.

Electric motors have been used [22, 38], but they must either be quite large or be highly geared, which will limit bandwidth. They remain appealing, however, because they typically exhibit well known dynamic behaviour. The RoboWalker [28] uses a proprietary electric-drive series-elastic actuator that is designed to overcome the shortcomings of some electric actuators. The series-elastic actuator converts a position controlled electric-drive motor into a force controlled actuator by placing an elastic element between the gear train output and the load. While limited success was reported, the rigid nature of the actuator does not allow the RoboWalker to be worn while seated. Due to this severe limitation, the electric-drive series-elastic actuator was ruled out.

Hydraulics have also been used in powered exoskeletons, but have proven to be slow and heavy [39]. Pneumatics, on the other hand, can be both fast and light. Researchers, however, have moved away from traditional pneumatic actuators due to the stiction caused by seals in pneumatic cylinders. Their focus has instead, for use in powered orthoses, moved towards other forms of pneumatic actuators.

Yamamoto el al. describe a power-assist for nurses in [24] that uses an alternative pneumatic actuator. Yamamoto et al. briefly considered using a pneumatic muscle actuator (PMA), described below, but felt that it exhibited too much hysteresis. Instead they developed a pneumatic rotary actuator, shown in Figure 2.8, for use in the power-assist suit. An extensor torque is generated by inflating a pressure cuff, though no flexor torque can be generated. The technology was successful in reducing hysteresis, but is severely limited for STS. Like the electric-drive series elastic actuator, it does not allow the user to sit while wearing the orthotic.

While the hysteresis of a PMA was found to be up to about 25% in [40], the concerns expressed in [24] about the hysteresis of pneumatic muscle actuators have been largely voided as PMA technology has advanced. Pneumatic muscle actuators are now a common pneumatic alternative, and are known by many names. They are called pneumatic muscle actuators, fluidic actuators, McKibben muscles, Rubbertuators, and air muscles. They have been used successfully in a variety of novel applications including powered exoskeletal devices [23, 26, 27] and biomimetic

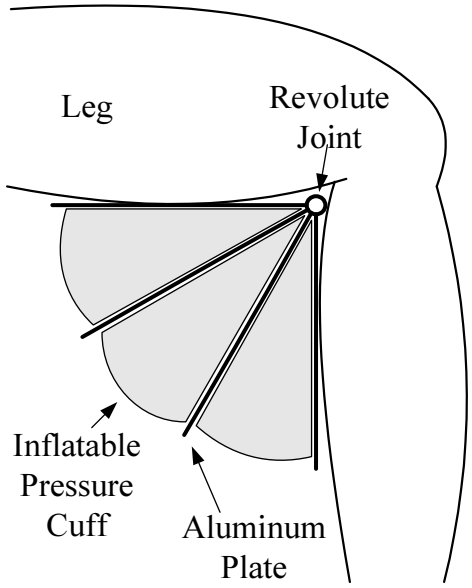

Figure 2.8: Pneumatic rotary actuator using pressure cuff

robots [39, 41, 42, 43, 44, 45, 46, 47, 48, 49, 50, 51].

Pneumatic muscle actuators have found favour for a number of reasons. They pose little risk to human operators in the event of failure, and, since they are driven by compressed air, they can be vented directly to atmosphere [39, 52]. Pneumatic muscle actuators typically have a power-to-weight ratio that is approximately 5 times higher than either electric or hydraulic actuators [39]. The muscle created by Festo "develops up to ten times more force than a conventional pneumatic cylinder and consumes only 40% of the energy for an identical force" [53].

The functional principle behind the PMA is quite simple. The pneumatic muscle is composed of an inner tube covered in a three-dimensional rhomboidal mesh. As air is admitted and the internal pressure of the PMA increases, the inner tube will expand radially. As is shown in Figure 2.9, the radial expansion of the air muscle forces a corresponding change in the alignment of the rhomboidal mesh. As the indicated angle α of the rhomboid increases, an axial tension is generated. A stroke of 25% of the initial unloaded length may be achieved [53].

In the axial direction, pneumatic muscles, like biological muscles, are capable only of exerting a tensile force. Therefore, to fully actuate a revolute joint, an antagonistic pair of pneumatic muscles must be used. This is shown in Figure 2.10,

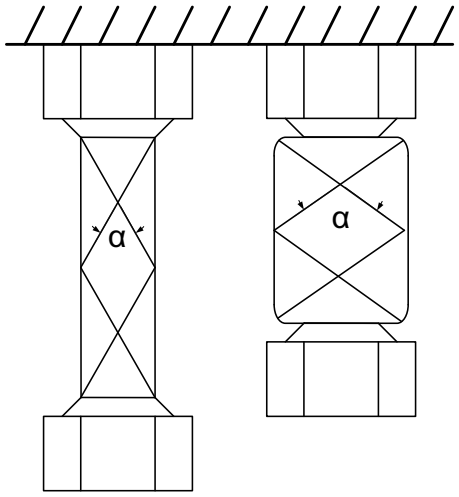

Figure 2.9: Functional principle of pneumatic muscles. Note the increasing angle α of the rhomboidal mesh as the pneumatic muscle contracts.

where two muscles are used to drive a one degree-of-freedom revolute joint. As the agonist contracts, the antagonist must relax in order to allow movement of the joint. The agonist and antagonist may also contract and relax simultaneously in order to control the joint stiffness, or in the human user to control the joint stability. The antagonist muscle, in certain designs, may be replaced with a tension spring in order to reduce the complexity of design. When developing an actuation strategy, it is important to consider that pneumatic muscle actuators can only exert tension.

While pneumatic muscles have grown in their diversity of application, they have yet to reach their full potential. The simple concept of the pneumatic muscle belies the complexity of control. A variety of approaches, with varying success, have been attempted. PID control [40, 47, 54], neural networks [40, 55], and adaptive control [54, 56, 57], among others, have been utilized. While PID control is well known, the results are particularly sensitive to errors in the feedforward term. Adaptive and neural network control may be more robust, but suffer from slow convergence and long training sessions respectively. Thus, adaptive control is not well suited for the fast movements required of an orthotic actuator. Analogously, neural control, with its training workspace, does not handle unique or unexpected situations well.

Ultimately, given the ability of humans to adapt to force transfers [10], a well controlled actuator technology coupled with a well designed human-machine inter-

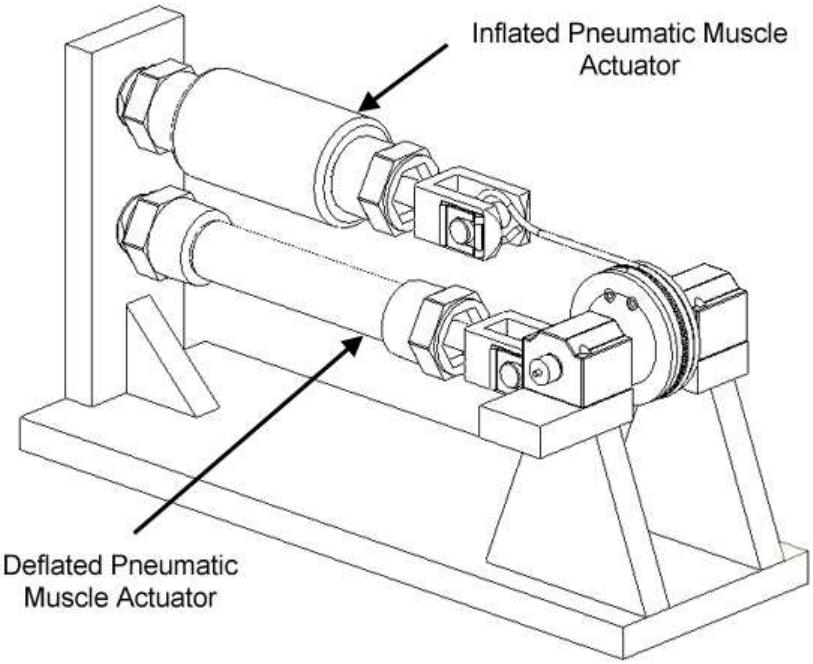

Figure 2.10: Antagonistic muscle pair actuating a 1 degree-of-freedom joint. (reprinted from [9])

face should allow for the implementation of a useful powered orthotic device. The design and simulation of such a device are explored in the following chapters.

Chapter 3

Modelling of the Powered Lower-Limb Orthotic Contribution to STS

Modelling of the sit-to-stand (STS) task with a powered orthotic is quite complex. It includes modelling human movement, actuator response, and the interaction between the human and the orthotic. The model should provide important insight into the design of the orthotic, by allowing orthotic parameters to be simulated before being implemented. The model, based on kinematic and dynamic requirements of STS, should allow the development of reasonable expectations regarding how much aid the orthotic can provide. The model should also provide a clue to the most effective control strategies.

In order to meet the stated goals, the model for assisted STS must be broken into three distinct categories. The STS inverse dynamics model will be used to estimate the inaccessible net torques exerted in STS based on the observable kinematics.

The inverse dynamics STS model will be used to generate a desired torque output for the powered orthotic. It will allow objective evaluation of the performance of the knee brace by quantifying the error between the desired and actual torque exerted by the orthotic.

Modelling of the brace will include parameters such as PMA length, origin and insertion points, and moment arm. It is through the brace that the force exerted by the actuator is converted into a torque about the knee of the user.

For pneumatic muscle actuators, modelling of the actuator may be subdivided into PMA and pneumatic valve, or the components may be viewed as an integral system. Currently, there are many different models for PMAs, which are explored in this chapter. DC motors, on the other hand, have a relatively standard form, which is also presented in this chapter.

An inverse dynamics model of the STS task is considered first, since it provides a framework for understanding the contribution of a powered lower-limb orthotic to STS.

3.1 Sit-to-Stand Model

In this section relevant biomechanical conventions are introduced, the STS task is described, and a model for the sit-to-stand task is developed.

3.1.1 Conventions for Measurement of STS

The STS process is typically analyzed in the sagittal plane, under the assumption of bilateral symmetry. Figure 3.1 illustrates how the sagittal plane bisects the subject, as viewed from the front. Typically, the analysis is done viewing the right-hand side of the subject. This is the case for the model developed in this thesis.

The anatomical position is used as the reference position by biomechanists, clinicians, and therapists when measuring human movement. In the anatomical position, the subject stands erect with head, eyes, palms and toes pointing forward, feet together and arms at the side.

With reference to the anatomical position, the hip, knee, and ankle angles can be seen in Figure 3.2. Note the segments labelled shank, thigh, and HAT. The HAT represents the Head, Arms, and Trunk, and is shown as a single rigid link. Also shown are the relative coordinate frames of each segment, located at the center of mass of the segment.

In the field of biomechanics, the convention for measuring angular position is to consider flexion, bending about a joint such that the angle between adjacent bones decreases, as negative and extension, bending about a joint such that the angle between adjacent bones increases, as positive. Similarly, dorsiflexion, pulling

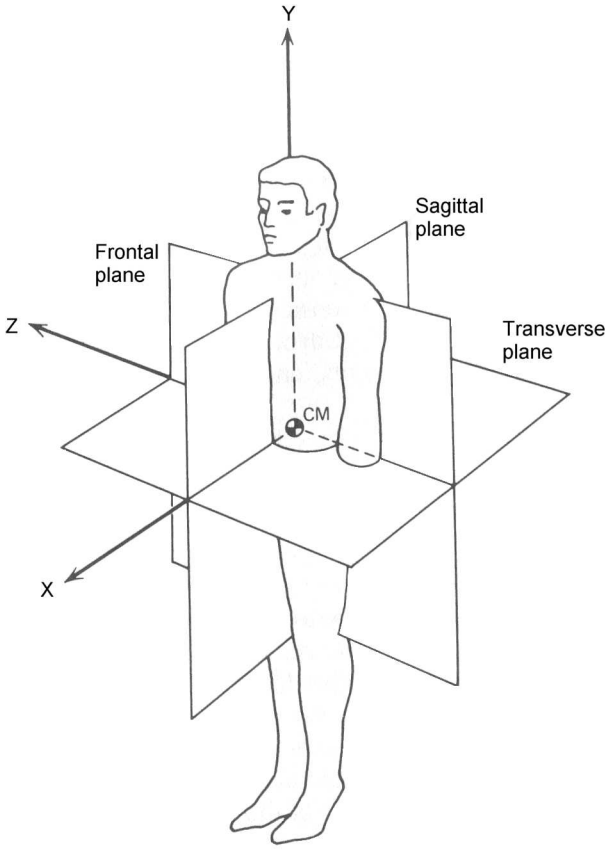

Figure 3.1: Spatial coordinate system. (reprinted from [29])

the foot up at the ankle, is negative. Extending the foot downward at the ankle is known as plantarflexion and has a positive angular position.

One important issue to note is that the ankle angle convention varies slightly between human gait and the STS task. During STS, the foot is usually kept flat on the floor. This allows a simplification to be made so that the ankle angle is measured as the angle between the shank and vertical, rather than between the shank and foot.

3.1.2 Phases of STS

To better understand the subtleties of moving from sitting to standing, it is possible to break the task into phases. The STS task, as reported in [58,59], has five distinct

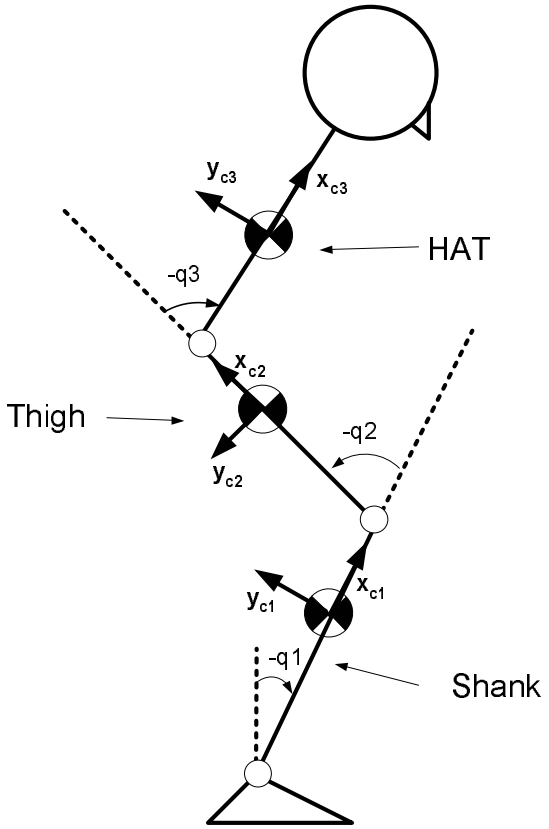

Figure 3.2: Biomechanical joint angles

functional phases. An STS model should capture these phases. The five phases of STS are:

Phase 1 The first phase is the angular acceleration of the HAT. In this phase the subject leans forward over his legs, first exerting a hip flexor torque, then later exerting a torque in the opposite direction to begin counterbalancing gravity.

Phase 2 The second phase of the task is the angular deceleration of the HAT. An extensor torque is exerted at the hip to decelerate the HAT against gravity.

Phase 3 In the third phase the hip is locked, allowing momentum to be transferred from the HAT to the whole body through a rotation about the knee and ankle. At this point seat-off occurs, and the subject is now self-supported.

Phase 4 The fourth phase is whole body linear acceleration where the subject

straightens at the knee and hip. In this phase, the subject is also decelerating about the ankle.

Phase 5 The final phase is whole body linear deceleration where the subject is nearly straight and approaching the vertical position. The subject exerts a plantarflexor torque in order to halt the rotation about the ankle, and comes to a rest in a straightened and near vertical position.

3.1.3 Link Segment Model of STS

Link segment models represent the human skeletal system as a set of rigid links connected by revolute joints. The number of segments used in the model is dependent on the task modelled and the accuracy required. The purpose of link segment models is to provide a realistic, though simplified, description of the task.

Inverse dynamic link segment models are often used because the muscle forces responsible for actuating movement are virtually inaccessible. In live subjects, dynamic data may only be accessed using painful and invasive surgical techniques, such as inserting a buckle force transducer onto a tendon. Even then, it is not possible to record the contribution of every muscle involved in the task.

Therefore, when joint torque information is required, researchers turn to inverse dynamic link segment models [8, 60, 61, 62, 63]. The simplification of the human system to a series of rigid links connected by revolute joints allows an estimate of the dynamics to be found. The inverse dynamics model is driven by kinematic data, often of actual motion, to estimate the net torques required at the modelled joints.

For a basic understanding of the torques involved in the sit-to-stand task, simple three-link models (shank, thigh, HAT) may be used [62,63]. A more complete model may be required when examining dynamic contributions [61,64], the assumption of bilateral symmetry [60,65,66], or control strategies [8]. It may include as separate links the pelvis, the trunk, the head, as well as the left and right feet, shanks, thighs, and arms.

3.1.3.1 Considerations for Link Segment Models of STS

The models used in the citations above use a two-dimensional model for the sit-to-stand task. Intuitively, it would seem that a two-dimensional model would be an

appropriate simplification of the three-dimensional reality, particularly for models using revolute joints. Schultz et al., in [8], argue that a two-dimensional model is reasonable since subjects "rise in an essentially sagittally symmetric manner". For the task at hand, and given the support in literature, a two-dimensional model is considered acceptable and is developed.

Link segment analysis allows for static analysis, where gravity and contact forces are the only forces considered. It also allows for the development of dynamic models where inertial effects are taken into account. Miller et al. explain that without the use of arm support the STS task can only be done dynamically, since the center of gravity is well behind the feet [64]. Hutchinson et al., however, found that segment dynamics account for less than 1% of the torques at the knee and ankle [61]. Also, given that impaired elderly subjects generally place a high priority on postural stability at liftoff [8], which places the center of gravity anterior of the foot, they may be able to perform the task nearly statically. While it may be possible to rise from sitting to standing in a nearly static manner, it appears that dynamics have a role in some STS trials, and therefore the model developed here incorporates dynamic effects.

Work performed in [66] suggests that subjects rise from sitting in an essentially sagittally symmetric manner. Work by Ikeda [60], Lundin [65], and Hutchinson [61] suggests that while the left and right torque profiles are similar, there are peak moment asymmetries. However, compared to normal physiological variability, both inter-subject and intra-subject, the sagittal asymmetry is not a reason for concern. It suggests that while all data used should be taken for the same leg, the assumption of bilateral sagittal symmetry in the model remains valid.

In [67], Gruber et al. found that the use of rigid links can result in severe errors when modelling high impact activities, such as landing a jump-shot in basketball. A wobbly mass model was suggested in an attempt to mimic the movement of muscle over the rigid bone. While muscle movement may be a valid concern when modelling high impact activities, its effects are negligible in the slower and low-impact STS task. Therefore rigid links are used in the model developed.

3.1.3.2 Equations of Motion for a Three-Link Planar Model of STS

Using a three-link segmental model for use in the analysis of the STS task, under the assumption of bilateral symmetry and viewed in the sagittal plane, the model resembles a three-link planar robot. Figure 3.3 shows a three-link planar model with the reference frames used in deriving the dynamic equations. Notice that the first, second, and third links match with the shank, thigh, and HAT respectively, and are actuated at the ankle, knee, and hip joints. The position and orientation of the reference frames follow the Denavit-Hartenberg convention [68]. Note that the model follows the right-hand rule used in robotics, rather than the biomechanical convention of extension as positive and flexion as negative.

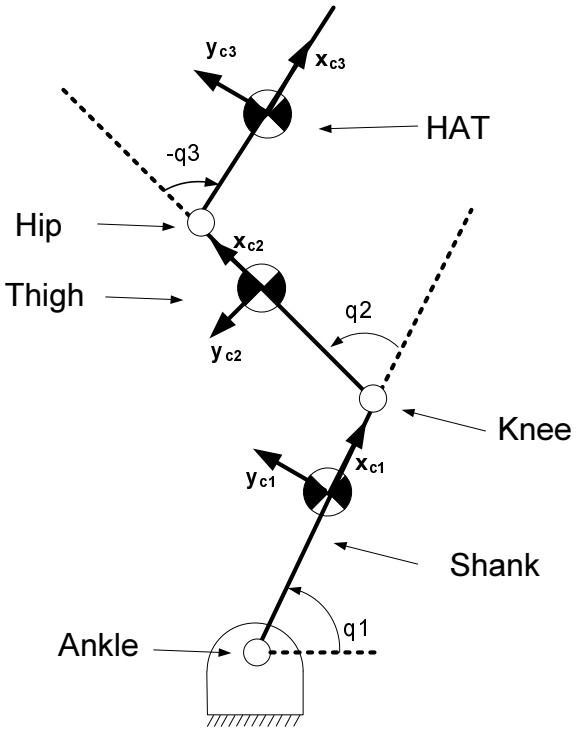

Figure 3.3: Link segment model of the sit-to-stand task

A closed-form system of equations for the three-link planar model was developed in [69]. The form of the equations [68] is given in Equation 3.1.

$$T_k = \sum_{j=1}^{n} d_{kj}(\alpha)\ddot{\alpha}_j + \sum_{i=1}^{n}\sum_{j=1}^{n} c_{ijk}(\alpha)\dot{\alpha}_i\dot{\alpha}_j + \phi_k(\alpha) \tag{3.1}$$

where,
α_k: Angular displacement of the k-th joint
T_k: Torque at the k-th joint
d_{kj}: k,j-th element of the inertia matrix $D(\alpha)$
c_{ijk}: i,j-th element of the Christoffel matrix $C(\alpha)$, containing Coriolis and centrifugal effects for the k-th joint
ϕ_k: k-th element of $\Phi(\alpha)$, the derivative of the potential energy of the system taken with respect to the k-th joint.

A state-space representation was also developed in [70]. Once expanded, the representation in [69] is equivalent to that of [70], therefore the more compact state-space form is presented in Equation 3.2.

$$\begin{bmatrix} T_1 \\ T_2 \\ T_3 \end{bmatrix} = \begin{bmatrix} I_{1,1} & I_{1,2} & I_{1,3} \\ I_{2,1} & I_{2,2} & I_{2,3} \\ I_{3,1} & I_{3,2} & I_{3,3} \end{bmatrix} \begin{bmatrix} \ddot{\alpha}_1 \\ \ddot{\alpha}_2 \\ \ddot{\alpha}_3 \end{bmatrix} + \begin{bmatrix} v(\alpha,\dot{\alpha})_1 \\ v(\alpha,\dot{\alpha})_2 \\ v(\alpha,\dot{\alpha})_3 \end{bmatrix} + \begin{bmatrix} G(\alpha)_1 \\ G(\alpha)_2 \\ G(\alpha)_3 \end{bmatrix}. \tag{3.2}$$

The following convention is used in the expansion of the terms of Equation 3.2
m_x: Mass of the x-th link
l_x: Length of the x-th link
l_{cx}: Distance to the center of mass of the x-th link from the x-th joint
I_x: Inertia of the x-th link about its center of mass
C_x: $\cos(\alpha_x)$
C_{xy}: $\cos(\alpha_x + \alpha_y)$
S_x: $\sin(\alpha_x)$
S_{xy}: $\sin(\alpha_x + \alpha_y)$.

The three moments of inertia are

$$\begin{aligned} I_{1,1} &= I_1 + m_1 l_{c1}^2 + I_2 + m_2(l_1^2 + l_{c2}^2 + 2l_1 l_{c2} C_2) + I_3 + \\ &\quad m_3(l_1^2 + l_2^2 + l_{c3}^2 + 2l_1 l_2 C_2 + 2l_1 l_{c3} C_{12} + 2l_2 l_{c3} C_3), \\ I_{2,2} &= I_2 + m_2 l_{c2}^2 + I_3 + m_3(l_2^2 + l_{c3}^2 + 2l_2 l_{c3} C_3), \\ I_{3,3} &= I_3 + m_3 l_{c3}^2. \end{aligned} \tag{3.3}$$

The coupling inertia terms, where $I_{i,j} \quad \forall i,j = 1..3, i \neq j$ is the effect on joint i

of angular acceleration at joint j, are given below. Note that the inertia matrix is symmetric therefore $I_{1,2} = I_{2,1}, I_{1,3} = I_{3,1}, I_{2,3} = I_{3,2}$.

$$\begin{aligned} I_{1,2} &= m_2(l_{c2}^2 + l_1 l_{c2} C_2) + I_2 + \\ &\quad m_3(l_2^2 + l_{c3}^2 + l_1 l_2 C_2 + l_1 l_{c3} C_{12} + 2 l_2 l_{c3} C_3) + I_3, \\ I_{1,3} &= m_3(l_{c3}^2 + l_1 l_{c3} C_{23} + l_2 l_{c3} C_3) + I_3, \\ I_{2,3} &= m_3(l_{c3}^2 + l_2 l_{c3} C_3) + I_3. \end{aligned} \tag{3.4}$$

The Coriolis and centrifugal terms are

$$\begin{aligned} v(\alpha, \dot{\alpha})_1 &= -[(m_2 l_1 l_{c2} + m_3 l_1 l_2) S_2 + m_3 l_1 l_{c3} S_{23}](2\dot{\alpha}_1 \dot{\alpha}_2 + \dot{\alpha}_2^2) - \\ &\quad [m_3 l_1 l_{c3} S_{23} + m_3 l_2 l_{c3} S_3](2\dot{\alpha}_1 \dot{\alpha}_3 + 2\dot{\alpha}_2 \dot{\alpha}_3 + \dot{\alpha}_3^2), \\ v(\alpha, \dot{\alpha})_2 &= -[(m_2 l_1 l_{c2} + m_3 l_1 l_2) S_2 + m_3 l_1 l_{c3} S_{23}]\dot{\alpha}_1^2 - \\ &\quad m_3 l_2 l_{c3} S_3(2\dot{\alpha}_1 \dot{\alpha}_3 + 2\dot{\alpha}_2 \dot{\alpha}_3 + \dot{\alpha}_3^2), \\ v(\alpha, \dot{\alpha})_3 &= (m_3 l_1 l_{c3} S_{23} + m_3 l_2 l_{c3} S_3)\dot{\alpha}_1^2 + m_3 l_2 l_{c3} S_3(2\dot{\alpha}_1 \dot{\alpha}_2 + \dot{\alpha}_2^2). \end{aligned} \tag{3.5}$$

The gravity terms are

$$\begin{aligned} G(\alpha)_1 &= m_1 l_{c1} g C_1 + m_2 g(l_1 C_1 + l_{c2} C_{12}) + m_3 g(l_1 C_1 + l_2 C_{12} + l_{c3} C_{123}), \\ G(\alpha)_2 &= m_2 g l_{c2} C_{12} + m_3 g(l_2 C_{12} + l_{c3} C_{123}), \\ G(\alpha)_2 &= m_3 g l_{c3} C_{123}. \end{aligned} \tag{3.6}$$

In order to complete the model the mass, length, and inertial parameters of the links must be determined. The selection of these parameters is considered next.

3.1.3.3 Segment Parameters of the STS Model

Modelling of the shape of the shank, thigh, and HAT segments has an effect on the inertial properties of those segments. That said, it was decided that each segment should be modelled as a line link with non-uniform mass distribution. This greatly simplifies the mathematics, but should not affect accuracy significantly. Recalling the relative coordinate system for each link, previously shown in Figure 3.3, it may be seen that under the assumption of sagittal plane motion there is no acceleration in the z-direction (out of page). Therefore, the z-component of inertia may be set to

zero. The y-component (transverse axis) of inertia is ignored. This seems acceptable based on the relatively small width of the human body segments in contrast to their length. A similar simplification was performed by Winter [29] in analysis of human gait. Thus, the determination of the inertial component in the x-direction, which is along the length of the segment, remains.

Due to the complex shape and composition of the human body, determining accurate values for the inertial parameters of the human body is not an easy task. Techniques exist to determine the parameters from both live subjects and cadavers. As well, regression equations and other mathematical methods exist to determine inertial properties. Indeed, Reid and Jensen, in their report on human body segment inertia [71] claim that a mathematical model is preferable to other clinical methods in order to account for body shape. Accuracy aside, mathematical models also present an important problem. Typically three or more width and length measurements are required [72, 73] for use in the mathematical models for each segment. As well, the HAT is modelled as three individual segments. Thus, the use of a mathematical estimation technique requires the accurate measurement of many parameters. The benefit of increased accuracy from the mathematical inertia estimation is limited compared to the cost in complexity.

Another method that may be employed is the use of anthropometric data. Provided and used in [29], anthropometric data is normative data collected from a range of subjects. Included in the data is the radius of gyration (ρ) about the center of mass, normalized by segment length. If the mass (m) and length (l) of the segment is known, then the inertia (I) of that segment may be calculated as

$$I = m \times (l \times \rho)^2. \tag{3.7}$$

Just as the radius of gyration of a segment is provided in [29], so is the location of the center of mass, the mass, and the length of the segment. These are scaled based on subject weight and height. Appendix A uses anthropometric data to calculate the values of the segment length, mass, inertia, and the center of mass for the shank, thigh, and HAT.

3.1.3.4 Bottom-Up Model

The net torque at the ankle can be estimated using an inverse dynamics approach. However, the ankle joint is prone to parameter error, especially since the ankle torque is coupled with parameters of the thigh and HAT. Based on this reasoning, it is recommended in [70] that ground reaction forces be used to correct the inverse dynamics estimate at the ankle. The comparison of the inverse dynamics estimate of ankle torque with the bottom-up estimate of ankle torque also provides a means of assessing the validity of the STS model. It is for the purposes of validation that the bottom-up model is developed here.

To determine the torque at the ankle, a torque balance about the estimated center of rotation is performed. An examination of Figure 3.4 reveals that two ground reaction force measurements, F_{GRF1} and F_{GRF2}, will be used. Taking more vertical reaction measurements is not practical due to the soft and compliant nature of the foot. The two force sensors are located on the the harder areas of the foot, namely the calcaneus or heel bone and the distal end of the first metatarsal.

Note that there are no horizontal ground reaction force measurements taken. Research has indicated that the horizontal forces remain near zero until late in the STS task, and even then they are small in comparison to the vertical forces [64]. Multiplying the small vertical forces with a small moment arm, the effects of horizontal ground reaction forces should be negligible.

Recognizing that the joint forces $F_{y-ankle}$ and $F_{x-ankle}$ pass through the center of rotation, a force balance yields:

$$M_{ankle} = x_2 F_{GRF2} - x_1 F_{GRF1}. \tag{3.8}$$

Given the two vertical ground reaction force measurements it is possible to estimate the torque at the ankle. This estimate will be compared with the inverse dynamics estimate of ankle torque to determine the validity of the STS model.

3.2 Brace Model

The brace is used to convert a force generated by the actuator into a torque acting about the knee of the user. While the powered orthotic has not been implemented

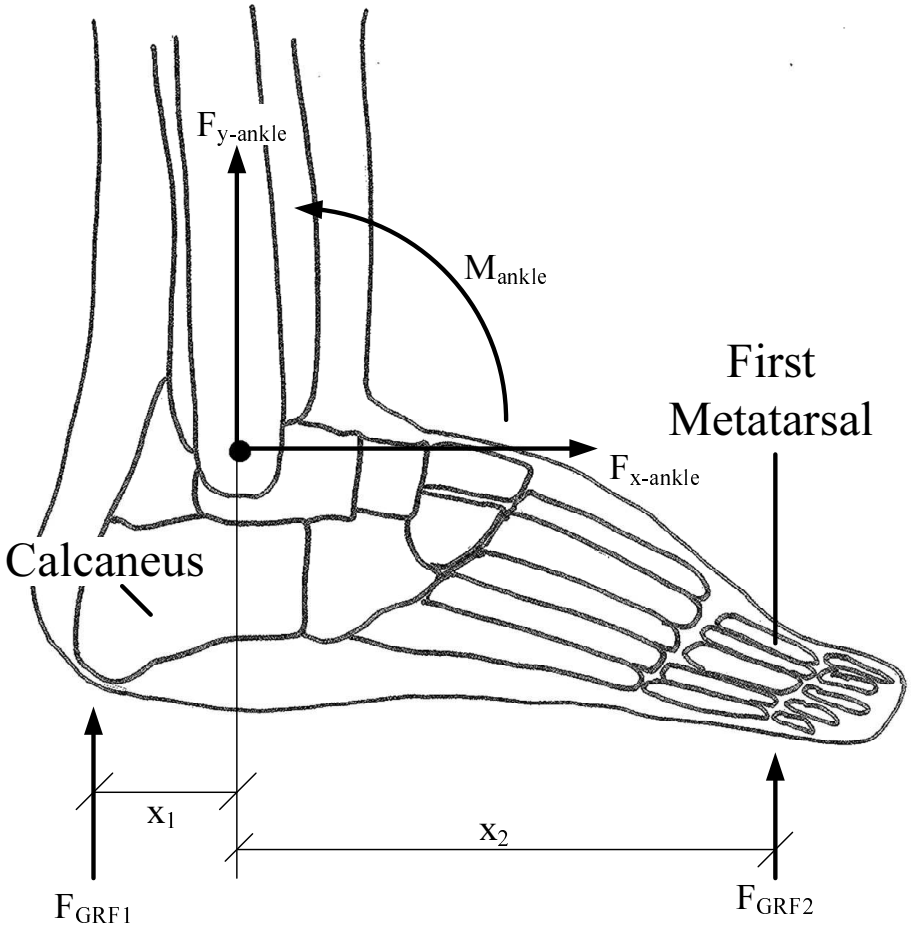

Figure 3.4: Model of foot for determining ankle torque

for this project, the model is based upon the Tradition X2K[1] knee brace, a photo of which is shown in Figure 3.5. The brace is an off-the-shelf orthotic for use in stabilizing the knee after Anterior Cruciate Ligament (ACL) injury. The brace, like the significant majority of custom ACL braces, includes symmetric gearing between the thigh and shank segments.

Figure 3.6 shows a side view of the knee brace, including gearing, with lever arm and actuator cable modifications. The brace is symmetric, and therefore calculations are based solely on the upper half of the brace, using the variables shown in Fig-

[1]Manufactured by Breg, Inc. Vista, CA. www.breg.com

Figure 3.5: Photo of the unmodified Tradition X2K knee brace.

ure 3.7. An actuator could also be used on the lower half of the brace, which would balance the torque on the lever arm, and double the torque producing capability of the powered brace.

The torque T produced by the actuator through the brace at the joint is

$$T = F \times r \tag{3.9}$$

where F is the tension developed by the actuator and r is the effective moment arm.

A series of equations follow that can be used to obtain r as a function of the knee position. Using Figure 3.7, then, from the right-triangle sine rule

$$\sin\phi = \frac{r}{r_{actual}}. \tag{3.10}$$

Using the Pythagorean theorem and the sine law

$$\sin\phi = \frac{\left(l_1 + \sqrt{\frac{b^2}{4} + r_{waste}^2}\right)\sin\theta}{l_{span}} \tag{3.11}$$

where the parameters are again shown in Figure 3.7.

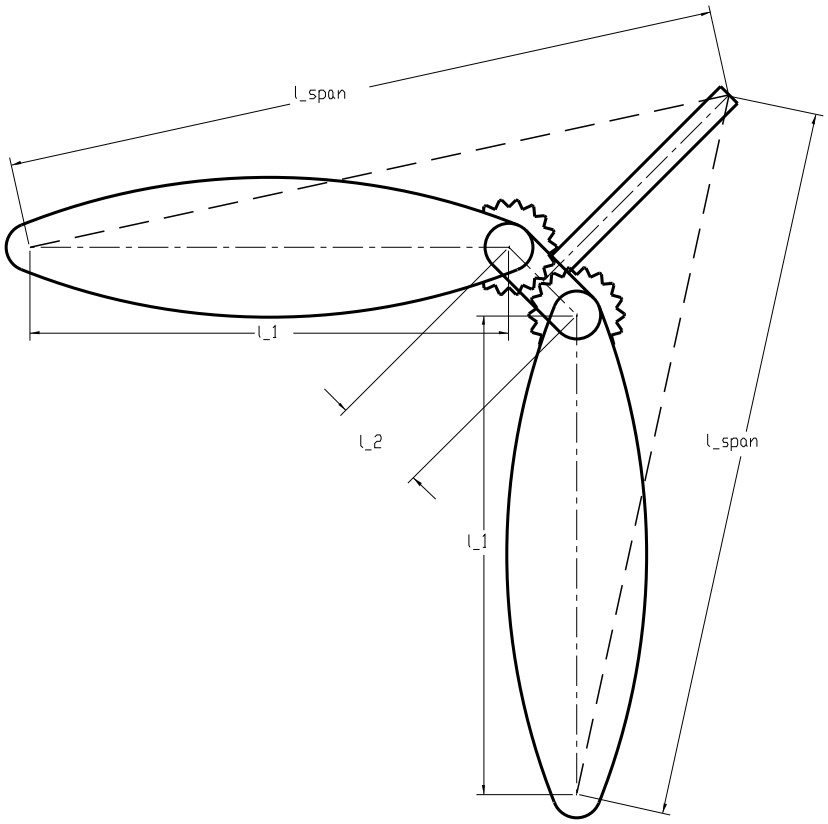

Figure 3.6: Schematic of the Tradition X2K knee brace. A lever arm and actuator cable l_{span} are modifications to the brace.

Eliminating $\sin\phi$ from Equation 3.11 with the use of Equation 3.10 and rearranging gives

$$r = \frac{\left(l_1 + \sqrt{\frac{b^2}{4} + r_{waste}^2}\right)\sin\theta}{l_{span}} \times r_{actual}. \tag{3.12}$$

This, however, can be further simplified into a set of known constants and the variable knee position. A set of equations are now presented in order to allow the reduction of Equation 3.12.

Using the right-triangle tangent law and rearranging

$$r_{waste} = \frac{l_2/2}{\tan\gamma}. \tag{3.13}$$

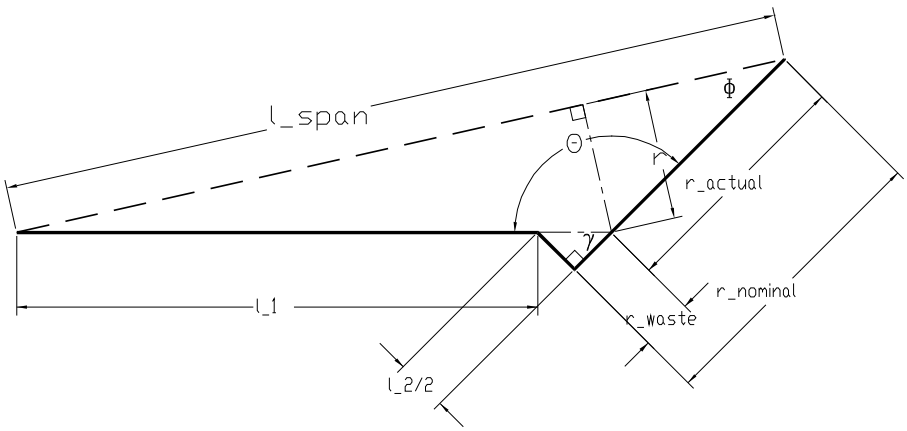

Figure 3.7: Schematic of upper portion of the Tradition X2K knee brace. Only the center lines and variables relevant to the torque calculations are shown.

Also,

$$r_{actual} = r_{nominal} - r_{waste}. \tag{3.14}$$

With the use of Equation 3.13, r_{waste} is eliminated from Equation 3.14, giving

$$r_{actual} = r_{nominal} - \frac{l_2/2}{\tan\gamma}. \tag{3.15}$$

Using the cosine law produces

$$l_{span} = \sqrt{\left(l_1 + \sqrt{\frac{b^2}{4} + r_{waste}^2}\right)^2 + r_{actual}^2 - 2\left(l_1 + \sqrt{\frac{b^2}{4} + r_{waste}^2}\right) r_{actual}\cos\theta}. \tag{3.16}$$

Finally, recognizing that the brace is geared to move symmetrically,

$$\theta = \frac{180^\circ + \theta_{knee}}{2} \tag{3.17}$$

and

$$\gamma = \frac{180^\circ - \theta_{knee}}{2}. \tag{3.18}$$

Equations 3.13 - 3.18 can be used to reduce Equation 3.12 to the known physical parameters l_1, l_2 and $r_{nominal}$, and to the variable θ_{knee}. For a given knee brace, the effective moment arm r is a function only of the knee position θ_{knee}. In Figure 3.8, for $l_1 = 30cm$, $l_2 = 2cm$ and $r_{nominal} = 10cm$, the effective moment arm is shown as a

function of knee position. l_1 was chosen to obtain a large l_{span} without compromising wearability. l_2 is a physical parameter of the Tradition X2K. The lever arm $r_{nominal}$ was selected as a compromise between effective moment arm and speed of rise.

Intuitively, the torque requirement at the knee is largest while it is bent. This indicates that the actuator must generate a large tension early in STS, complicated by the fact that the effective moment arm is smaller when the knee is bent more, as shown in Figure 3.8. Therefore the brace actuator must be designed so that the powered orthotic can generate the largest torque with the smallest moment arm.

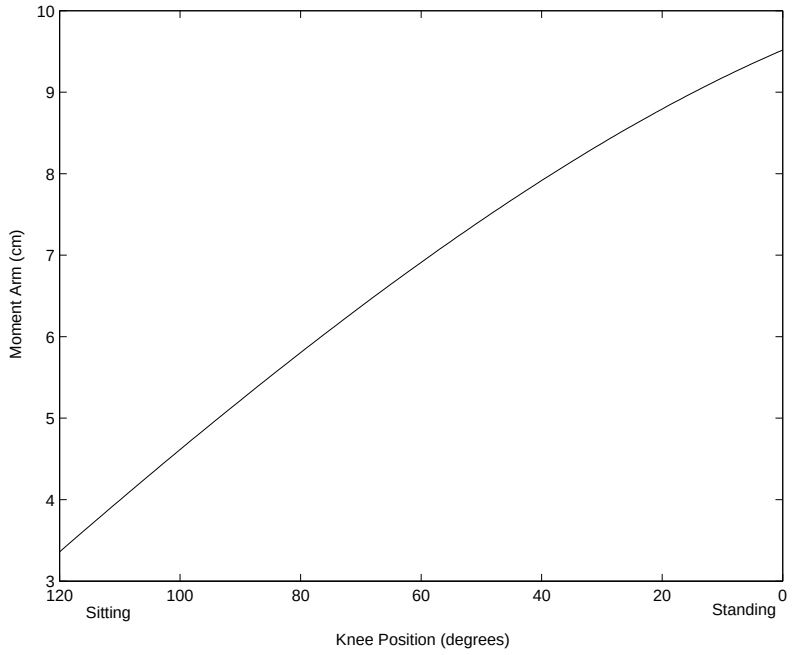

Figure 3.8: Effective moment arm versus knee position

3.3 Pneumatic Muscle Actuator Model

The Pneumatic Muscle Actuator is one type of actuator being considered for use in a powered lower-limb orthotic. The PMA was first introduced in Section 2.3. As the internal pressure of the PMA increases, there is corresponding radial expansion. The radial expansion changes the alignment of the rhomboidal mesh, which was previously shown in Figure 2.9, generating an axial force. The force that is generated

is a function of both pressure and contraction ratio.

The pressure of the PMA is regulated by a valve, which must also be modelled. While it may be possible to model the pneumatic muscle and the pneumatic valve separately, there is no benefit in doing so here. Since the pneumatic muscle and valve may be viewed as a single actuator entity, with desired pressure as the input control signal and force as the output, there is no need to model them separately. Also, since the characteristics of the actuator are strongly dependent on the type of pneumatic muscle and the valve used, it is useful to mention the equipment here.

The pneumatic muscle selected for use in the project is the Festo fluidic Muscle Actuators Single acting pulling, in the $10mm$ diameter option. The muscle is called the MAS-10[2], and was chosen due to the minimal hysteretic behaviour of the muscle and its force producing capabilities. The valve used is the Techno Airfit PRE-U-01 pressure regulating piezo valve[3].

3.3.1 Static Model of the PMA

Modelling of the force producing capabilities of pneumatic muscles has typically centered on the consideration of virtual work and conservation of energy. The original work by Chou and Hannaford [74] made the assumption that the PMA remained perfectly cylindrical, and that the wall of the PMA was infinitely thin.

Based on pressure P and change in volume δV, the work done on the PMA δW_{in} to inflate its bladder is

$$\delta W_{in} = P\delta V. \tag{3.19}$$

Based on the axial tension F and the change in length δL, the work done to actively shorten the PMA δW_{out} is

$$\delta W_{out} = -F\delta L. \tag{3.20}$$

Then, using the principle of virtual work

$$P\delta V = -F\delta L. \tag{3.21}$$

[2]Manufactured by Festo AG & Co. Mississauga, ON. www.festo.com

[3]Manufactured by Hoerbiger Origa. Glendale Heights, IL, USA. www.hoerbiger-origa.com

Using Equation 3.21, Chou and Hannaford developed a static tension-pressure-length model that used parameters including the length and diameter of the cylinder, the weave angle of the mesh, the number of turns of the threads making up the mesh, and the length of the threads. Tondu et al. [75] and Tondu and Lopez [55] used Equation 3.21 to develop a more useful model, given by

$$\begin{aligned} F(\epsilon, P) &= (\pi r_0^2) P[a(1-\epsilon)^2 - b], \qquad 0 \leq \epsilon \leq \epsilon_{max} \\ \epsilon &= \frac{(l_0 - l)}{l_0} \\ a &= \frac{3}{\tan^2 \alpha_0} \\ b &= \frac{1}{\sin^2 \alpha_0} \end{aligned} \tag{3.22}$$

where,
F: PMA generated force
ϵ: Contraction ratio
P: Control pressure
r_0: Resting radius of PMA
l_0: Resting length of PMA
l: Length of PMA
α_0: Resting weave angle of PMA.

Reportedly, it is the same equation used in the Bridgestone Rubbertuator reports [55]. The equation is also very similar in form to that used by Umetani et al. [23] in their spacesuit exoskeleton research.

Tondu et al. [75] recognized that the model given by Equation 3.22 predicted forces higher than were actually being generated. They pointed out that the more a PMA contracts, the less cylindrical it becomes. The ends of the muscle take on a conic shape. To account for this systematic error, a factor k was introduced. The factor amplifies the contraction ratio ϵ, thereby reducing the predicted force at high contraction ratios. The modified model is given as

$$F(\epsilon, P) = (\pi r_0^2) P[a(1-k\epsilon)^2 - b], \qquad 0 \leq \epsilon \leq \epsilon_{max}. \tag{3.23}$$

For a sample PMA with $r_0 = 0.7cm, \alpha_0 = 20^\circ, k = 1.30$, the static model is given in Figure 3.9. Note how the pressure isobars are quite linear, and how they intersect at

a 30% contraction ratio. Despite adjusting the parameters, the model developed by Lopez was not able to match well with the data prepared by Festo for the MAS-10[4]. The force-length-pressure curve developed by Festo is presented in Figure 3.10.

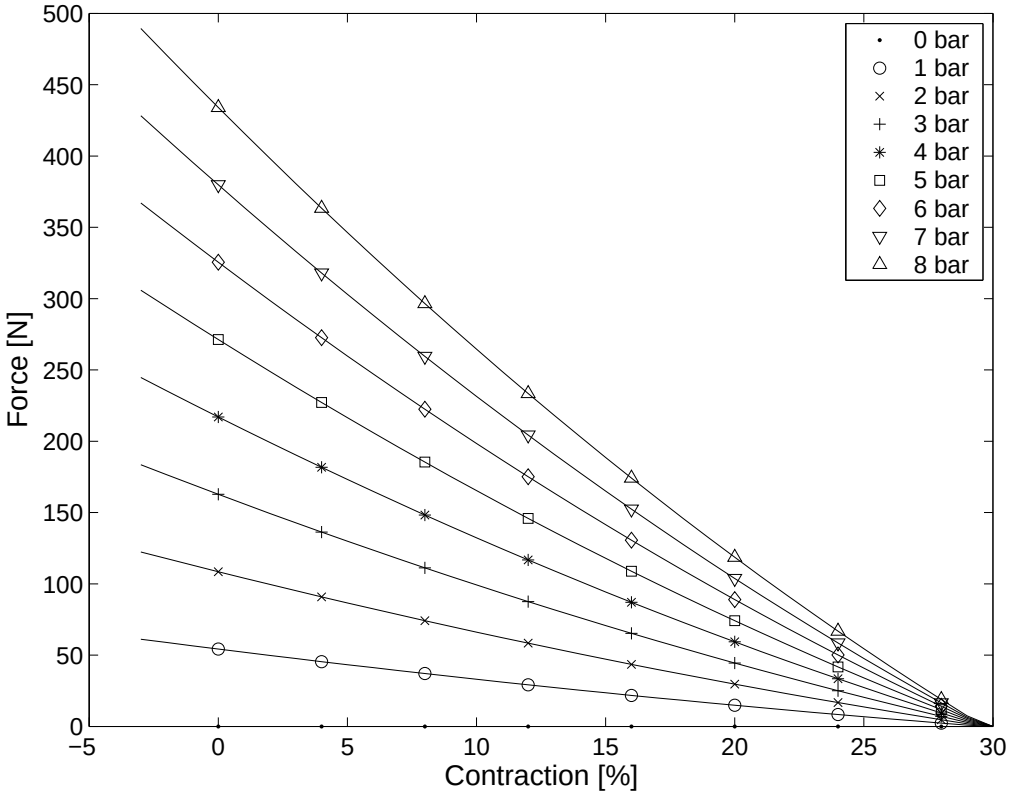

Figure 3.9: Static Lopez force-length-pressure curve for a PMA

The reason for the difference between the Lopez model, which is reported to accurately predict the force generation, and the actual results of the MAS-10 is most likely due to the structure of the MAS-10. While the pneumatic muscles of the published literature use an inner tube covered by a rhomboidal mesh, the mesh of the Festo pneumatic muscles is embedded in the tubing. Therefore, the assumption of an infinitely thin inner tube may be invalid. On the other hand, hysteresis due to the friction between the mesh and the inner tube is drastically reduced in the Festo pneumatic muscles. The claimed and experimentally verified value of 5% hysteresis was found.

[4]For purposes of legibility, the Lopez model and the Festo data are presented separately

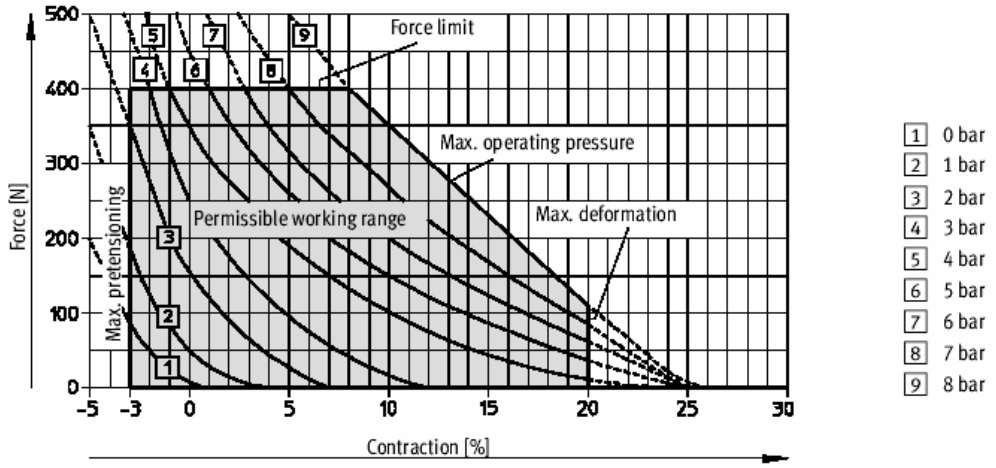

Figure 3.10: Static force-length-pressure curve for a MAS-10 as presented by Festo. (reprinted from [53])

Since the Chou model and its variants are not accurate force predictors for the MAS-10, a new model is developed. Using the force-length-pressure data for the MAS-10, exponential best fit curves are presented in Figure 3.11. The exponential fit matches with the MAS-10 data much better than the Lopez model. One clear disadvantage of the exponential fit is that the predicted force will only reach zero at an infinite contraction ratio. However, this can be remedied by setting the force to zero if the predicted force is near zero.

The form of the equation used to curve fit in Figure 3.11 is

$$F = ae^{-b\epsilon} \tag{3.24}$$

where,
F: PMA generated force
ϵ: Contraction ratio
a, b: Curve fit parameters corresponding with a given pressure isobar.

The values for the a and b parameters are presented in Table 3.1. The a and b parameters are also plotted in Figure 3.12 and Figure 3.13 respectively. In order to allow the interpolation of the parameters for predicting the force generated by the MAS-10 at various pressures, a curve fit is added to the figures. A linear fit was used for the a parameter and a second order polynomial fit was used for the

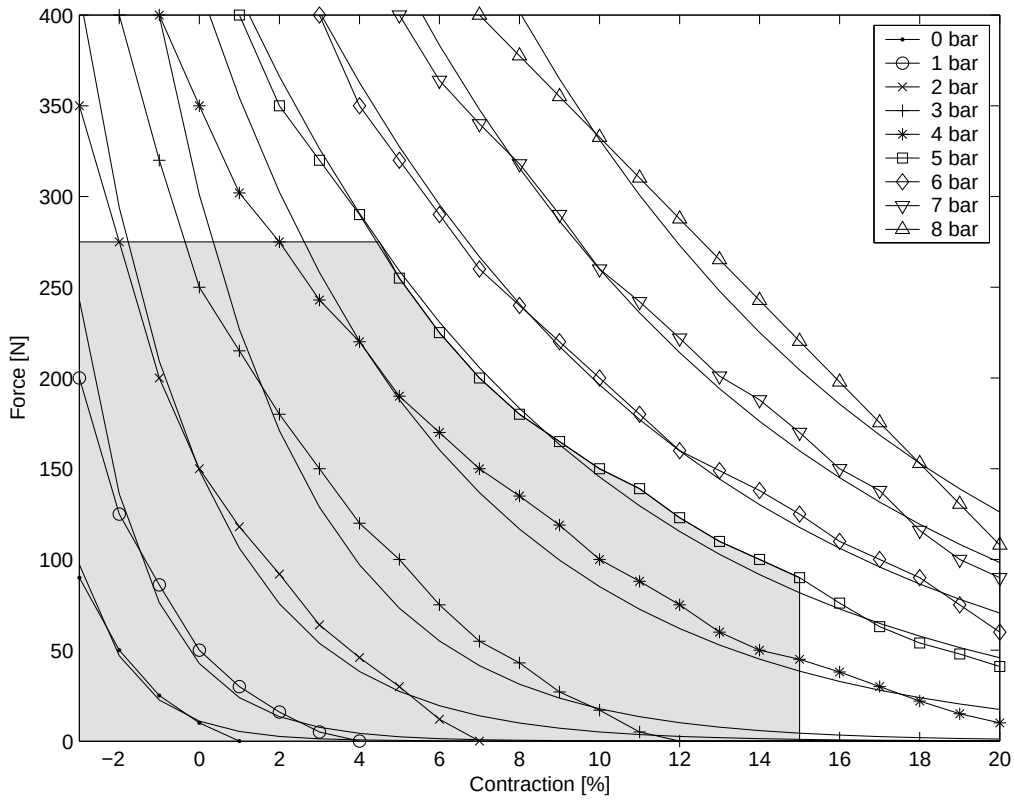

Figure 3.11: Static force-length-pressure curve for a MAS-10 with exponential best fit. The curves with markers represent the actual data, while the curves without markers represent the best fit. Utilized working area of the PMA for the powered lower-limb orthotic is shaded.

b parameter. There is no physical reasoning for the type of fit used, though the results are reasonable.

Using the linear fit curve for the a parameter and the second order polynomial fit curve for the b parameter, the static force-length-pressure curve with an exponential fit was regenerated. The exponential force predicting fit is very sensitive to the values of the a and b parameters. Thus, the Festo data and the model are drastically less accurate than that shown in Figure 3.11. Therefore, a linear interpolation will be used to estimate the a and b parameters between pressure isobars, rather than a curve to represent the whole pressure range.

In summary, the static model used to estimate the force generated by the MAS-

Table 3.1: Summary of a and b parameters for MAS-10 exponential static force-predicting model

Pressure	a-param	b-param
0 bar	10.92	72.85
1 bar	42.68	57.97
2 bar	149.04	33.95
3 bar	300.97	28.29
4 bar	415.38	15.86
5 bar	461.23	11.54
6 bar	546.31	10.24
7 bar	687.01	9.72
8 bar	869.30	9.65

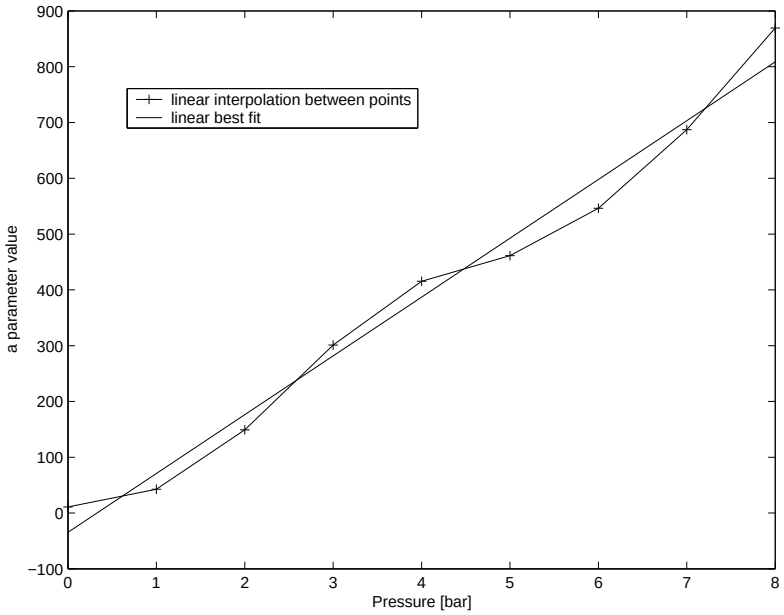

Figure 3.12: Plot of a-parameter for MAS-10 exponential static force predicting model

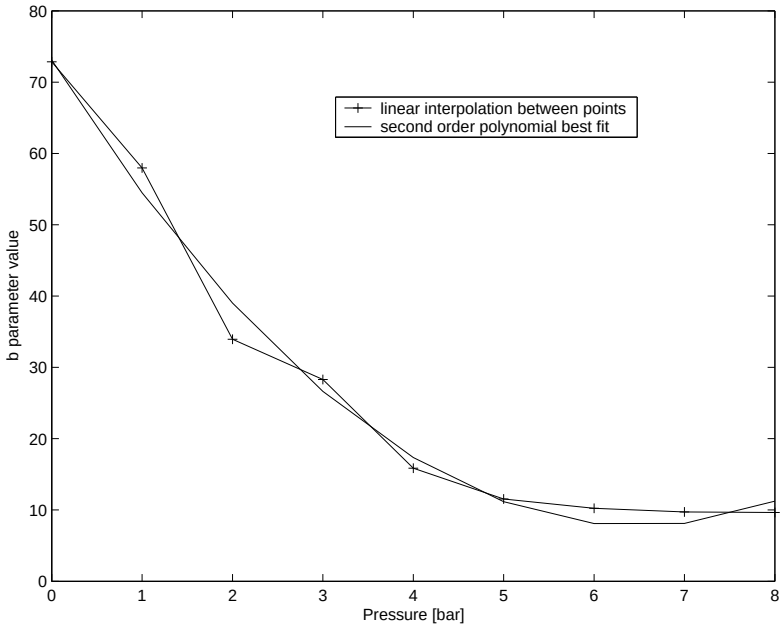

Figure 3.13: Plot of b-parameter for MAS-10 exponential static force predicting model

10 is based on the contraction ratio and pressure of the PMA. The force estimator is given by Equation 3.24 and Table 3.1, with linear interpolation used to estimate the parameters between pressure isobars.

3.3.2 Dynamic Model of the Actuator

Various approaches to modelling the dynamic characteristics of a pneumatic valve and muscle have been attempted. Modelling the dynamics of the actuator, however, can be a daunting task given that pneumatic muscles are highly nonlinear. Fortunately, there is over a decade of research into modelling the dynamics of a pneumatic valve coupled with a pneumatic muscle actuator. It seems as though different research groups continue to use different modelling approaches, some of which are examined below before a model is selected.

3.3.2.1 System Identification of the Actuator

The approach taken by Caldwell and his associates in the early to mid part of the 1990's was to use standard system identification. In [47], an off-line least squares approach was used to estimate the parameters for a discrete transfer function. The form of the transfer function, which must be determined *a priori* in least squares techniques, was 5 parameters with three time delays. However, given the nonlinearities of pneumatic muscles, this approach was only valid for a small stroke length. In [54], an on-line recursive least squares identification was used, as it allows the model parameters to be updated. The use of parameter update requires that the system change relatively slowly, which is generally not the case for augmented tasks like assisted STS.

With an off-line approach similar to that used in [47], it was found that the *a priori* form of the transfer function was reasonable. Experimentation, however, was limited to isometric muscle contraction. While a higher order system did seem to provide somewhat improved results, it was also found that a second order system could approximate the system well. The second order Bode response of an isometric contraction is given in Figure 3.14. The system identified is not so important as the fact that a second order system could approximate the actual results so well. Tondu reports that "although highly nonlinear, the McKibben muscle actuator can be approximated by a linear second-order system" [55]. This is confirmed by an examination of the second order Bode response given in Figure 3.14. It also lends credence to the research that treats the system as a spring-mass-damper system.

3.3.2.2 Spring-Mass-Damper Model of the Actuator

Work presented by Repperger and Phillips in [39] treated the pneumatic muscle as a spring-mass-damper system. For a mass M being driven by a pneumatic muscle, they ran a number of experiments over the working tension and pressure range of the muscle. From the experiments, they obtained a position dependent spring constant $K(x)$ and a velocity dependent damping coefficient $B(\dot{x})$. It was found that the parameters were different for inflation and deflation. This should be expected because inflation charges a closed space, while deflation vents to an infinite space. Four second-order equations were used to describe the two parameters as they inflate and as they deflate. These equations could then be used in the standard spring-

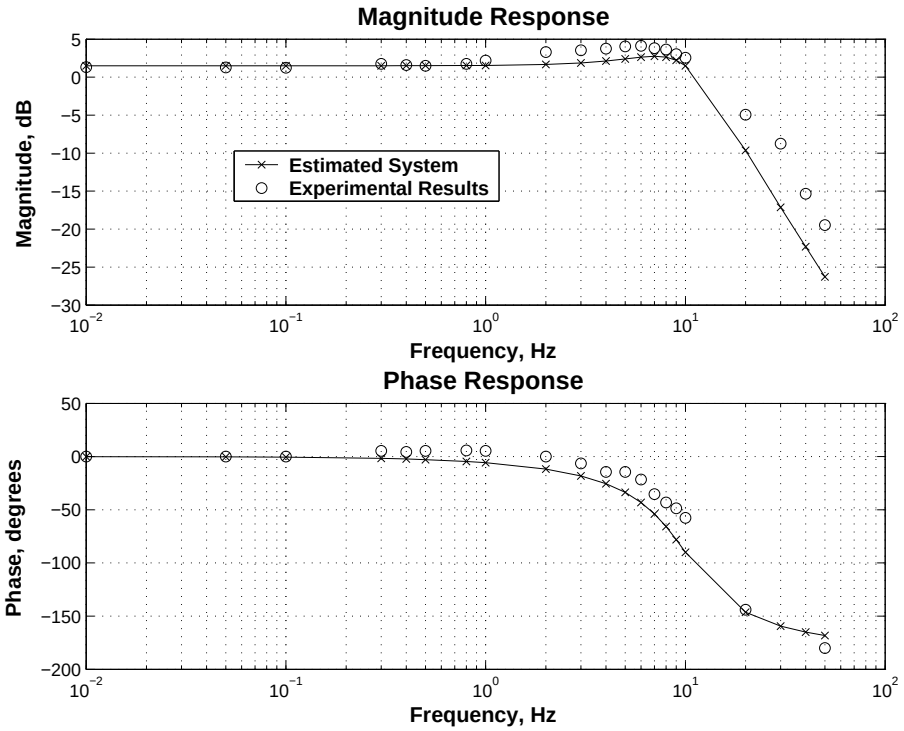

Figure 3.14: Bode response of second order system

mass-damper system, given as

$$M\ddot{x} + B(\dot{x})\dot{x} + K(x)x = u \tag{3.25}$$

where u is the control variable with units of force. Unfortunately, no results were presented in [39] upon which to evaluate the effectiveness of the model.

Work by Colbrunn et al. in [76] continued with the spring-mass-damper model. Their work, more so than Repperger and Phillips, is based on the underlying physical properties of the muscle. They explicitly incorporated effects that they felt to be of relevance, rather than fitting empirical data. They reported that their model was adequate for use in robotic simulations. While some of the effects that Colbrunn et al. incorporated are not necessary for the Festo PMA, with its integrated mesh, their model used and supported the use of fluid dynamics. The fluid dynamics model is therefore developed.

3.3.2.3 Fluid Dynamics Model of the Actuator

Colbrunn et al. [76] and Chou and Hannaford [74] both used fluid dynamics to develop a model of a pneumatic muscle actuator. Chou and Hannaford explain why it is not easy to analyze pneumatic circuits using fluid dynamics. First, pneumatic circuits are distributed-parameter systems, meaning that the state variables are functions of both time and space. Secondly, the systems are very sensitive to geometry, and many boundary conditions must be met in order to solve the system. Finally, while laminar flow allows for an analytical solution, the turbulent flow, associated with the high fluid velocities that the PMA would experience, is more difficult to solve.

In [74], a lumped-parameter approach is used to overcome some of the mentioned difficulties. The authors suggest three models, in order of increasing complexity. Their first model examines only two node pressures of the system P_1 and P_2. The gas viscosity of the system is modelled as a linear resistor R, and the accumulator as a linear capacitor C. Then the mass flow ω can be expressed as

$$\frac{P_1 - P_2}{R} = \omega \tag{3.26}$$

where,

$$\omega = -C\frac{dP_2}{dt} \tag{3.27}$$

which gives

$$P_2 - P_1 = RC\frac{dP_2}{dt}. \tag{3.28}$$

The first model, given by Equation 3.28, is a low-pass filter. The second model increases in complexity by taking into account the cross-section of the tubing and connectors. The third model extends the second by including the inertia of the gas. Since the model parameters are specific to the pneumatic circuit implementation, it makes sense to use the most generic model, the low-pass filter, unless very accurate results are required for a specific circuit.

3.3.2.4 Final Dynamic Model of the Actuator

Given the support for the low-pass filter model in [74], the model developed by Wight in [9], which is based on the same PMA and valve selected in this thesis, will

be used. The flow rate of the valve limits the dynamics of the system. The valve also controls the force output of the PMA by controlling the internal pressure.

The model developed in [9] is presented in Figure 3.15. The model, as was suggested is necessary in [39], incorporates both inflation and deflation of the PMA. It also includes a 15ms experimentally observed transport delay. While the model of [9] uses the minimum of the inflation and deflation model to implicitly choose the mode, the model developed here explicitly selects the mode.

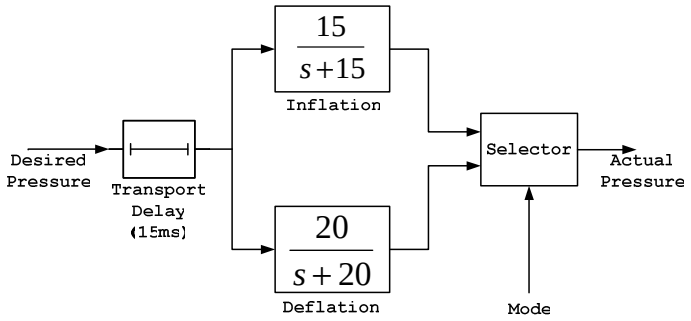

Figure 3.15: Model of fluidic flow

Wight suggests that the time required to inflate and deflate the PMA is accurately modelled by the low-pass filters, though the intermediate pressures may include some error. During inflation, the mode of the system is largely subsonic. Subsonic flow is a function of pressure difference, and therefore the low-pass filter offers a good approximation to the experimental results, to within about 5%. The mode of deflation, on the other hand, is largely sonic. Sonic flow is a function of only the source pressure. Therefore, while total charge time estimates were found to be accurate, up to 25% error was found for the intermediate pressures.

Given the pressure model suggested by Chou and Hannaford [74] and implemented by Wight [9], how can it be incorporated into the larger model? To use the dynamic model, first determine the current force and length requirements of the PMA. Using the static PMA model, determine the new pressure signal. Apply the pressure signal to the low-pass filter. Given the filtered pressure signal and the length of the muscle, it is possible to use the static model again to estimate the force generated by the PMA. The process is shown in Figure 3.16, and is incorporated into a control strategy in Section 5.2.

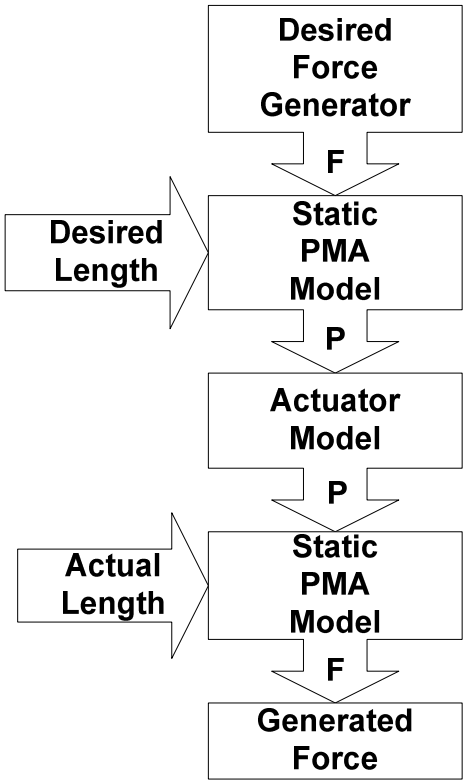

Figure 3.16: Flow diagram of PMA model

3.4 DC Motor Model

The DC motor has widespread application, being used everywhere from small remote controlled vehicles to large industrial robotics. Due to their ubiquity, the background of the DC motor is not examined. Instead, the ideal DC motor model is presented first, followed by load and configuration considerations. Finally, a model for the torque generated at the knee by a DC motor is presented.

3.4.1 Standard DC Motor Model

The standard model for a DC motor [9, 68] is given by Equation 3.29 and is shown pictorially in Figure 3.17. As shown, the angular velocity $\dot{\theta}$ of the motor shaft is controlled by an applied voltage V_{ref}. The shaft velocity is also modified by the back-EMF, which is an electromagnetic field generated by the spinning of the motor.

The EMF induces a voltage V_{EMF} that opposes the flow of current, and which is proportional to $\dot{\theta}$ by the motor constant K_{EMF}

The forward component of the DC motor model can be divided into an electrical component and a mechanical component. The electrical component has inductance L and resistance R. The torque T_{motor} is proportional to the current I drawn by the motor by the torque constant K_T. The mechanical component of the motor has actuator and load inertia J and damping ratio B.

The standard model for a DC motor is

$$\frac{\dot{\theta}(s)}{V_{ref}(s)} = \frac{K_T}{(Ls+R)(Js+B)+K_{EMF}K_T}. \tag{3.29}$$

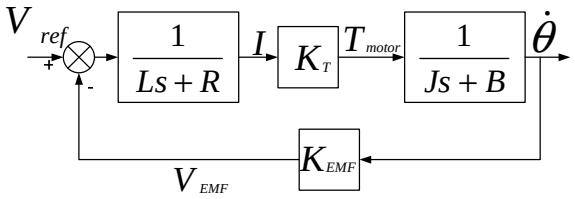

Figure 3.17: Standard DC motor model

The model can be rearranged, to that given by Equation 3.30 and given in Figure 3.18, so that torque is the output. Developing a relationship between voltage and torque allows the torque to be controlled in the simulations to follow.

The rearranged DC motor model, with torque output, is

$$\frac{T_{motor}(s)}{V_{ref}(s)} = \frac{K_T(Js+B)}{(Ls+R)(Js+B)+K_{EMF}K_T}. \tag{3.30}$$

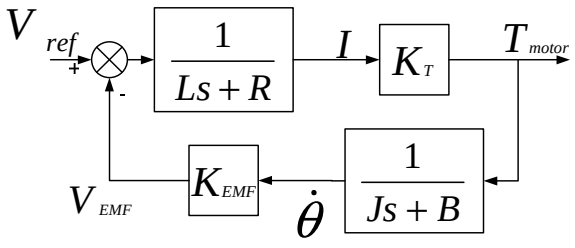

Figure 3.18: DC motor model with torque output

3.4.2 Motor Drive Configuration

While there are many possible configurations in which to use a DC motor as part of a powered knee brace, a spooling configuration is examined here. With reference to Figure 3.7, l_{span}, which represented the PMA, is replaced with a cable. The motor is then used to create a tension in the cable, by spooling the cable onto a spindle.

The drawback of a spooling configuration, as opposed to a direct drive or gear train configuration, is that the device is not back-drivable because the cable would simply unravel off the spindle. For STS, where the torque at the knee is always extensor, this is not a problem. For other tasks, such as walking, where both flexor and extensor torques may be required, a spooling configuration could still be used, but with antagonistic pairing. A spooling configuration has advantage over direct drive and gear train configurations because it is easier to modify a brace to accept the spooling configuration. It also has the advantage that the motor can be torque controlled, rather and torque and position controlled, as outlined next.

With a DC motor in the spooling configuration, it is possible to control torque and neglect the position of the motor. The motor cannot outpace the user, since the torque is limited to 50% of the required torque. A more reasonable concern, since the orthotic is designed to be used by a user who has at least limited ability to rise from sitting, would be for the motor to have difficulty spooling quickly enough to contribute a torque to the task. However, if this happens, the load on the motor is reduced, which means that for a given input voltage the motor will speed up until it is again contributing to the STS task. Therefore, torque control of the motor alone should provide good assistance to the user.

3.4.2.1 Motor Drive Requirements

In the spooling configuration, there are three factors which must be considered when selecting a motor. They are: 1)torque, 2)speed, and 3)spindle radius. The torque and speed of the motor are related, usually linearly, with maximum torque occurring when the motor is stopped and maximum velocity occurring with no load. The spindle radius determines how much cable is taken up per revolution and acts as the moment arm to create tension in the cable, and it must therefore be considered when selecting a suitable motor. Note that other factors, such as weight, power usage, and cost, are important, but only play a role if the first three requirements

are met.

In order to achieve the stated goal of providing 50% of the required torque at the knee during the STS task, a maximum tension of $2200N$ must be exerted in the cable on each knee. If an actuator is used both on the lower and upper portion of the brace, as was done with the PMA, then each motor must create a maximum tension of $1100N$.

As the knee is extended during the STS task, the cable must be shortened in order to maintain a tension in the cable. Again, this is similar in concept to the shortening PMA. The peak velocity of shortening of the cable is $8cm/s$, and the velocity of shortening during peak torque is even less than that.

3.4.2.2 Motor Selection

The Kollmorgen Direct Drive Rotary DC motor, model RBE-03013-A[5], has been selected as the DC motor actuator for use in the simulation. Sometimes known as a pancake motor due to its large diameter compared to its width, the RBE-3013-A has a diameter of less than $13cm$, and is $8cm$ in width. The motor weighs a very reasonable $1.8kg$.

The selected motor is capable of generating a peak torque of $76Nm$, and can operate at a maximum speed of $1700RPM$. With a spooler spindle of $3cm$ in radius, the motor is able to shorten the cable at a rate of $8.9cm/s$, which is above the required $8cm/s$. Additionally, the peak tension that can be generated, estimated simply by peak torque divided by the moment arm of $3cm$, is over $2500N$. On the other hand, with a spooler spindle of $6cm$ in radius, the motor has a peak shortening velocity of $17.8cm/s$ and a peak torque of over $1250N$. The working ranges are shown in Figure 3.19. The speed-tension requirement of the motor is within the working range of the motor for each of the shown spindle radii.

While each of the spindle radii shown in Figure 3.19 ensure that the speed tension requirement is met, the $5cm$ spindle radius matches well with the slope of more demanding upper half of the speed-tension curve. At $5cm$ neither the speed nor the torque limits of the motor are strained, and the model therefore uses a spindle with a radius of $5cm$.

[5]Manufactured by Kollmorgen, Wood Dale, IL. www.kollmorgen.com

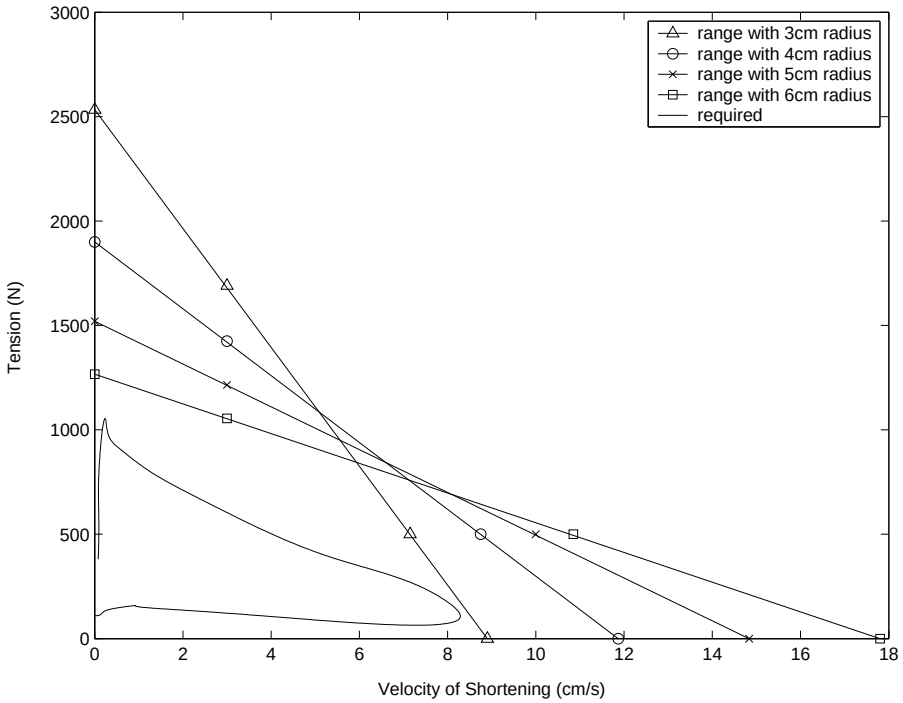

Figure 3.19: Speed-tension requirement of DC Motor and working ranges of various spindle radii

3.4.2.3 Usage of Motor Model

Kollmorgen has provided specifications for the RBE-03013-A, which are reiterated here, to be used in Equation 3.30. The rotor inertia J is $9.40 \times 10^{-4} kg \cdot m^2/s^2$ and the mechanical damping B is $2.01 \times 10^{-6} Nm \cdot s/rad$. The electrical inductance L is $6.4 \times 10^{-1} H$ and the electrical resistance R is 1.78Ω. The torque constant K_T is $1.91 Nm/A$ and the back EMF constant K_{EMF} is $1.1 V \cdot s/rad$. Based on these parameters, and using Equation 3.30, it is possible to predict the torque generated by the motor.

The tension in the cable can then be estimated as torque generated by the motor divided by the radius of the spindle, which acts as a moment arm. As with the PMA, and as shown in Figure 3.20, the tension generated by the cable l_{span} acts on a lever to generate a torque at the knee. The torque generated at the knee is different than the torque generated by the motor model, but they are related by the radius of the spindle and the effective lever arm of the knee brace.

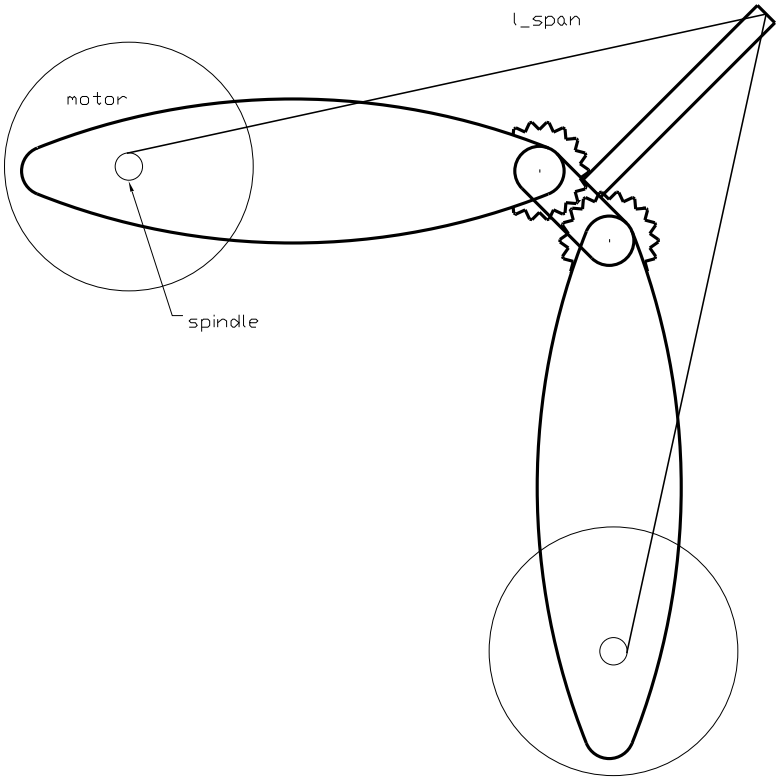

Figure 3.20: Schematic of the Tradition X2K knee brace with DC motor in spooling configuration shown.

Finally, the weight of the motor is not neglected. It is included by modifying the mass and inertia matrices of the STS model.

3.5 Concluding Comments

A model for assisted STS has been presented in this chapter. Though simple, the STS model, which is a three-link planar model, should be complex enough to accurately describe the sit-to-stand task. The knee brace model, which is based on the Tradition X2K, uses trigonometry to estimate the torque that an actuator can generate at the knee. The PMA model and the DC model, both of which are based on real actuators, are consistent with published literature. The PMA model

is sensitive to the configuration of the actuator, valve, and piping, but is considered accurate for the specified setup.

Recall that the reason for developing a model for assisted STS was to allow a simulation of the task, which will ultimately be used to guide the implementation of a powered lower-limb orthotic. A simulation based on the model for assisted STS requires kinematic data and a controller. The STS model is driven by kinematic data, which is presented Chapter 4. Controllers for the PMA and the DC motor are developed in Chapter 5. Simulations, using the model presented here, driven by the experimental data of Chapter 4 and controlled by the controllers of Chapter 5, are finally presented in Chapter 6.

Chapter 4

Experimental Data and Validation of the STS Model

The sit-to-stand model previously outlined is an inverse dynamics model, thus it must be driven by kinematic data. This chapter develops an experimental protocol for the collection of the data and provides a validation of the STS model. The data is presented following the convention established in the field of biomechanics, which is outlined in Section 3.1.1.

4.1 Experimental Protocol

A single adult male, with mass $77.11kg$ and height $1.85m$, was used in the collection of the experimental data. The subject was seated in a armless chair of height $0.43m$, and was instructed to sit erect and avoid the use of the backrest. To minimize the effects of the upper limbs, the subject kept his arms folded in front of his body for the duration of the experiment, as was done in [61,77]. The subject performed three trials each of the STS tasks at the self-selected speeds of slow, natural, and fast. Joint angle data for the ankle, knee, and hip was collected, as was force data for the foot. Based on the collected data, one representative trial for each of the three speeds was selected for use in the simulation. Representative trials were used instead of averaging in order to capture the inherent variability of physiological movements.

4.1.1 Equipment

An Optotrak[1] motion capture system was used to collect the data from which the joint kinematic data was derived. The Optotrak system measures the position of LED markers. These markers were placed along the long axis of the bone, as recommended in [78]. Specifically, they were located at the bony landmarks of the lateral malleolus (distal shank), head of the fibula (proximal shank), femoral condyle (distal thigh), greater trochanter (proximal thigh), iliac crest (lower HAT), and the anterolateral edge of the acromion (upper HAT).

Foot force data was collected using a pair of FlexiForce[2] force sensors. The force sensors are piezoresistive, and must therefore be driven by a voltage. The driving circuit is shown in Figure 4.1. In this configuration, the output voltage V_{out} is given as

$$V_{out} = V_{in}\left(1 + \frac{R_{feedback}}{R_{flexiforce}}\right). \tag{4.1}$$

The resistance of the FlexiForce sensor $R_{flexiforce}$ varies with applied pressure. The feedback resistor $R_{feedback}$ was selected to produce an output voltage of $1V$ with no load and an output voltage of $5V$ under full body weight. While it would have been possible to produce a circuit with a 0-$5V$ scale, another voltage source would have been required.

The FlexiForce data was collected on a computer system using a Quanser Data Acquistion Unit[3]. The Optotrak data was collected on a computer system using the Northern Digital proprietary Data Acquisition Unit. The two systems were synchronized with a trigger signal from the Quanser unit to the Optotrak system using the Optotrak External Trigger feature.

4.1.2 Processing of Data

This section describes the protocol used to process the collected data. As much as possible, the protocol established here follows the standards and guidelines set out by other biomechanics researchers.

[1]Manufactured by NDI, Waterloo, ON. www.ndigital.com
[2]Manufactured by Tekscan, Boston, MA. www.tekscan.com
[3]Manufactured by Quanser, Markham, ON. www.quanser.com

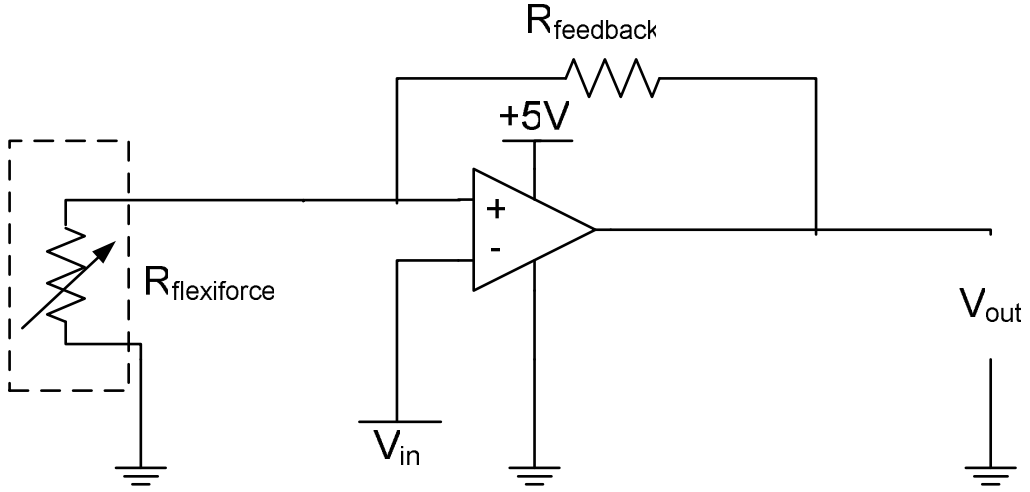

Figure 4.1: FlexiForce Driver Circuit

4.1.2.1 Kinematic Data

In order to determine the joint angles, the Optotrak marker position data was used to create vectors representing the floor, shank, thigh, and HAT. The cross product of each adjacent vector was taken to determine the trajectory of the ankle, knee, and hip. The collection of the segmental data, however, suffers from noise known as movement artifact. While the goal is to track the movement of the underlying bone, the marker is located on the skin above the bony landmark. Therefore, when the skin moves over the bone, noise is introduced to the data. This problem is remedied using smoothing techniques [61, 77, 78, 79].

A second-order dual-pass Butterworth filter, with a cutoff frequency of $3Hz$ was used to smooth the data, as was done in [77]. The filter design is also known as a fourth-order zero-phase-shift filter [78], where data is filtered, reversed, and filtered again. The dual-pass approach is useful in eliminating the phase shift seen in single-pass Butterworth or lowpass filter designs. In [78], Winter explains that a Butterworth filter has a shorter rise time than critically damped filters, but that the Butterworth filters exhibit overshoot in response to step and impulse inputs. Winter goes on to conclude that the Butterworth filter should be used since impulse type movements are rarely seen in humans.

It should be noted that $3Hz$ is a reasonable cutoff frequency because that is approximately the maximum bandwidth of larger human body segments. However,

since the Butterworth filter is used in a dual pass system, the actual cutoff frequency is less than the nominal cutoff frequency. Therefore, for a second-order dual-pass system, a nominal cutoff of $3.95Hz$ must be used to obtain the actual cutoff frequency of $3Hz$. See [80] for more details and the equation relating nominal and actual cutoff frequencies.

For use as a reference, the step response of the single-pass and dual-pass Butterworth filter with a cutoff frequency of $3Hz$ is shown in Figure 4.2. Note that both responses overshoot, as was expected with a step input. The single-pass filter, however, has a phase lag while the dual-pass filter does not.

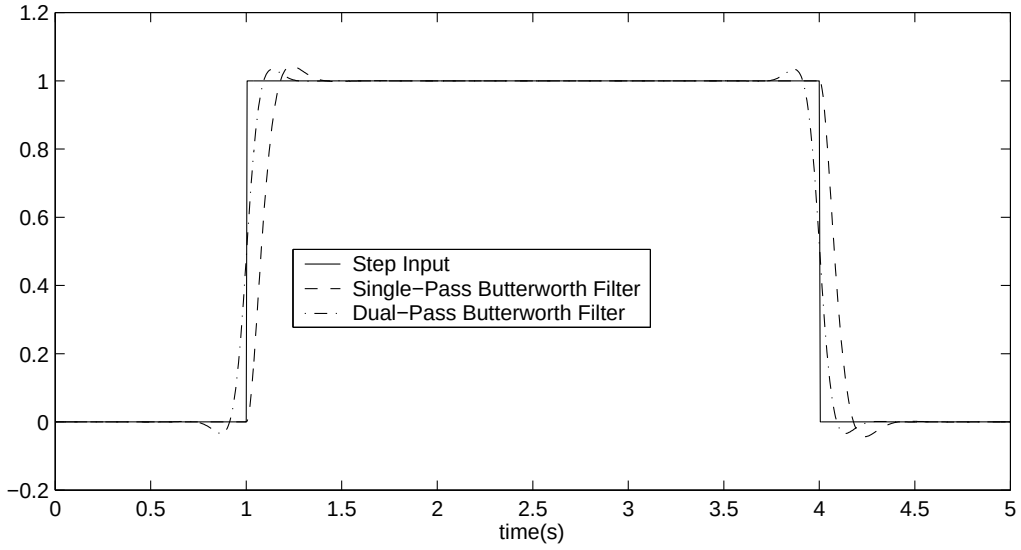

Figure 4.2: Butterworth Filter Step Response

In order to properly drive the inverse dynamics model, the angular velocities and accelerations are also required for the joints. These were obtained by taking the forward numerical first and second time derivative of the angular position. This data was also smoothed using a second-order dual-pass Butterworth filter with a cutoff frequency of 3Hz.

4.1.2.2 Foot Force Data

The force sensors used to collect data at the calcaneus (referred to henceforth as heel) and first metatarsal (referred to henceforth as toe) produced results that were quite

noisy. This was expected, given that the voltage source for the FlexiForce driving circuitry was noisy. The signal to noise ratio could be improved by using the vastly more expensive force platform, redesigning the driving circuitry for the FlexiForce sensor, or by filtering the data. Filtering of the data was performed using a second-order dual-pass Butterworth filter with a cutoff frequency of $3Hz$. The data from one trial is given in Figure 4.3, with the filtered data superimposed. As is discussed later, filtering produces the results that were expected. It is acknowledged that, if the force sensor data is to be used in the control of a powered orthotic, a single-pass filter would need to be used instead. While not shown here, the use of a single-pass filter does not affect the trends seen in the force data.

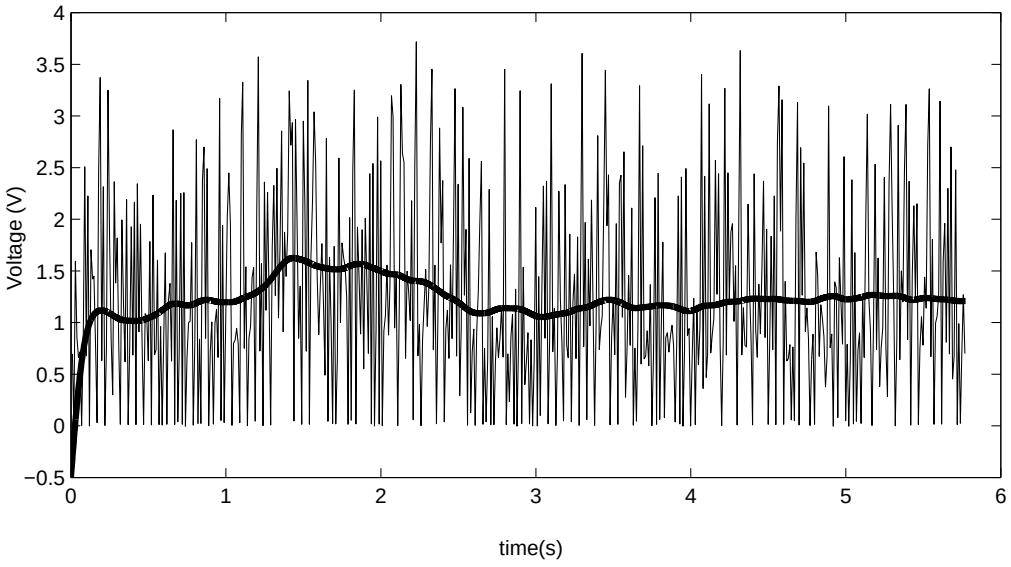

Figure 4.3: Flexiforce Data for the heel in a slow STS trial.

4.1.2.3 Onset of Back Flexion, Liftoff, and Steady Stance

Onset of back flexion was used as an indication that STS had begun. It was determined using a graphical display of hip kinematic data, as done by [61], and verified using the load cell data of the heel. Steady stance, indicating completion of STS, was found by examining a graphical display of the ankle kinematic data.

Liftoff is defined as the time when the subject looses contact with the chair. Ideally, the seat would have been instrumented with force sensors or a force plate.

However, the laboratory lacks the equipment required to instrument the seat. Liftoff was instead estimated using load cell data of the heel. It is indicated by a sharp increase in the force measured by the force sensor.

The key timing points for one experiment are shown in Figure 4.4. There is certainly room for some debate when determining onset of back flexion, liftoff, and steady stance. However, the torques generated using these points are consistent with what would be expected.

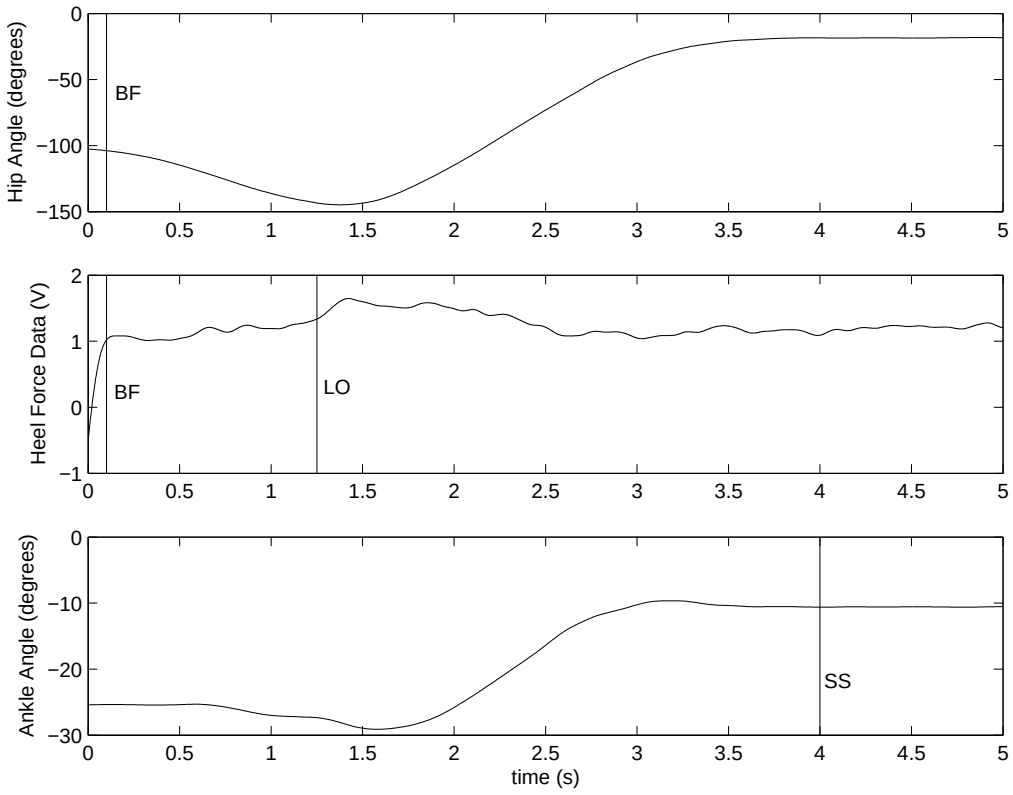

Figure 4.4: STS Timing. Back Flexion is indicated by BF, liftoff by LO, and steady stance by SS

Based on the start and stop criteria for the STS task, the slow speed trial took 3.9s, the natural speed trial took 3.4s, and the fast speed trial took 2.1s.

4.1.2.4 Inclusion of Seat Contact Force

The STS model developed in Section 3.1.3 is valid only for the self-supported phase of STS. It does not inherently include the effects of the chair contact force on the subject. The implementation of the model, however, allows external forces to be exerted on the model. Therefore a vertical force has been added, acting three-quarters up the thigh, approximately where contact is made while rising from a stool.

As was explained previously, it would have been ideal to measure the seat contact force during the STS task by instrumenting the seat with force sensors or a force plate. The use of a force plate, in particular, would allow for the inclusion of very accurate seat contact forces into the simulation. However, the laboratory lacks the equipment required to measure the seat contact forces directly. Therefore it was estimated instead.

Originally, the seat contact force was to be estimated by modelling the chair as a spring-damper system. While it is still believed that the chair force could be modelled as a nonlinear spring-damper system, no compelling reason was found to do so. This is particularly true since the model parameters would still need to be updated between trials. While the chair remained unchanged, the seat contact force, more properly, must include the interaction between the chair and thigh. The thigh has variable stiffness and damping based on the strength of contraction, thus modelling the seat contact force as a spring damper system adds complexity with little benefit.

Failing to find a compelling reason to model the seat contact force as a spring-damper system, the force was instead created to generate a reasonable torque at the knee for the period between back flexion and liftoff. After liftoff, the force of the seat on the thigh is null. The difference between the calculated torque at the knee without a seat force and the desired knee torque was divided by the moment arm of the chair force in order to find a seat contact force that would generate the desired knee torque. The knee torque without a seat contact force and with a seat contact force are shown in Figure 4.5 for a representative trial. Note the large dorsiflexor torque required at the ankle and the large extensor torque required at the knee when no seat force is included. They become much more reasonable once a seat force is added.

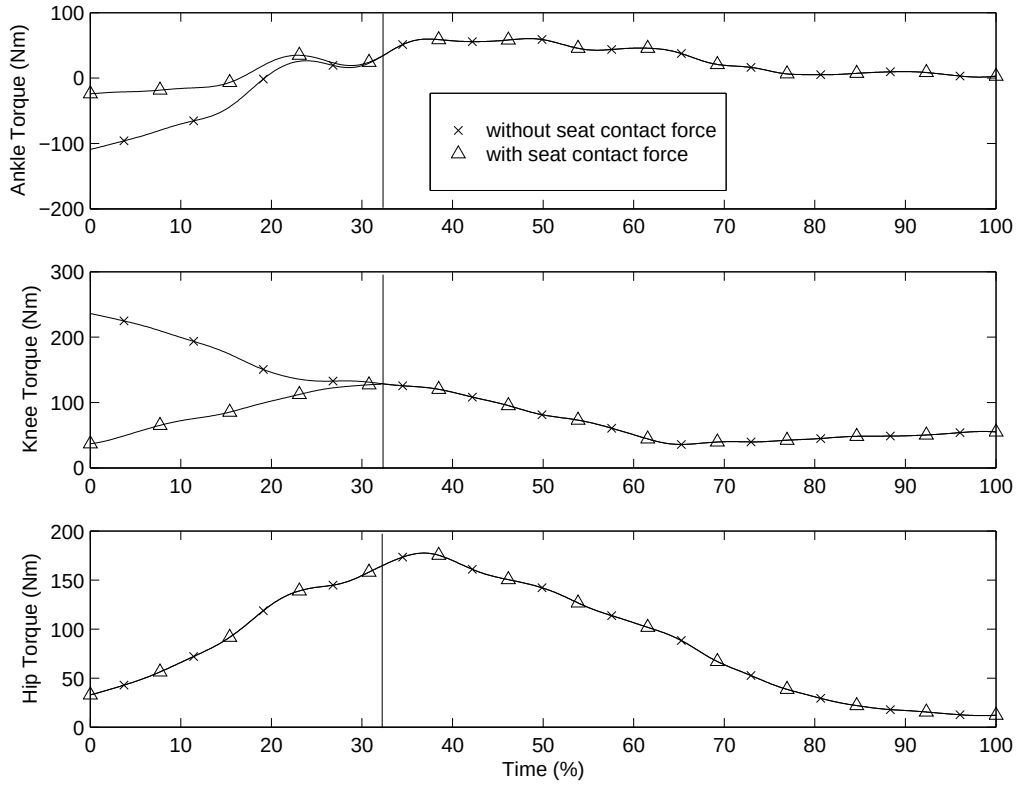

Figure 4.5: Torques at the ankle, knee, and hip as calculated with no seat contact force and with seat contact force. The vertical line indicates when the subject has lost contact with the seat.

It is acknowledged that this is somewhat akin to forcing the results to what was desired and then claiming that the results are in accordance with what was expected. Clearly it would be preferable to have the ability to directly measure the seat contact force. In the absence of that ability, however, a couple of methods exist to verify the estimated seat contact force.

First, the seat force should be between zero and body weight. Since the seat only acts in compression, there should never be a negative force, which would indicate that the seat is holding the subject down. Also, even with dynamic effects, the chair generally does not need to support more than body weight. Note that the chair contact forces for the slow, natural, and fast trials, shown in Figure 4.6, ares always greater than zero and less than the body weight of $755N$. Each of the three trends are also similar, adding confidence to the estimate of the force.

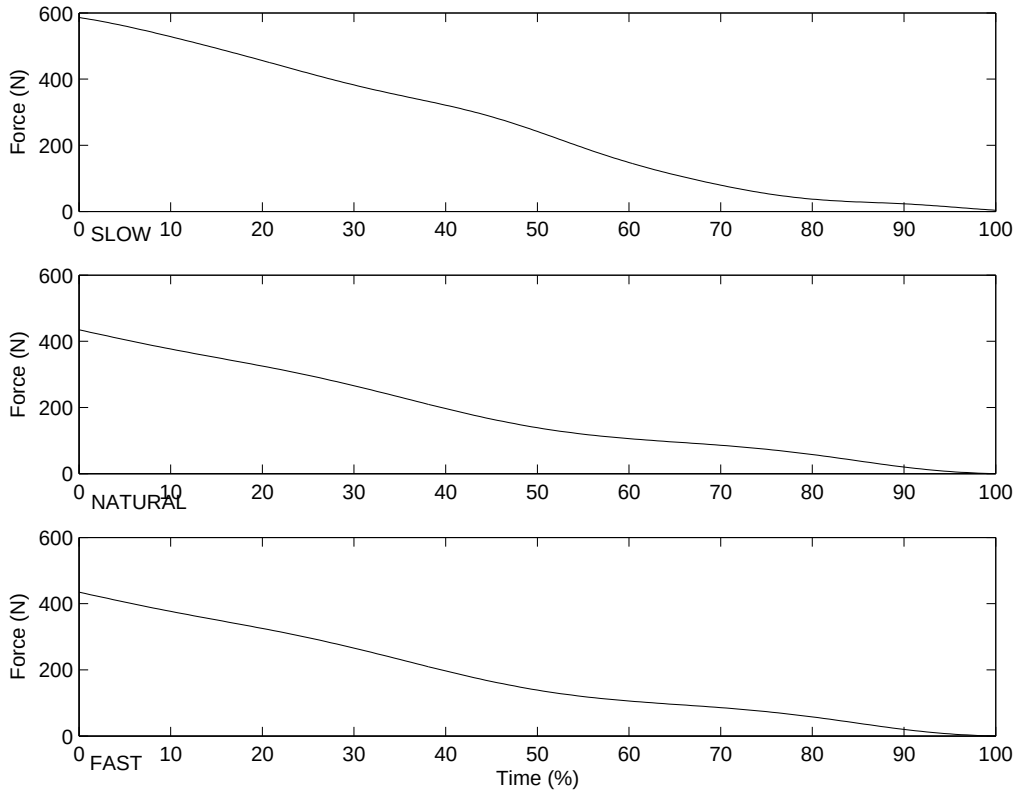

Figure 4.6: Seat contact force for slow, natural, and fast STS. The time axis is scaled from back flexion to lift off, thus the graphs do not represent equal time periods.

Second, and as expected, the knee torque profiles align well with work done by others [61, 77]. More significantly, the ankle torques also align well with the work of [61, 77], and with the foot force data. The torques are presented in Section 4.2.2 and the foot force data in Section 4.2.3. Thus, while some subtleties may be lost by estimating the seat contact force instead of measuring it, the overall effect on the simulations is small.

4.2 Experimental Data

In this section, the processed kinematic data is presented. The required joint torques for the recorded trials, as determined through inverse dynamics analysis, are also presented. Finally, the collected foot force data is presented.

4.2.1 Kinematic Data

The joint trajectory data used to drive the simulations is presented in Figure 4.7. For each of the three trial speeds, the trend is similar. The task can be characterized as a flexion of the hip, bringing the center of mass of the subject over his feet, followed by an extension of the ankle, knee, and hip to bring the subject to the standing position.

The joint velocities are shown in Figure 4.8. Again, for each of the three trials the trends are similar. As expected, the peak velocities increase with increasing speed of ascension. The difference between the slow and natural paced peak torques is small, but this is reasonable once it is recognized that the slow rise took $3.9s$ and the natural rise took $3.4s$. To contrast, the fast rise took only $2.4s$, and has noticeably larger peak velocities.

The joint accelerations are shown in Figure 4.9. For each of the three trials the trends appear similar, except for an anomalous peak in the ankle acceleration of the slow paced STS at about 22%. The origin of this peak can be seen in Figure 4.7(a) and Figure 4.8(a). Most likely it indicates a correction in balance, but it does produce an anomalous torque, shown in Figure 4.10(a)

4.2.2 Dynamic Data

The torque data given in Figure 4.10 for the three trial speeds was calculated by running the STS simulation with the presented kinematic data. The trends are again similar, though a torque anomaly at the ankle during the slow rise is obvious at 22% of STS. In the fast speed trial there is also some clear stabilizing torques at the ankle and knee during the last quarter of STS. This was expected with increased speed of STS as dynamic effects become more prominent.

Each of the peak torques are within range of those presented in [8,61,77]. There are, however, some slight deviations in the results from what would be expected based on the phases of STS given in Section 3.1.2. An examination of the kinematic data reveals that the subject has oriented the HAT just flexed of vertical. Therefore, no initial flexor torque at the hip is required to accelerate the HAT forward. Instead, the subject enters immediately into phase 2 of STS, and decelerates the HAT against gravity.

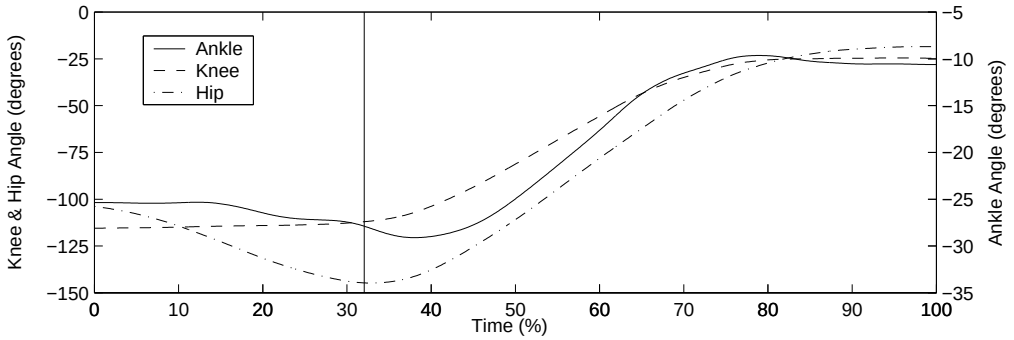

(a) Slow

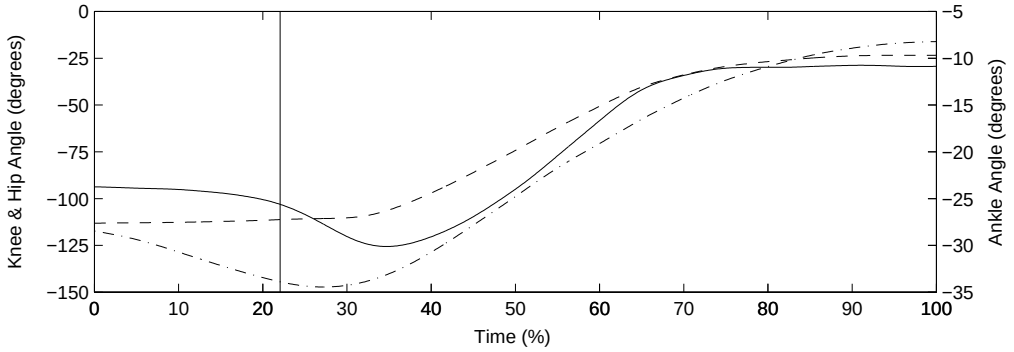

(b) Natural

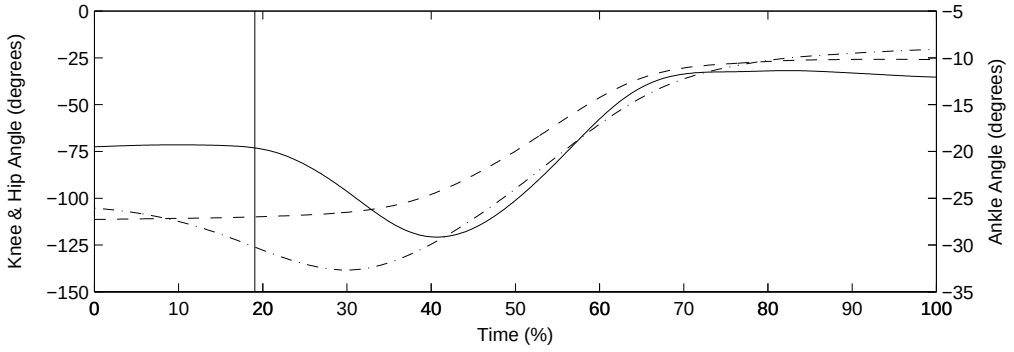

(c) Fast

Figure 4.7: Joint trajectories for (a)Slow, (b)Natural, and (c)Fast STS trials. The vertical line indicates the time of liftoff.

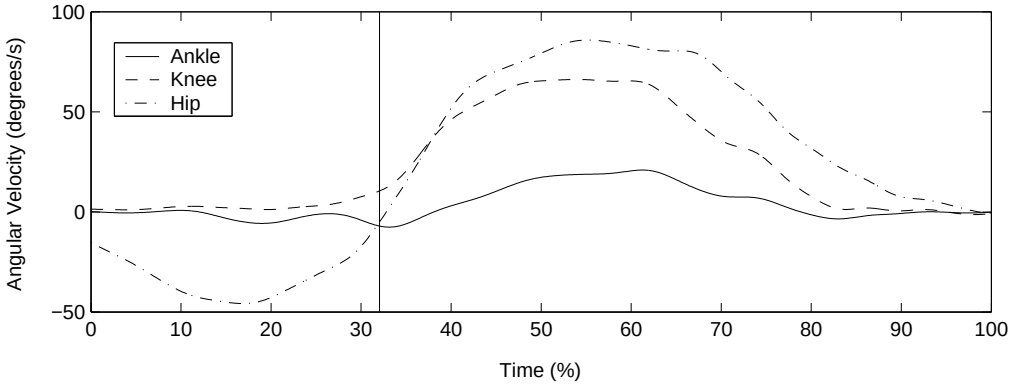

(a) Slow

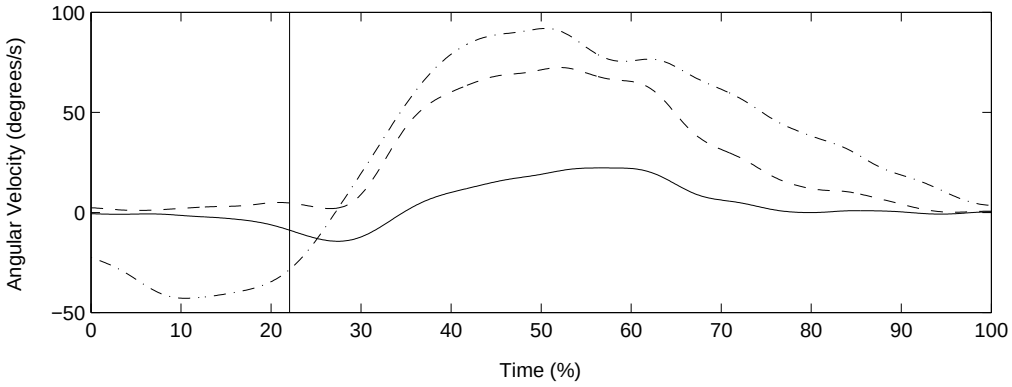

(b) Natural

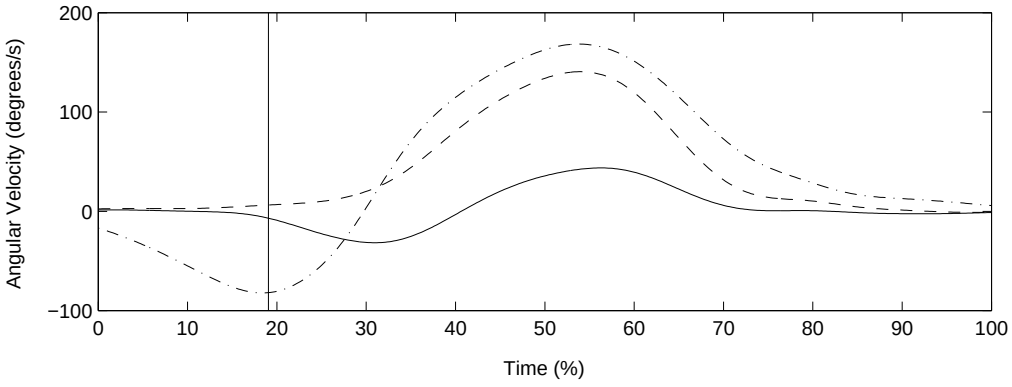

(c) Fast

Figure 4.8: Joint angular velocities for (a)Slow, (b)Natural, and (c)Fast STS trials. The vertical line indicates the time of liftoff.

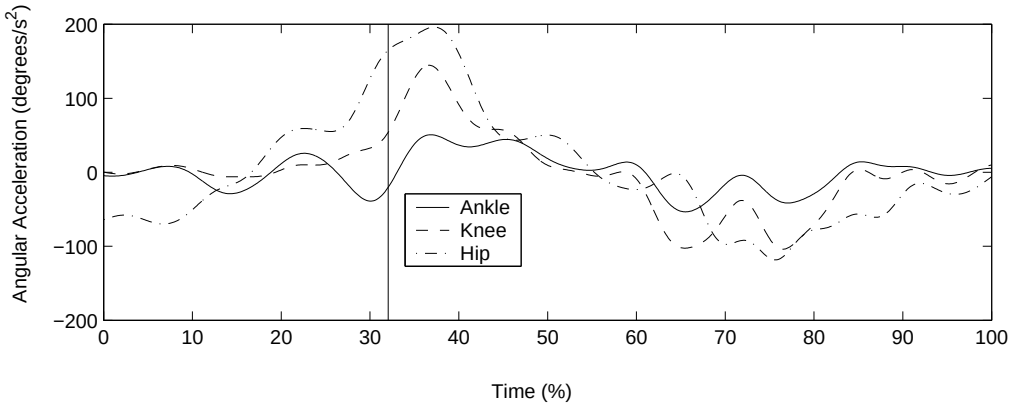

(a) Slow

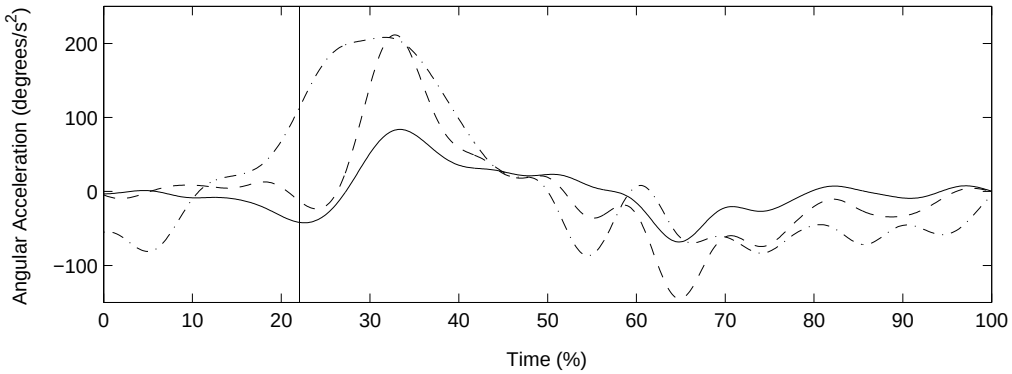

(b) Natural

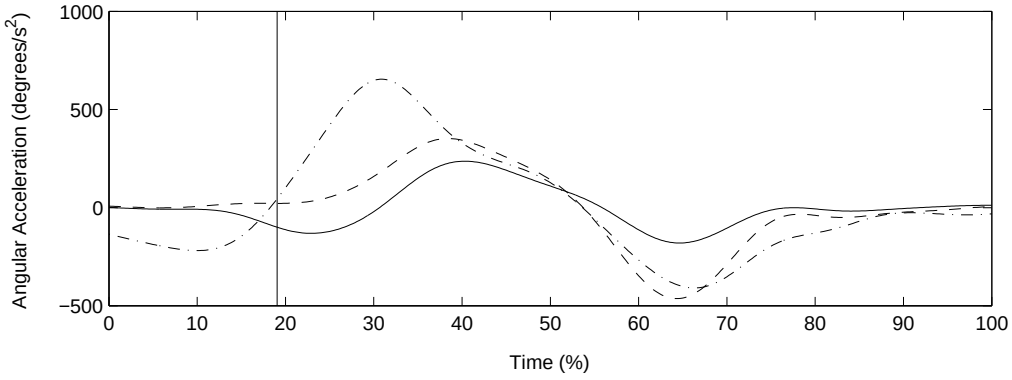

(c) Fast

Figure 4.9: Joint angular accelerations for (a)Slow, (b)Natural, and (c)Fast STS trials. The vertical line indicates the time of liftoff.

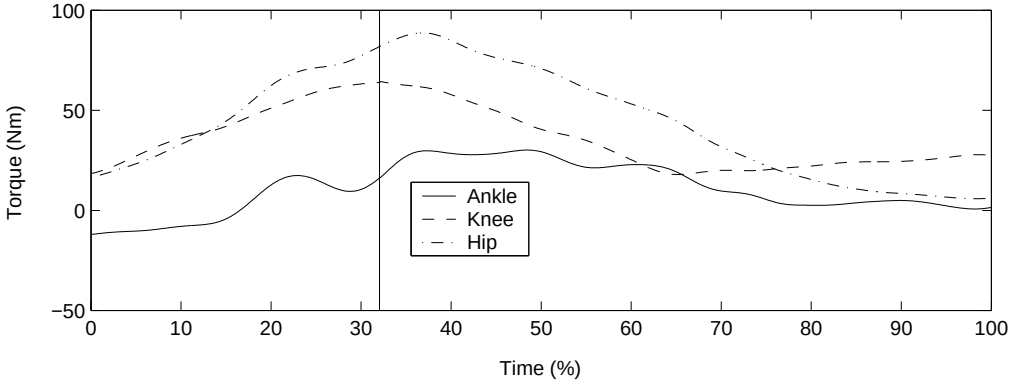

(a) Slow

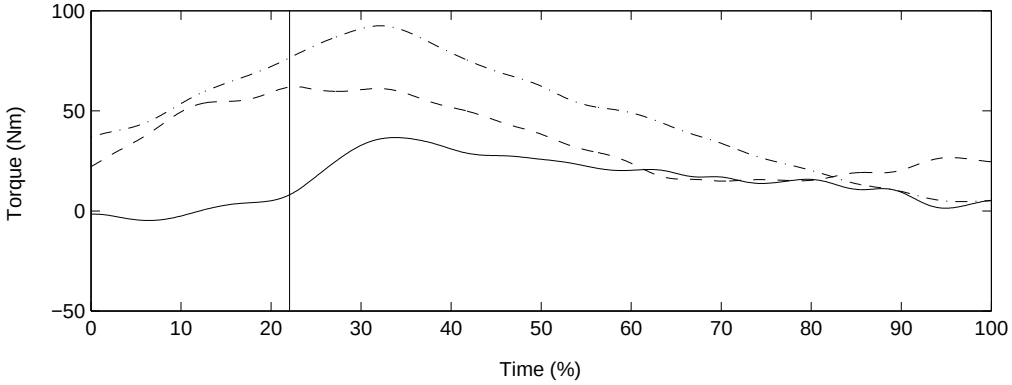

(b) Natural

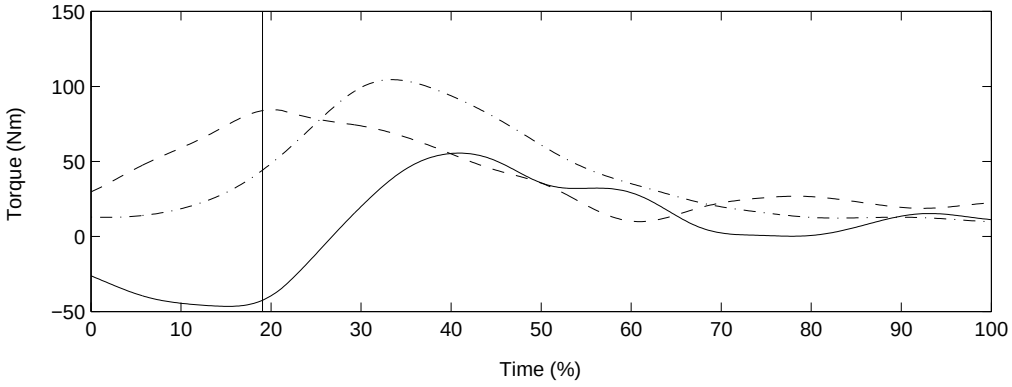

(c) Fast

Figure 4.10: Unassisted joint torques for (a)Slow, (b)Natural, and (c)Fast STS trials. The vertical line indicates the time of liftoff.

Typically STS is concluded with the body center of mass just forward of the ankle. This is normally accomplished with a near zero torque at the knee and hip, with a slight plantar-flexor torque at the ankle. The position of the body can be envisioned as a single straight and rigid link from the ankle to the top of the HAT. The subject in these experiments, while also bringing the body center of mass just forward of the ankle, did so with a slight bend at the knee. The hip and ankle torques were reduced to near zero, but a small extensor torque was seen at the knee to maintain the knee angle. This odd end position may have been a result of a weak ankle, but more likely was due to an evident tightness of the hamstring muscle, which is responsible for the flexing of the knee.

4.2.3 Foot Force Data

The calibrated foot force data is given in Figure 4.11(a) for the heel, and Figure 4.11(b) for the toe. Note that the trend is similar for the slow and fast paced data. The heel and toe data for the natural trial is not similar to the slow or fast trial.

In the slow and fast trial, the subject placed his weight over his heel for the early stages of STS, and only transferred the weight forward as the rotation about the ankle was halted at the end of the task. In the natural trial, the user placed his weight over his toe, and only near the end did he transfer weight back to the heel. An examination of Figure 4.12 reveals one possible explanation for the two strategies. For the slow and fast trial, the center of gravity is behind the ankle for a much longer duration. The subject must therefore exert a large heel force to remain in a balanced stance. It is only near the end of the task, as the subject halts the rotation about the ankle, that a large toe force must be exerted. With the natural trial the center of gravity was over the toe much earlier in the trial. Therefore, a large toe force was exerted to remain in a balanced stance, and only near the end of the trial did the subject moved his weight back on his heel.

The first strategy indicates that the user was balanced throughout the task. The second strategy represents an escalation in the effort required to remain balanced. Although the foot remained in contact with the floor for the duration of each trial, the second strategy could have been further escalated to include a heel-off event. By lifting the heel off the floor, an extra degree of rotation is introduced, providing

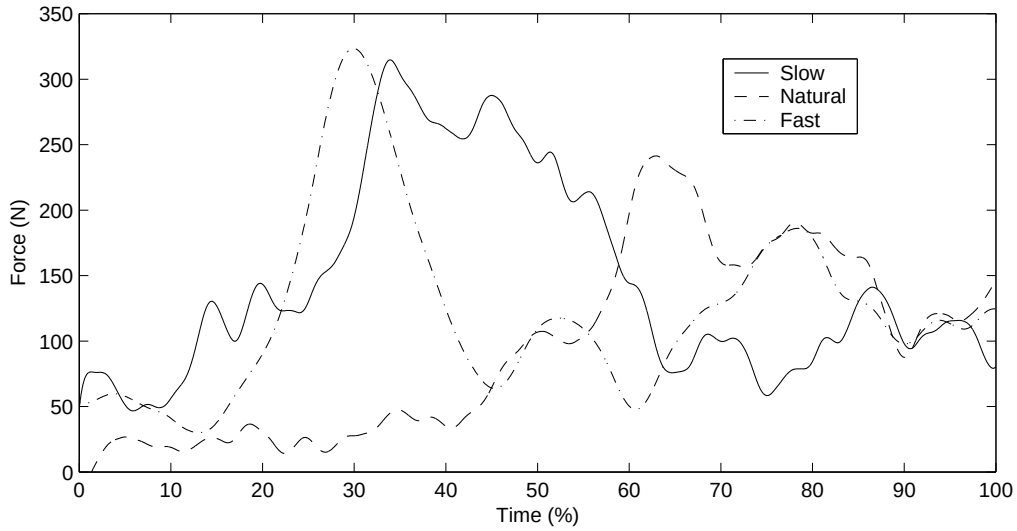

(a) Heel Force

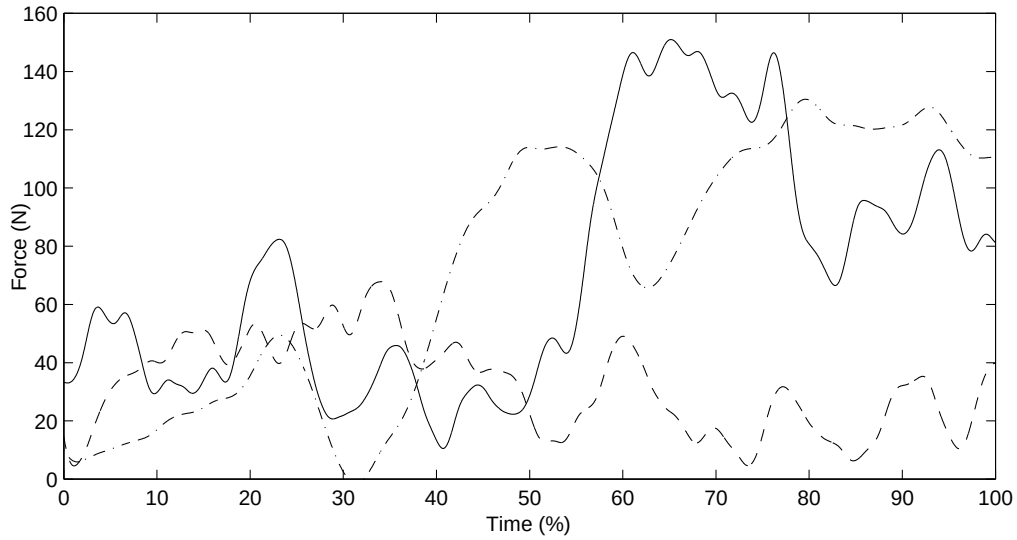

(b) Toe Force

Figure 4.11: Calibrated foot force data for slow, natural, and fast paced STS trials. Note that the two graphs use different vertical scales.

another opportunity to preserve the STS attempt.

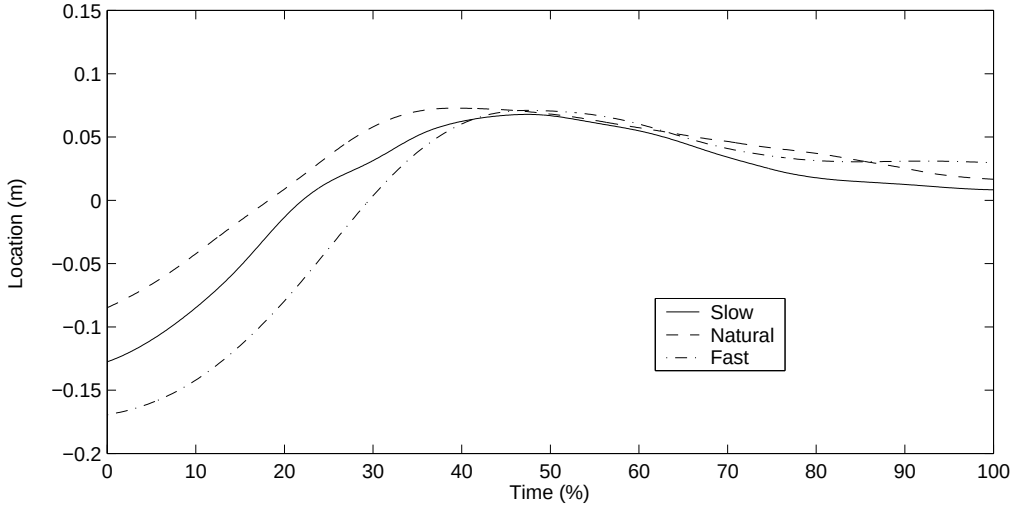

Figure 4.12: Horizontal location of the center of gravity.

4.2.3.1 Comparison of Inverse Dynamics with Foot Sensor Data

The torques computed at the ankle through the inverse dynamics simulation, along with the torques estimated using the foot sensor data and Equation 3.8, are presented in Figure 4.13. The ankle torque from the foot sensor data for the slow trial appears to suffer from a phase lag. The ankle torque profiles for the natural and fast paced trials are aligned a little better with the torques estimated using inverse dynamics, though the magnitudes are only half of what was expected. The two methods of determining the ankle torque did not produce particularly similar results.

Recall that the model used to estimate the torque about the ankle from the foot force data is quite simplistic. It supposes only two points of contact, at the heel and at the toe, at which points the floor contact forces are measured. These contact forces are multiplied by their moment arm to produce a net torque about the ankle. In reality, there is a continuum of contact with the floor over the width and length of the foot. The musculoskeletal system of the foot also has variable stiffness, which affects how forces are converted into a torque about the ankle. Even in light of these simplifications, there seems to be little agreement between the

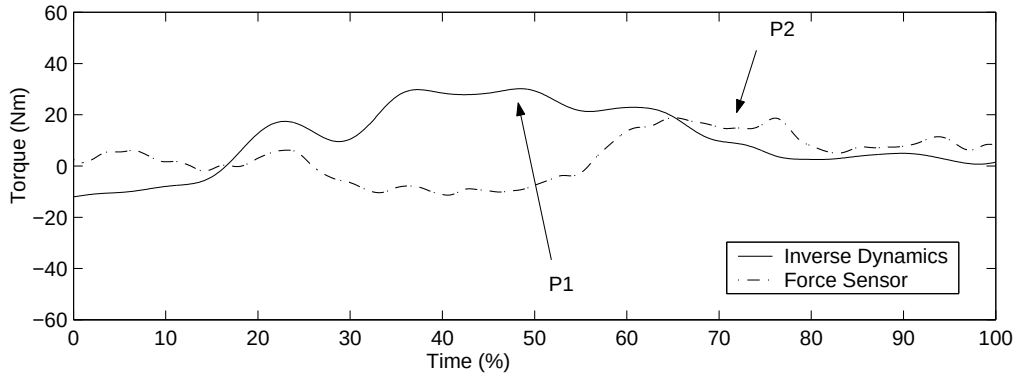

(a) Slow

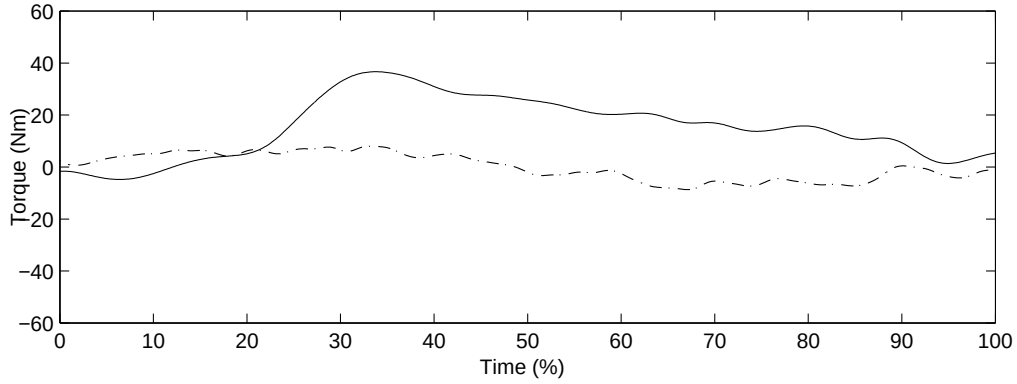

(b) Natural

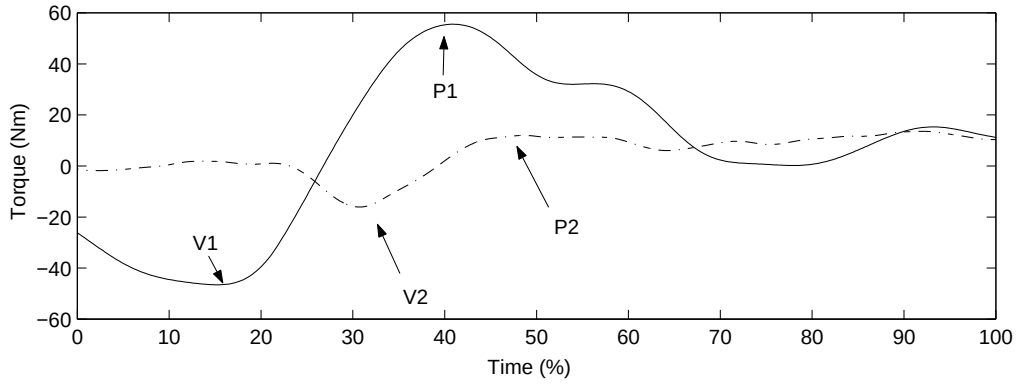

(c) Fast

Figure 4.13: Ankle torques for (a)Slow, (b)Natural, and (c)Fast STS trials.

inverse dynamics torque and the foot sensor data torque. Though not done here, it may be beneficial to optimize the STS model parameters so that they are in closer agreement with the foot sensor data torque. It may well be that a small change in the model parameters could produce much better agreement.

4.3 Analysis

In this section, an analysis of the experimental data is performed. The suitability of the inverse dynamics model is examined. Further consideration is then given to the use of a powered knee orthotic in STS.

4.3.1 Support for the Inverse Dynamics Model

The suitability of the inverse dynamics model for STS was verified by running three simulations with representative data for slow, natural, and fast paced rising. The torque profiles were found to be generally in accordance with those found by Hutchinson et al. [61] and Pai and Rogers [77]. The peak torques for the ankle, knee, and hip also were in line with published data [8, 61, 77].

The simulation results were also compared with the results from the foot sensor data. Optimization of the STS model parameters may strengthen the agreement between the inverse dynamics model ankle torque and the foot model ankle torque, but is not done here. Agreement with other published data is considered to provide reasonable support for the model. The inverse dynamics model will therefore be used in simulations along with the powered-knee orthotic models to determine the contribution that a powered-knee orthotic can make to the STS task.

4.3.1.1 Evidence for the Use of a Powered Knee Orthotic in the STS Task

It was noted by Hutchinson et al. in [61] that the peak dorsiflexor torque and peak knee and hip extensor torques occurred within $0.06s$ of each other, shortly after liftoff. The time just after liftoff may indicate a critical period of STS where sit-back failure occurs most frequently. While the very tight relationship with the ankle dorsiflexor torque was not observed in the experimental data, there is a close

timing between between peak knee and hip extensor torques, which still indicates a critical period of sit-back failure. The difficulty is that it may be possible to generate individually the required knee torque or the required hip torque, but together the maximum torques may not be able to be generated.

Hutchinson et al. alluded to, but did not specifically mention the cause of the problem. It may be common in robotics to consider each joint as being singly-actuated. The human locomotor system, however, is composed of both single joint actuators and biarticulate actuators. The rectus femoris of the quadriceps muscle group is a biarticulate muscle which both extends the knee and flexes the hip. For maximum effort in flexing the knee, the rectus femoris must be activated, but this also generates a hip flexor torque. The long head of the biceps femoris, the semitendinosus, and the semimembranosus of the hamstring muscle group are biarticulate muscles which both flex the knee and extend the hip. They must be recruited during maximum effort flexion of the hip. Therefore, a dilemma is introduced during maximum effort where either the knee can be flexed and the hip extended, or the knee extended and hip flexed, but the knee and hip cannot both be extended.

In healthy subjects, the single joint muscles may be strong enough to generate the peak knee and hip extensor torques, thereby avoiding the recruitment of the biarticulate muscles. Weaker subjects, however, may need to recruit the biarticulate muscles to generate the peak torques, thus forcing the biarticulate dilemma and increasing the chances of sit-back failure. A reduction in the peak knee extensor or hip extensor torque would reduce the chance of entering into the biarticulate dilemma. This is supported by the finding that compared to able-bodied groups, the old unabled group "opted for a marked reduction in the required joint torques at the knees ... but not at the ankles and hips" [8]. This indicates that the incidence of sit-back failure may be reduced by generating an external knee extensor torque with a powered lower-limb orthotic during the period shortly after liftoff.

4.3.1.2 Use of Foot Sensor Data for Triggering the Powered Knee Orthotic

An examination of the ankle torques does not reveal an identifiable event upon which the triggering of the powered-knee orthotic could be based. On the other hand, the heel force data could be used to identify the start of STS. For the slow

and fast trials, the knee orthotic could be triggered based on a threshold crossing at about $75N$. It did not work for the natural trial, but recall that the natural trial represented a less stable rise, where the weight was forward over the toes. Using the heel force data to trigger the knee brace would therefore require user training, but would also help to ensure that the task is only executed from a balanced position.

Considering that the intent is for the orthotic device to be worn in daily living, heel force alone is not enough to trigger the brace. Ankle and knee position information should also be used to ensure that the user is in fact beginning in a seated position. User trials will need to be performed in order to determine that the combination of heel force and position information uniquely describes the user intent to rise.

Chapter 5

Control of the Powered Lower-Limb Orthotic

In this chapter the control strategy for the modelled orthotic is examined. The challenge of control can be broken into determining user intent and actuating that desired command. Determining user intent essentially reduces to determining the desired assistive torque to be provided by the orthotic. Actuating the desired command is the more familiar challenge of compensating for actuator dynamics so that the actual orthotic torque is close to desired orthotic torque.

5.1 User-Orthotic Interaction

The human augmentation control system may be seen in Figure 5.1. While the figure contains only a very simplified model of the human control strategy, it serves to illustrate the interaction between the human and the powered lower limb orthotic.

First, consider briefly the human system. The human path planner generates a control signal to actuate the muscles, based on conscious, subconscious, and reflexive components. The muscle controller causes the muscles to generate a force, which acts upon the human skeletal system to produce an output position. Through the feedback mechanisms of sight, balance, and proprioception, the human achieves position control.

Second, consider the orthotic system. A Human-in-Loop controller uses information from the human kinematics to generate a desired orthotic torque. The powered

orthotic, shown as the actuator, takes the desired torque as an input, and is controlled through a feedback torque controller. The torque produced by the orthotic acts on the human, so there must be appropriate user-orthotic interaction.

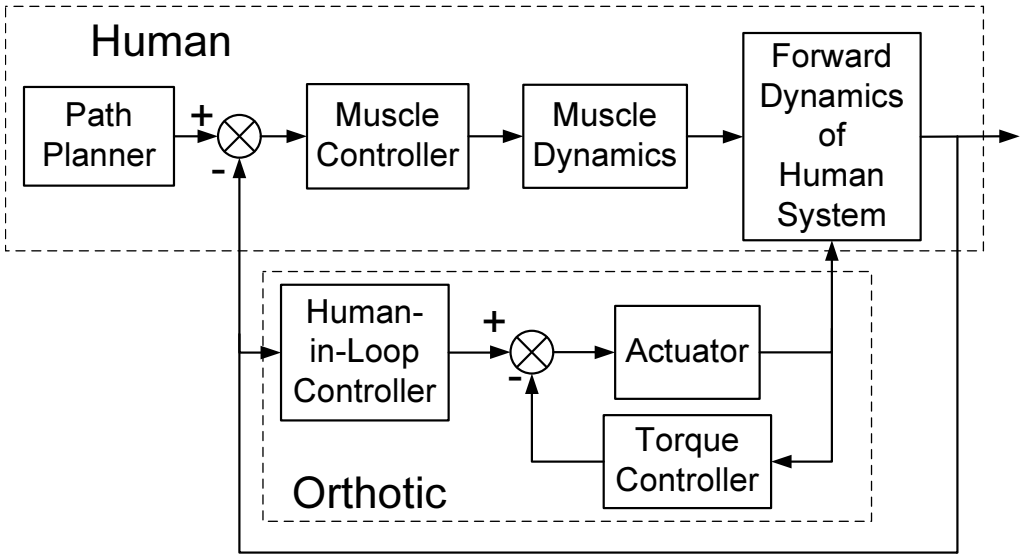

Figure 5.1: Human augmentation control system

The position control strategy of the human must interact with the torque control strategy of the orthotic actuator. Wight proposed that a force control strategy could in fact be used to augment a position controlled system [9]. In this case, the Human-in-Loop controller, which is described below, acts as a supervisor to decide how much assistance the orthotic actuator should provide. The Human-in-Loop controller is independent of the actuator implementation. The torque controller, on the other hand, is implementation specific.

5.1.1 Human-in-Loop Control

The use of Human-in-Loop control allows the user to close the feedback loop to the powered lower-limb orthotic and determine the amount of assistance the orthotic will provide. While user training will remain an important part of orthotic usage, Human-in-Loop control seeks to limit the amount the user must adapt to the device.

The control structure can be broken into two components. The supervisory controller exists to delegate the execution of a given task to the appropriate agent,

where the agent is a controller designed to control a single task. At present, the only task which is augmented is STS. Therefore, the supervisor has the duty of handing off and reclaiming control from only the STS agent. As the augmentation of more tasks is implemented, the supervisor will be responsible for delegating control to, for example, an STS agent, a walking agent, or a stair-climbing agent.

Presently the only task that is augmented is STS. Therefore, the supervisor logic is embedded with the STS agent rather than as a higher-level in the hierarchy. As more tasks are augmented, then the logic will have to be ported and extended into a distinct, higher-level of the hierarchy, but for now it is acceptable to implement the supervisory logic and the STS agent as a single layer.

5.1.1.1 Supervisory Controller

As the number of tasks which the orthotic can augment increases, so will the complexity of the supervisor. At the moment, the supervisor need only be designed to provide and revoke the authority of the STS agent. This is done with *begin* and *end* trigger events. The begin trigger event occurs when the heel force increases beyond $75N$, as discussed in Section 4.3.1.2, and the knee is flexed between 80° and 115°. The end trigger event occurs when the knee position is nearly extended and when the knee angular velocity is $0°/s$. Recall that for the subject for which the data was collected, 30° represents extended, as was previously explained.

Logic to capture a failed STS attempt has been deliberately left out. The danger of incorrectly judging a sit-back failure is that the orthotic will deactivate in mid lift, requiring a sudden and drastic increase in the torque by the user. The issue of sit-back failure is an issue that would be better investigated with the implementation of the orthotic, and its handling should be based on a consultation between the user and the prosthetist.

5.1.1.2 STS Agent

The control strategy employed by the STS agent is straight forward. The requested torque is a function of knee position, and is not dependent on speed of ascension. A plot of required torque versus knee position at various chair rise speeds is shown in Figure 5.2. Also included is the torque assistance that the STS agent requests from the powered orthotic, given as a function of knee position.

Note that there is a sharp increase in the torque with very little change in knee position, beginning from the seated position. It is a transient effect associated with chair contact. Since chair contact is a reactionary force, it has an effect only to the degree to which the user places his or her weight on the chair. Therefore the transitory period is not reproduced by the STS agent.

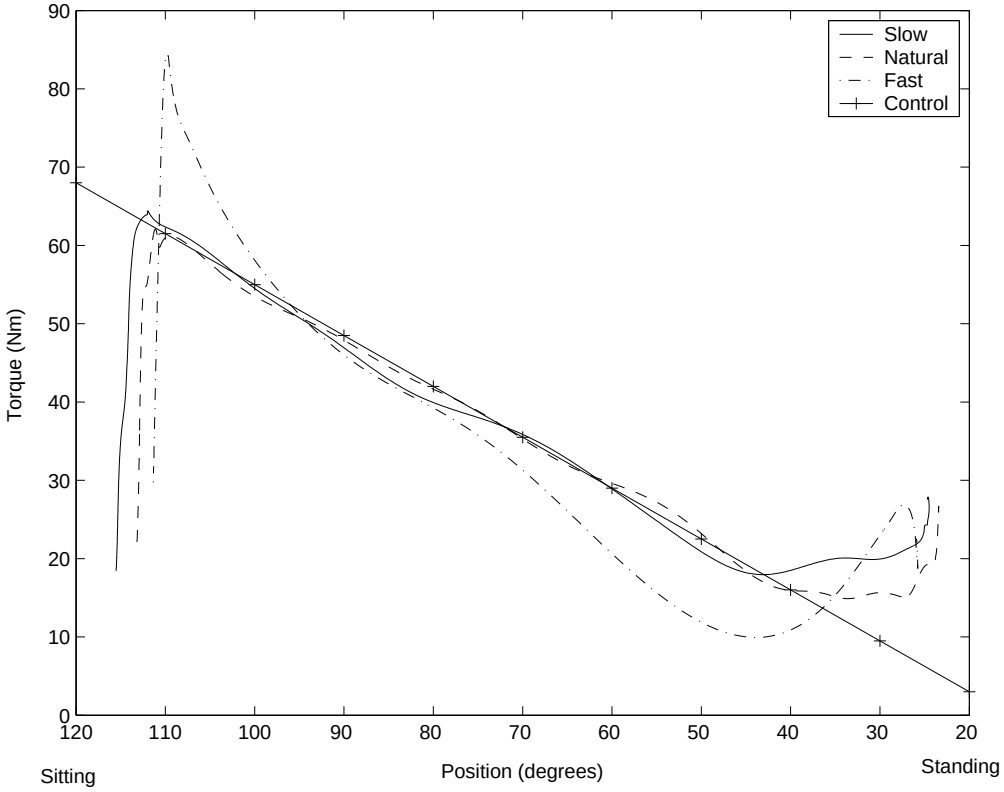

Figure 5.2: Required torque versus position of the knee

The STS agent sets the orthotic reference signal as a first order function of knee position. The relationship is based on a graphical best-fit to the natural paced STS, with strong weighting against the transitory effects. The relationship is given specifically as

$$T_{ref} = 0.65 \times \theta_{knee} - 10. \tag{5.1}$$

5.2 Pneumatic Muscle Actuated Orthotic Control

In the previous section, the knee actuator was generalized as a plant which took a desired torque as input and produced an actual torque. The control of the PMA actuated orthotic, however, can be reduced to the problem of controlling the pressure of the PMA.

In order to reduce the problem to controlling the pressure of the PMA, the torque to force converter and the force to pressure converter must be brought outside of the control loop. This is shown in Figure 5.3. The torque to force converter (T to F) quite simply divides the desired torque of the Human-in-Loop controller by the moment arm of the knee brace, and by the number of air muscles generating a force on the brace. Recall from Section 3.2 that the moment arm is a kinematic transformation, dependent only on the knee brace configuration and the angle of the knee.

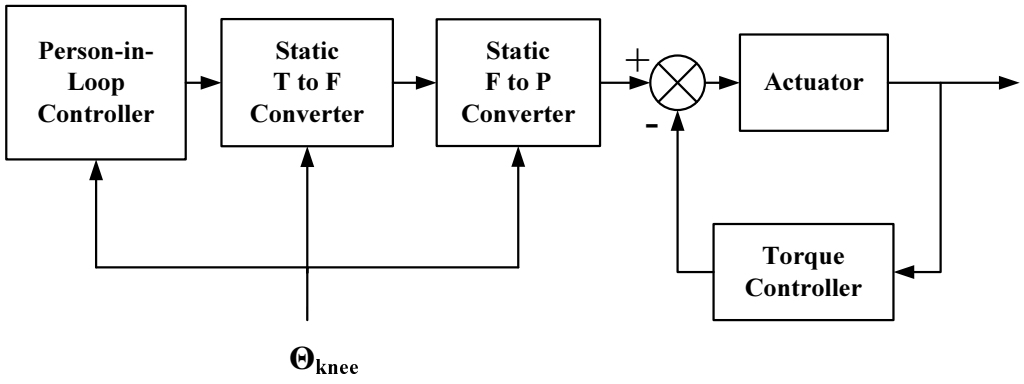

Figure 5.3: Reduction complexity of PMA actuated orthotic control

The force to pressure (F to P) converter is somewhat more complex. From Figure 3.11, the force exerted by the air muscle is dependent on both the contraction of the air muscle and the pressure. As well, the pressure isobars are exponential curves. Thus, for the general case, a search algorithm must be employed to find the pressure that generates a particular force at a given contraction.

For the specific case where the the Human-in-Loop torque is a function only of knee position, it is possible to generate a position-pressure curve offline. This is ad-

vantageous because it is more computationally efficient than performing the torque to force and force to pressure conversions online. Results, presented in Chapter 6, indicate that it is reasonable to use a speed invariant controller.

It is now possible to generate a position-pressure curve offline as follows. Under the speed invariant simplification, there exists only one possible desired torque at a given knee position. At a given knee position, the knee brace moment arm is known, meaning a one-to-one mapping exists between desired orthotic torque and required PMA force. For a given knee position, the contraction of the PMA is known, and therefore there also exists a one-to-one mapping between required PMA force and require pressure. Therefore, there is a one-to-one mapping between desired orthotic torque and required PMA pressure in the case where desired torque is a function only of knee position.

Having presented a case for controlling the orthotic based on the dynamics of PMA pressure, the PMA controller design considerations are first presented, followed by a presentation of the implemented system.

5.2.1 Background of PMA Control

Control of pneumatic muscle actuators is an ongoing area of research due to some difficult nonlinearities [39,47,55]. The literature has presented increasingly complex control strategies to deal with the actuator nonlinearties. Caldwell's team began to address the position control problem with a PID and feedforward controller [47], but they found that the system was particularly sensitive to error in the feedforward term. The team has therefore begun exploring adaptive controller design, using a pole placement scheme [54]. While convergence is slow, they have been able to accurately control the actuators. Tondu's team also used a PID and feedforward controller [75] to control the position of the PMA. They also found the feedforward term to be sensitive to error, and have more recently investigated a variable structure controller [55]. Both Caldwell and Tondu, however, have been addressing the problem of position control in antagonistic PMA actuated robot joints.

Colbrunn et al. suggested the use of a state-space controller for controlling the force of a PMA actuator [76]. However, they did not present the architecture of the controller other than to suggest the use of state-space. Similarly, Repperger and Phillips indicated success with the use of a feedback force controller that used gain

scheduling [39], but again no architecture was suggested. It is from these hints that the PMA controller architecture is developed.

5.2.2 PMA Controller Architecture

This section briefly introduces the state-space representation. The actual architecture of the PMA controller is then presented.

5.2.2.1 Definition of State-Space Elements

In state-space, the plant is modelled as a set of first-order differential equations called the state equations, and an output equation which expresses the output as a linear combination of the state variables. This is shown in Equation 5.2.

$$\begin{aligned} \dot{\mathbf{x}} &= \mathbf{A}\mathbf{x} + \mathbf{B}u \\ y &= \mathbf{C}\mathbf{x} \end{aligned} \tag{5.2}$$

where,
u: Input
y: Output
$\mathbf{x}$: State vector
$\mathbf{A}$: System matrix
$\mathbf{B}$: Input matrix
$\mathbf{C}$: Output matrix.

In systems where not all of the states can be observed, an observer, also known as a state estimator must be employed. Similar to the plant, but with an error term $y - \hat{y}$, the observer is modelled as

$$\begin{aligned} \dot{\hat{\mathbf{x}}} &= \mathbf{A}\hat{\mathbf{x}} + \mathbf{B}u + \mathbf{L}\left(y - \hat{y}\right) \\ \hat{y} &= \mathbf{C}\hat{\mathbf{x}} \end{aligned} \tag{5.3}$$

where,
u: Input
$\hat{y}$: Estimated output
$\hat{\mathbf{x}}$: Estimated state vector
$\mathbf{A}$: Observer system matrix

B: Observer input matrix
C: Observer output matrix
L: Observer feedback matrix.

Note that the **A**, **B**, and **C** matrices for the plant and observer are generally not the same.

From the controller perspective, the important variables are
FF: Feedforward gain
K: Controller feedback matrix.

The controller variables are included here for completeness, but are detailed in the next section.

For more information on state-space representation, controller design, or observer design please see the excellent textbook by Nise [81].

5.2.2.2 PMA Controller Architecture

Recall the dynamic model of the PMA, presented first in Figure 3.15, and now presented again in Figure 5.4. The model behaves as a low-pass filter with a time delay, so the open loop response is stable. It was even suggested in [9] that closed loop control would possibly not be necessary. However, for improved response and disturbance rejection, closed loop control is pursued here. It was found that PID control had limited ability to damp oscillations, most likely due to the time delay. State-space control, with the ability to incorporate a Pade approximation of time delay, is used instead.

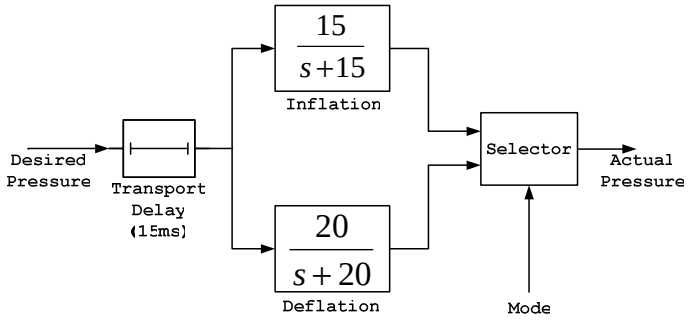

Figure 5.4: Model of fluidic flow

The architecture implemented, presented in Figure 5.5, is a state-space represen-

tation with feedforward gain FF, state feedback managed by the controller $\mathbf{K}$, and a closed loop observer. The details are further developed throughout this chapter. The observer details are shown in Figure 5.6. From the PMA model of Figure 5.4 it is clear that the PMA operates in a charge and discharge modality. Gain scheduling is used to handle these two modes.

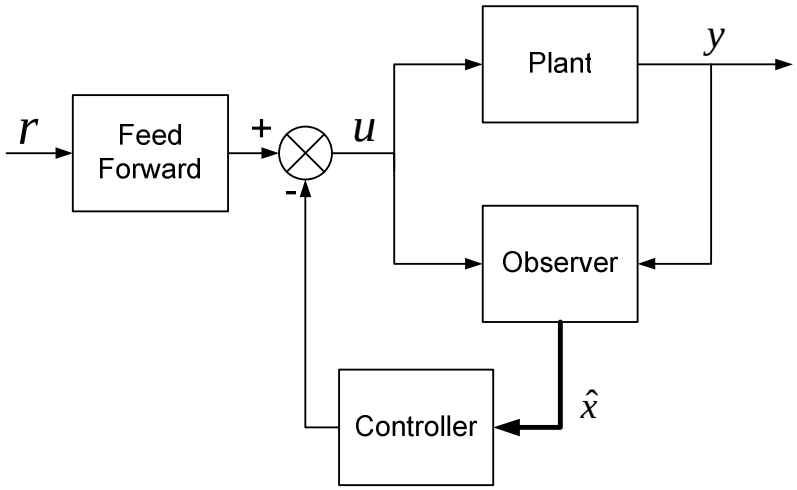

Figure 5.5: Control system architecture

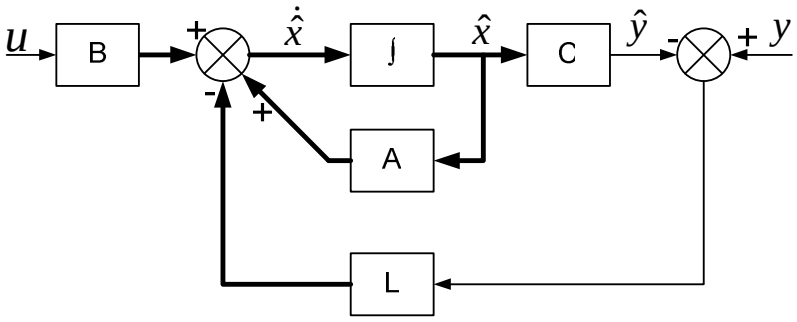

Figure 5.6: Observer architecture

The details of the PMA control architecture are expanded upon below. The following sections provide the level of detail required to implement the PMA model and controller.

5.2.3 Pade Approximation of Time Delay

Several well documented techniques exist to aid in the design of state feedback controllers, some of which are documented in [81]. These techniques, however, require that the system be represented as a rational transfer function, or the state-space equivalent. Systems with a pure time delay cannot be represented as rational transfer functions. However, Pade approximations allow rational systems that a have pure time delay to be replaced with a rational approximation. Pade approximations therefore allow linear design techniques to be used even on systems with a time delay. The approximation is commonly used in controller design and stability analysis [81, 82, 83].

The Pade approximation of the continuous time delay e^{Ts} is given by

$$e^{Ts} \approx \left[\frac{1 - Ts/2n}{1 + Ts/2n}\right]^n \tag{5.4}$$

where T is the time delay and n is the order of the approximation.

The step response of the second order Pade approximation used to model the $15ms$ transport delay of the PMA model is shown in Figure 5.7. For comparison, a first order Pade approximation is also shown. The second order response has a conjugate pair of zeros on the right hand side of the s-plane that cause a small drop below zero, but other than that the approximation is good.

The Pade approximation, along with the low-pass filter portion of the PMA model, is a rational estimate of the actual model of Figure 5.4. It is used as the state estimator in the control architecture, and it is upon this model which the feedback controller is designed.

The system with a pure transport delay still acts as the plant and, as with traditional control techniques, it is through the plant that the input signal is transformed into an output. However, the controller is designed based on a system with a Pade approximation of the time delay. The use of a second order Pade approximation introduces two new state variables to represent the time delay. Since these two additional states are artificial, they cannot be observed in the pure time delay PMA model. Therefore, unlike traditional feedback control techniques, the output of the plant alone is not sufficient input for the controller. The controller requires the plant output, or rather the estimated plant output, along with the estimates of the

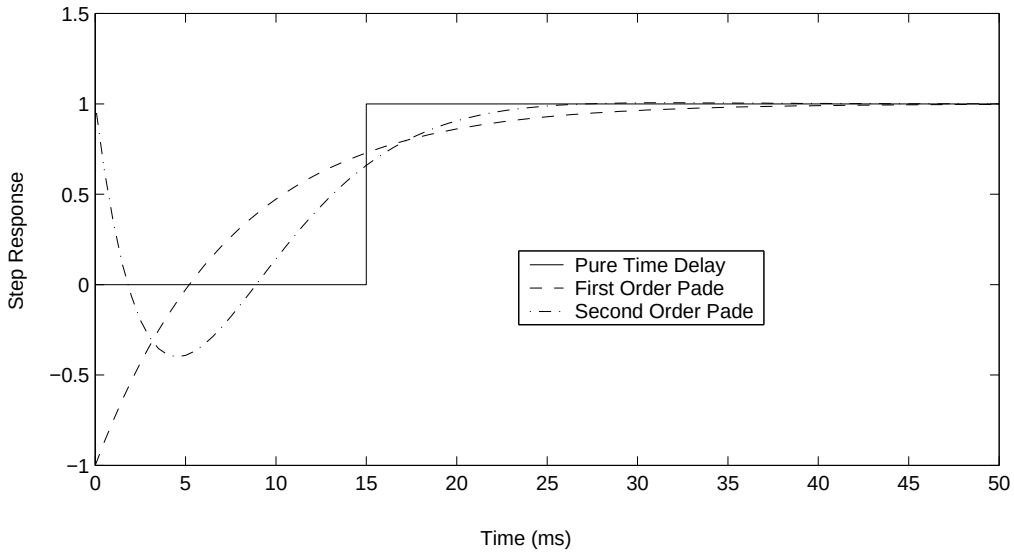

Figure 5.7: Second order Pade approximation of a $15ms$ time delay

two state variables representing the time delay. It is for this reason that an observer must be included in the control architecture.

5.2.4 Design of the State Feedback Controller

As opposed to traditional feedback techniques, where the output is fed back and compared with the reference, with state-space feedback the states are fed back into the controller matrix K. This is shown in Figure 5.5. The advantage over traditional methods is that, in a controllable linear system, arbitrary closed loop poles may be achieved with state-feedback control.

5.2.4.1 Controllability

The system given by Equation 5.2 is considered controllable if the controllability matrix, given by

$$\mathbf{C_M} = \begin{bmatrix} \mathbf{B} & \mathbf{AB} & \mathbf{A^2B} & \dots & \mathbf{A^{n-1}B} \end{bmatrix} \tag{5.5}$$

has a rank equal to n, the number of states in the system [81]. Based on this criteria, the second order Pade estimator is a controllable system.

The difficulty then becomes choosing the closed loop poles. The poles should be selected so that the system has a fast response, but must be constrained by control effort. In the case of the PMA, response speed is limited by the pressure of the source. If the system can handle a greater pressure, then with higher input pressure comes increased response speed.

5.2.4.2 Optimal Control and Observability

It is possible to design the state feedback gains to obtain an optimal linear control system with quadratic performance. The optimization is known as linear quadratic (LQ) optimal control, and automatically places the poles based on the weighting matrix $\mathbf{Q}$ and R. For a single input, single output (SISO) system, the performance criterion is the minimization of the cost function

$$J = \int_0^\infty (\mathbf{x}^T \mathbf{Q} \mathbf{x} + Ru^2)\, dt \tag{5.6}$$

where $\mathbf{Q}$ weights the importance of states and R weights the importance of the control input [68].

The cost of LQ control is that each state must not only be controllable, it must also be observable. The system given by Equation 5.2 is observable if the observability matrix, given by

$$\mathbf{O_M} = \begin{bmatrix} \mathbf{C} \\ \mathbf{CA} \\ \vdots \\ \mathbf{CA}^{n-1} \end{bmatrix} \tag{5.7}$$

has a rank equal to n, the number of states in the system [81]. Based on this criteria, the second order Pade estimator is an observable system, and therefore LQ optimization is an applicable design technique.

5.2.4.3 LQR Design

LQR design uses LQ optimization to obtain an LQ optimal regulator. The LQ state-feedback regulator $\mathbf{K}$ was determined with a state weighting of $\mathbf{Q} = \mathbf{C}^T * \mathbf{C}$ and an input weighting of $R = 1$. This produces a roughly similar weighting between the

states and the input. Based on these weightings, the input signal u was about 1.5 times the reference signal r. The practical effect is that, based on an 8 bar supply pressure, the maximum step change for which optimal control can be achieved is about 5 bar. For a step change above 5 bar, the input signal will experience a saturation at the 8 bar supply.

The Nonlinear Control Design Blockset was used to obtain a faster rise-time from the linear quadratic state-feedback regulator, essentially increasing the relative weighting of $\mathbf{Q}$ compared to R. However, it was found that in order to improve the response of the system, the control effort was increased significantly. Increased control effort results in a reduction in the maximum step change of the reference before saturation occurs. With the given orthotic configuration, the maximum required pressure step change is about 4 bar, occurring at STS initiation. Therefore, initial values of $\mathbf{Q}$ and R do produce an optimal regulator that does not saturate.

5.2.5 Design of the Observer

An observer is used to estimate the inaccessible states of a system. An open loop configuration may be used, but is susceptible to errors due to system approximations. In the case of the PMA, it was predicted that errors in approximating the transport delay could cause robustness issues. Therefore a closed loop configuration, which is shown in Figure 5.6, was examined.

With state feedback in the observer it is possible to design a transient response that is much faster than the controlled closed-loop system [81]. With a fast transient response, the observer error $y-\hat{y}$ is driven to zero, increasing the fidelity of the state estimator, and therefore the robustness of the entire control system.

5.2.5.1 Observer Feedback Matrix

The design of the observer feedback matrix $\mathbf{L}$ determines the response of the observer. Generally, in order to force the observer error zero quickly, the feedback matrix is chosen so that the closed loop poles are 10 times faster than the open loop poles of the observer. From the open and closed loop characteristic equations it is possible to find $\mathbf{L}$ by inspection. More details and examples can be found in [81].

5.2.5.2 Implementation Considerations

In attempting to design the observer feedback matrix, some implementation issues became evident. Even to double the speed of the closed loop poles required gains in the order of 10^5. Such large gains may cause stability issues in a real implementation. Also, with large gains it took over two minutes to simulate one second of the PMA system in Simulink. Thus it may be that the processing power required to control the system with a closed loop observer does not yet exist. The other possibility is that the long simulation time is a problem inherent with Simulink. Other work has indicated that C++ implementations can dramatically improve performance above that obtained with Simulink.

Considering the difficulty of using a closed loop observer in the PMA control, open loop observer control was re-examined. Despite initial robustness concerns, it was found that the system is resistant to errors between the actual system and the observer. Even doubling the transport delay did not alter the stability of the system. The step response of the system with an accurate estimate of transport delay and that of the system with an inaccurate estimate of transport delay are shown in Figure 5.8.

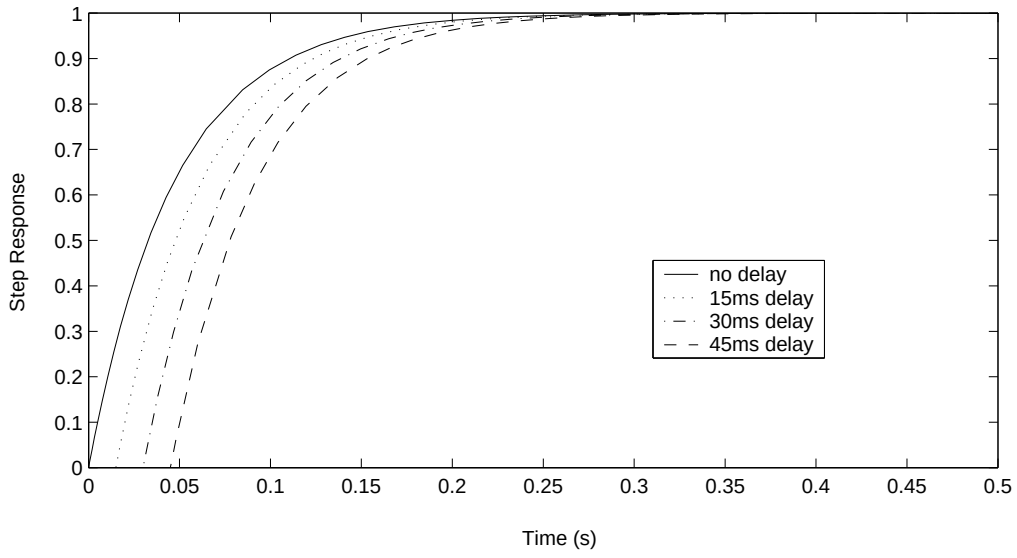

Figure 5.8: Demonstration of the resistance of the PMA Open Loop Observer to model inaccuracies ($15ms$ was the experimentally observed delay).

Given the apparent robustness of the open loop observer, and the implementation challenges of the PMA closed loop observer, the observer feedback matrix is set to $\mathbf{L} = \begin{bmatrix} 0 & 0 & 0 \end{bmatrix}^T$ in order to remove the observer feedback. The result is, in this case, a stable open loop observer.

5.2.6 Design of the Feedforward Term

The design of the feedforward term FF is straight forward. After the dynamic response of the controlled system has been designed, the feedforward term is used to adjust the steady-state value of the output. The most basic way to determine FF is to run the simulation with unity step input to determine the steady-state value. The feedforward gain is simply the inverse of the steady-state value.

5.2.7 Gain Scheduling

As has been discussed, the PMA model operates in two distinct modes. Gain scheduling is a technique that permits different gains in different operating regions, thus allowing for better control of the system despite the fact that the PMA behaves differently for inflation and deflation. The technique allows nonlinear systems to be divided into smaller systems that can be more reasonably modelled and therefore controlled as linear systems. In the case of the PMA, the system is divided into an inflation model and a deflation model, as was shown in Figure 5.4. Controllers were designed for both the charging and discharging mode of operation.

Determining the current mode of the PMA is a matter of determining if the pressure must increase or decrease at a given time step. If the reference pressure is greater than the actual pressure, then the pressure of the PMA must increase, and the PMA must therefore inflate. Likewise, if the reference pressure is less than the actual pressure, then the PMA must deflate.

Implementation revealed an algebraic loop. It arose since the mode of operation is dependent on the value of the actual pressure, and since the controller determines the pressure, then the pressure depends on the mode. To overcome the issue, a memory delay of one integration cycle was used on the actual pressure before comparing it with the reference pressure.

With the ability to determine the mode of PMA operation, the final implemen-

tation issue is determining how to swap controllers. Each of the controller gain matrices are swapped out at their site. This allows the controller integrators, which contain the state information, to be left in place. This solution avoids the difficulty of redefining the initial conditions every time the mode is changed.

5.2.8 PMA Controller Design Results

Based on the design considerations described above, the plant and estimator matrices are presented, for both the charging and discharging mode, in Table 5.1. Similarly, the controller gain matrices for both the charging and discharging mode are presented in Table 5.2.

Table 5.1: Plant Representation for Pneumatic Muscle Actuator

	Plant	Estimator
Charging	$A = \begin{bmatrix} -15 \end{bmatrix}$	$A = \begin{bmatrix} -415 & -115.89 & -12.207 \\ 512 & 0 & 0 \\ 0 & 128 & 0 \end{bmatrix}$
	$B = \begin{bmatrix} 4 \end{bmatrix}$	$B = \begin{bmatrix} 8 \\ 0 \\ 0 \end{bmatrix}$
	$C = \begin{bmatrix} 3.75 \end{bmatrix}$	$C = \begin{bmatrix} 1.875 & -1.4648 & 1.5259 \end{bmatrix}$
Discharging	$A = \begin{bmatrix} -20 \end{bmatrix}$	$A = \begin{bmatrix} -420 & -119.79 & -16.276 \\ 512 & 0 & 0 \\ 0 & 128 & 0 \end{bmatrix}$
	$B = \begin{bmatrix} 4 \end{bmatrix}$	$B = \begin{bmatrix} 8 \\ 0 \\ 0 \end{bmatrix}$
	$C = \begin{bmatrix} 5 \end{bmatrix}$	$C = \begin{bmatrix} 2.5 & -1.9531 & 2.0345 \end{bmatrix}$

Figure 5.9 shows the open and closed loop pressure response to a step input in charge mode. Figure 5.10 shows the open and closed loop pressure response to a step input in discharge mode. Similar results are obtained in both modes, where the closed loop response is faster, though not significantly, than the open loop response. Though not demonstrated in these figures, the more important consideration is the

Table 5.2: Controller for Pneumatic Muscle Actuator

	Controller
Charging	$FF = 1.4142$ $K = \begin{bmatrix} 0.77665 & 0.60676 & 0.63204 \end{bmatrix}$ $L = \begin{bmatrix} 0 \\ 0 \\ 0 \end{bmatrix}$
Discharging	$FF = 1.4142$ $K = \begin{bmatrix} 1.0355 & 0.80901 & 0.84272 \end{bmatrix}$ $L = \begin{bmatrix} 0 \\ 0 \\ 0 \end{bmatrix}$

disturbance rejection of the closed loop response.

Note that the step is from $0.5bar$ to $1bar$ for charging and from $1bar$ to $0.5bar$ for discharging. Note also that the control signal is within the working pressure range of $0bar$ to $8bar$, meaning the controller is active. For a system charging to $8bar$ or discharging to $0bar$, the open and closed loop responses would be identical since the controller will saturate and become ineffective.

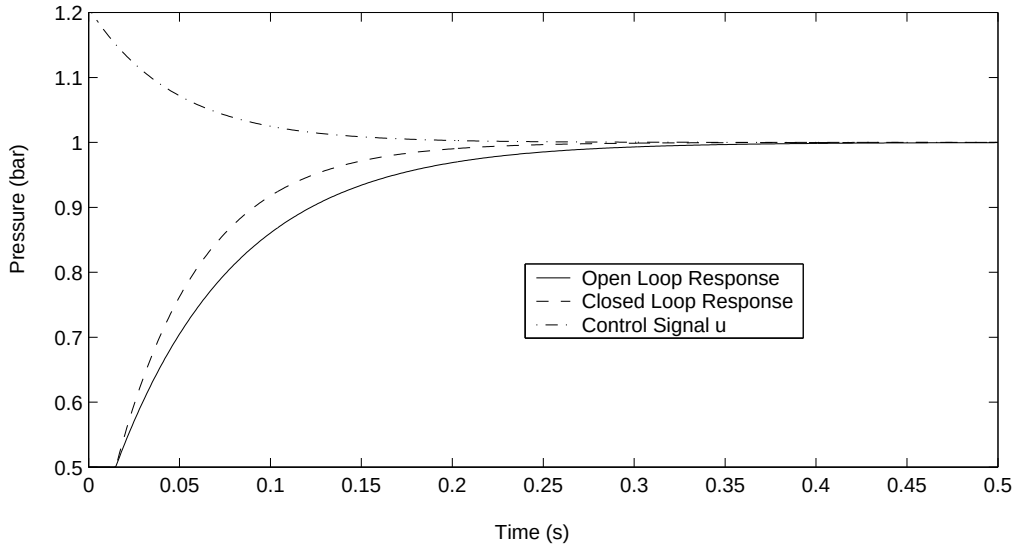

Figure 5.9: Step response of PMA in charge mode. Note that the step is from $0.5bar$ to $1bar$. This ensures that the controller remains active (i.e. does not saturate)

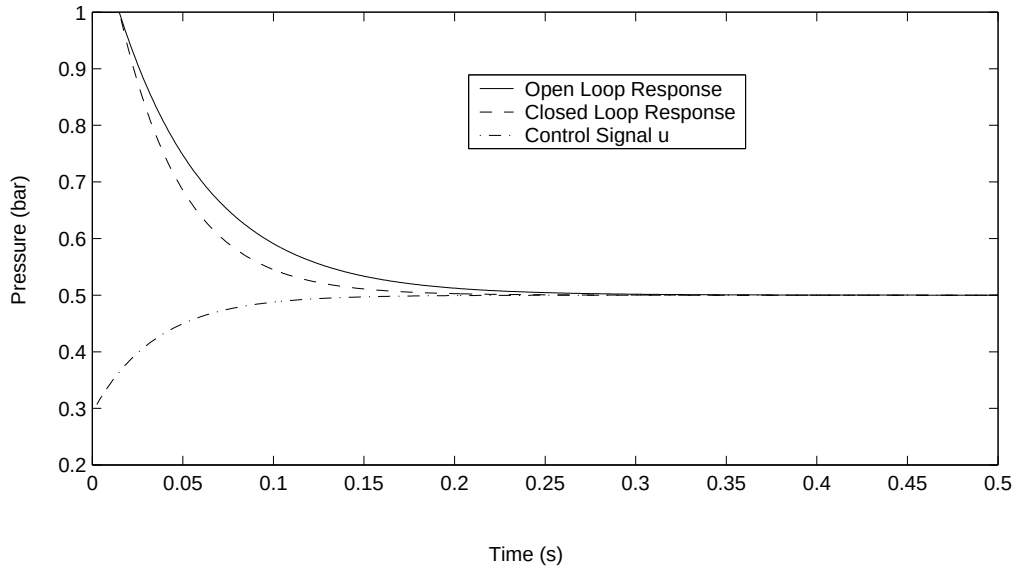

Figure 5.10: Step response of PMA in discharge mode. Note that the step is from $1bar$ to $0.5bar$. This ensures that the controller remains active (i.e. does not saturate)

5.3 DC Motor Actuated Orthotic Control

In many ways the DC motor model and its control are much simpler than the PMA and its control. While the basics of state-space control introduced in the previous section still apply, the more advanced topics are not relevant. This is the case for two reasons. First, the DC motor system has only one mode of operation. It is, therefore, not necessary to consider gain scheduling. Second, there is no significant time delay associated with the DC motor. The advantage, in this case, is that all of the states are therefore observable, which means that a state estimator and its controller are not required. Additionally, the same argument that was made for controlling the torque at the knee by controlling the dynamics of PMA pressure can be made for controlling the dynamics of DC motor torque. The resulting controller is examined.

5.3.1 DC Motor Controller Architecture

The state-space equations given in Equation 5.2 are used with the DC motor, since each state is observable and a state estimator is therefore not required. Recall the DC motor model, originally presented in Figure 3.18, and now presented again in Figure 5.11.

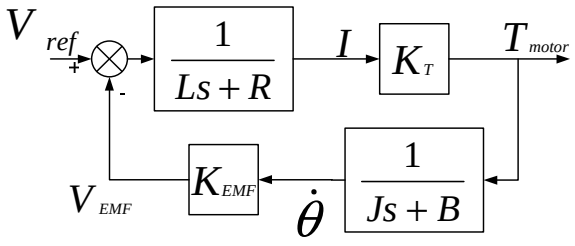

Figure 5.11: DC motor model with torque output

Since each state of the plant, the current I drawn by the motor and the velocity $\dot{\theta}$ of the motor, is observable, the architecture is simplified from that of the PMA controller. Schematically, the architecture for the DC motor is given in Figure 5.12. As was previously mentioned, the torque at the knee can be controlled by controlling the dynamics of the DC motor torque. Therefore y is the DC motor torque.

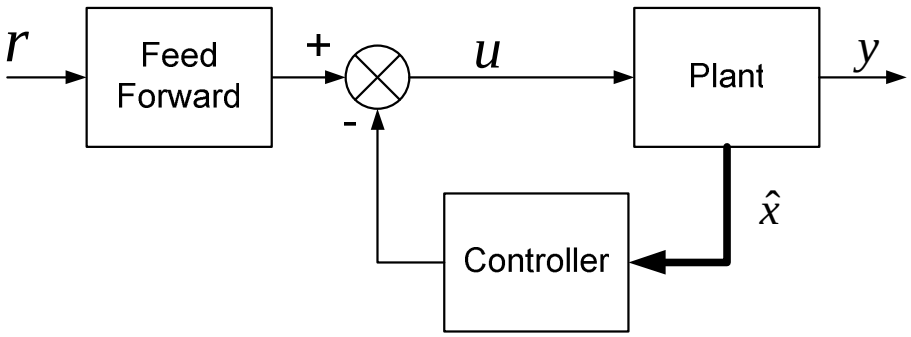

Figure 5.12: DC motor controller architecture

Thus, the motor model is written in state-space form as:

$$\begin{aligned} \frac{d}{dt}\begin{bmatrix} \dot{\theta} \\ T_{motor} \end{bmatrix} &= \begin{bmatrix} -\frac{B}{J} & \frac{1}{J} \\ -\frac{K_{EMF}K_T}{L} & -\frac{R}{L} \end{bmatrix}\begin{bmatrix} \dot{\theta} \\ T_{motor} \end{bmatrix} + \begin{bmatrix} 0 \\ \frac{K_T}{L} \end{bmatrix} V_{ref}, \\ T_{motor} &= \begin{bmatrix} 0 & 1 \end{bmatrix}\begin{bmatrix} \dot{\theta} \\ T_{motor} \end{bmatrix}. \end{aligned} \tag{5.8}$$

5.3.2 DC Motor Controller Design

It was found that the motor has very low damping and inductance. This caused difficulty in controlling the motor. Thus, for the purposes of the model, the damping of the system is increased so that B is $2.01 \times 10^{-1} Nm \cdot s/rad$. The inductance of the system is increased so that L is $6.4 \times 10^{-1} H$. The result of increasing damping and inductance is an increased rise time, which is acceptable. Also based on the experimental values of [9], and the values used in the simulation of [84], it seems reasonable to increase the damping and inductance values for the model. In fact, the damping of the mounted motor will be larger than that specified by Kollmorgen, and inductance is easily added with an electrical inductor.

Based on the revised values for B and L, and using Equation 5.8, the plant matrices are:

$$\mathbf{A} = \begin{bmatrix} -221.79 & 1106.2 \\ -3.2828 & -2.7813 \end{bmatrix}, \tag{5.9}$$

$$\mathbf{B} = \begin{bmatrix} 0 \\ 2.9844 \end{bmatrix}, \tag{5.10}$$

and,

$$\mathbf{C} = \begin{bmatrix} 0 & 1 \end{bmatrix}. \tag{5.11}$$

5.3.2.1 State-Feedback and Feedforward Design

As was already mentioned, the motor model is observable and a verification of observability was performed, as described in Section 5.2.4.2. It was also found, using the method described in Section 5.2.4.1, that the motor model is controllable. The LQR design of a state-feedback regulator $\mathbf{K}$ was previously described in Section 5.2.4.3 for the PMA. The same technique was applied to the design of the state-feedback controller for the DC motor.

The feedforward term FF was selected so that the closed loop steady-state error of the model output is zero. The method is described in Section 5.2.6.

5.3.2.2 DC Motor Controller Design Results

The optimal LQR state-feedback controller, with $\mathbf{Q} = \mathbf{C^T} * \mathbf{C}$ and $R = 1$, was found to be $\mathbf{K} = \begin{bmatrix} -0.0011308 & 0.083076 \end{bmatrix}$. The feedforward term is $FF = 6.4103$.

The open and closed loop response of the DC Motor is shown in Figure 5.13. The open and closed loop response are quite similar, obtaining steady-state within 0.2 seconds. The open and closed loop responses are also similar to that of the PMA, though with no delay, and are considered good. Note that while the open and closed loop response of the motor are similar, closed loop control is chosen due to its improved disturbance rejection.

5.4 Concluding Comments

The control of the assisted STS task is broken down into user-orthotic interaction and control of the actuators. The user-orthotic interaction section examines how

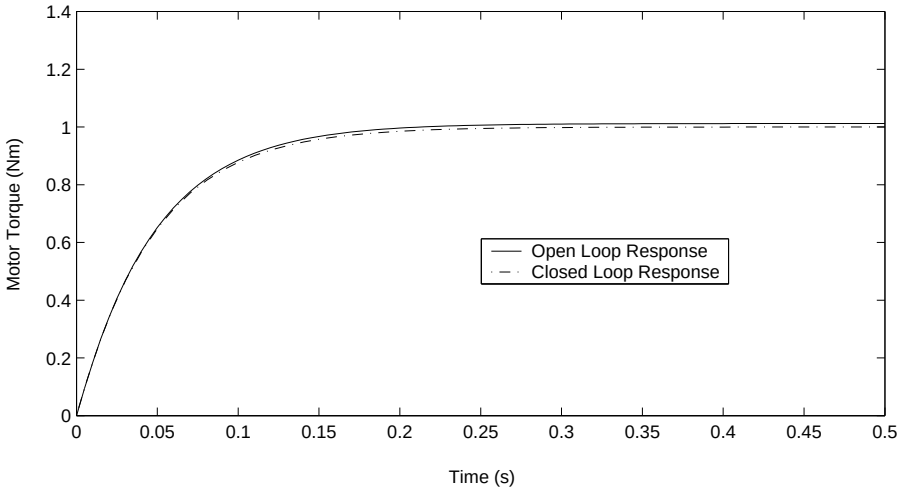

Figure 5.13: Step Response of DC Motor

to generate a control signal for the actuator, based on observable signals from the user. Its efficacy is examined though simulation.

The design of the controller for the PMA and the controller for the DC motor is based on accepted control techniques. It is believed that the controllers for the actuators are reliable and that they could be used equally well with the models and the actual actuators.

Chapter 6

Simulation of Assisted STS

In this chapter, the assisted STS model implementation details and simulation parameters are provided. The results of several simulations are presented and a discussion of those results follows.

6.1 Model Implementation and Simulation Parameters

The Assisted STS model is implemented with a mechanical modelling and simulation package[1]. Inverse dynamic functionality is included in the package.

The simulation of assisted STS was performed using a variable-step solver with a maximum step size of $5ms$. Rather than being constrained to a fixed time step, variable-step solvers alter the step size as dictated by the characteristics of the system. The solver used for the assisted STS is an ordinary differential equation 45 (ODE45). ODE45 is based on the Runge-Kutta formulation, and was developed by Dormand and Prince in [85]. It is therefore also referred to as the Dormand-Prince solver. ODE45 is a one step solver, meaning that it only requires the input and the solution at the previous time step. According to [86], ODE45 is the solver that works for most problems. It is the first solver that should be used, and it provides good accuracy. For a rigorous discourse on the Runge-Kutta family of solvers see [87].

[1] Matlab 6.5 Release 13, with Simulink 5.0 and SimMechanics 1.1

6.2 Results

Simulations were run using the models developed in Section 3, driven by the kinematic data of Section 4, and controlled by the controllers of Section 5. Figure 6.1 illustrates how the component research is used in the simulations to determine the amount of torque that the user must produce. The kinematic data drives the inverse dynamics STS model, with which the gross knee torque is found. The kinematic data is also used as an input to the human-in-loop controller, which provides a control signal to the actuator. The torque output of the actuator is subtracted from the gross knee torque to obtain the torque that the user must generate to produce the input trajectory.

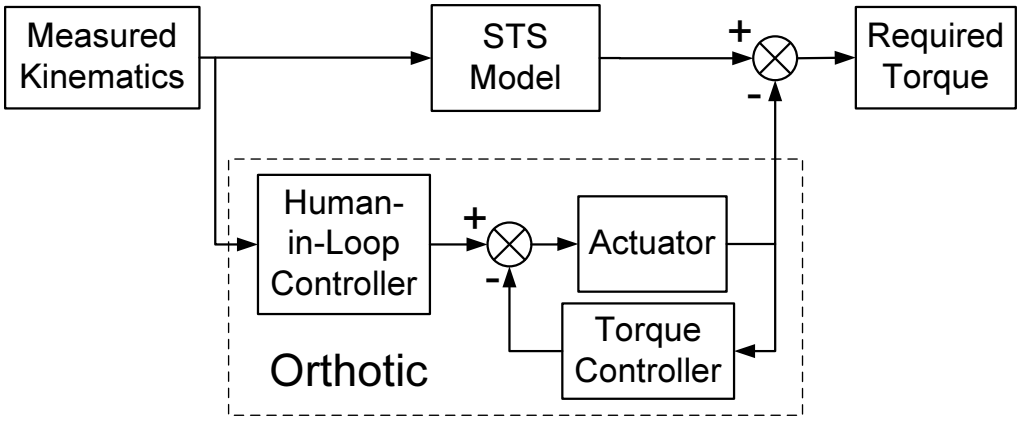

Figure 6.1: Overview of the simulation setup

The simulations were run to get an estimate of the torques that a PMA actuated knee orthotic and a DC motor actuated knee orthotic could contribute to the STS task. The data presented throughout this section gives the gross knee torque, or the torque required at the knee to produce the prescribed motion, and the assisting torque of the orthotic. The net torque, which is the torque that the user must supply, is not shown in the plots. It is, however, simply the gross torque less the orthotic torque.

Recall that the plots follow the biomechanical convention, thus a positive torque is extensor, and the torques are for a single knee. Also, recall that the goal of the project is to consider the feasibility of providing 50% assistance of the torque throughout the STS task.

Figure 6.2 presents the orthotic torque produced using the control strategy of Section 5.1.1.2. The dynamics of the actuators are not included in order to provide a clear view of the utility of the user interface strategy, which used a linear relationship between the required torque and the position of the knee. Results that include dynamics are presented after the user interface strategy is examined.

It was hypothesized that the steep slope of the relationship between required torque and knee position near the seated position, given previously in Figure 5.2, was a transient effect associated with seat contact. It was therefore ignored by the linearization. From the early stages of STS in Figure 6.2(b), it can be seen that neglecting the steep slope of the torque-position relationship results in an overestimation of the required torque. The result is that a flexor torque must be exerted by the user for about the first 5% of the slow and natural paced STS in order to produce the gross knee torque.

It turns out that the first 40% of the STS task falls within the steep section of the torque-position curve, where the knee position moves only a few degrees. Since the effect is not transitory it cannot be ignored. Figure 6.3 shows the results of a strategy that does not ignore the steep section of Figure 5.2. Instead, the control strategy is updated to use the torque-position curve of the natural paced STS, also shown in Figure 5.2. Again the dynamics of the actuators are ignored.

The expected result of the strategy, with actuator dynamics ignored, was that the orthotic torque of the natural paced trial will be exactly half of the gross knee torque. Indeed, that is the case for the natural paced trial, shown in Figure 6.3(b). For the slow trial, the orthotic does not produce a torque until 20% through the task. That is because the controller requested a flexor torque, due to the misalignment of the steep section of the slow-paced task and the natural-paced controller in Figure 5.2, when the orthotic is capable of extensor torques only. For the fast trial, the orthotic was still able to produce over 1/3 of the peak gross knee torque.

With the dynamics of the actuators being ignored, it may have been surprising that the PMA contribution and the DC motor contribution were not exact in each of the trials. They are not identical in Figure 6.3(a), the slow trial, due to the requested flexor torque and the slightly different way in which the PMA and motor respond. For the natural and the fast trial the PMA and motor contributions are virtually indistinguishable when dynamics are ignored.

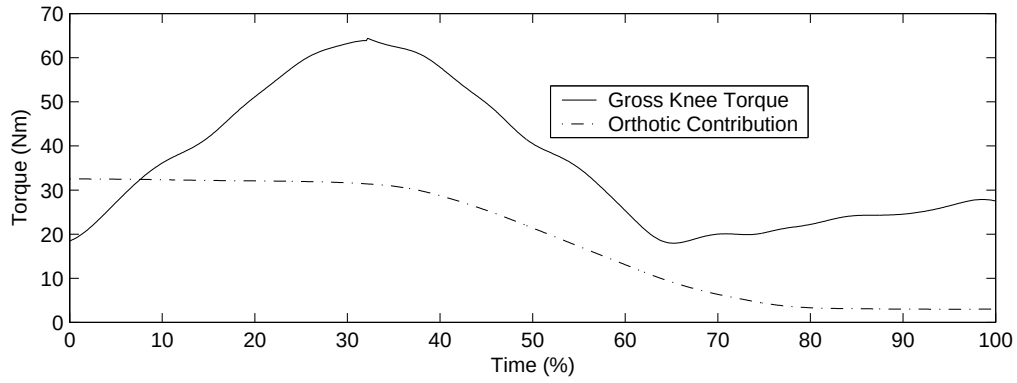

(a) Slow

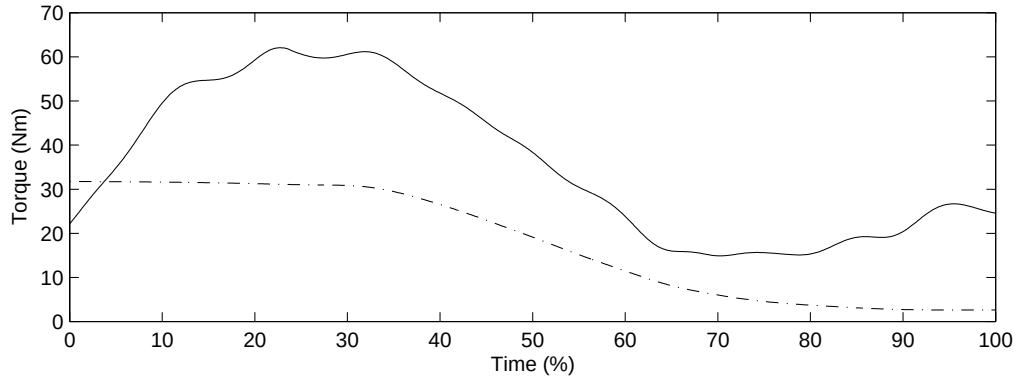

(b) Natural

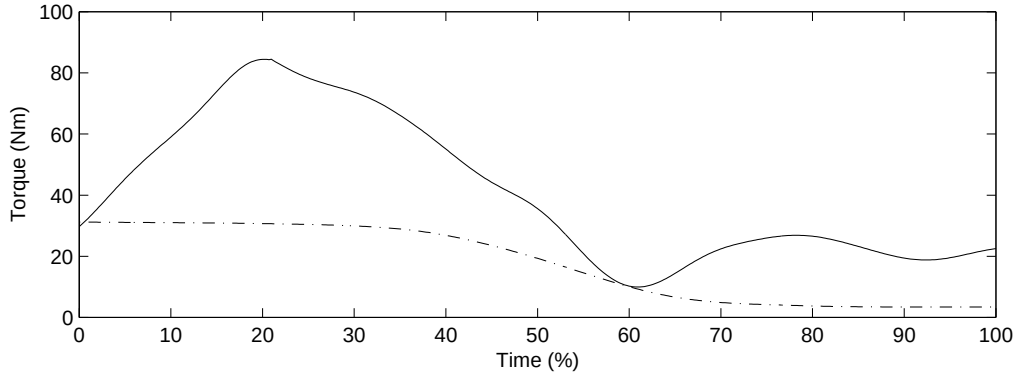

(c) Fast

Figure 6.2: Orthotic torques for (a)Slow, (b)Natural, and (c)Fast STS trials. The control signal is based on a linear relationship between knee position and required torque. Here the dynamics are not included in torque output of the actuator.

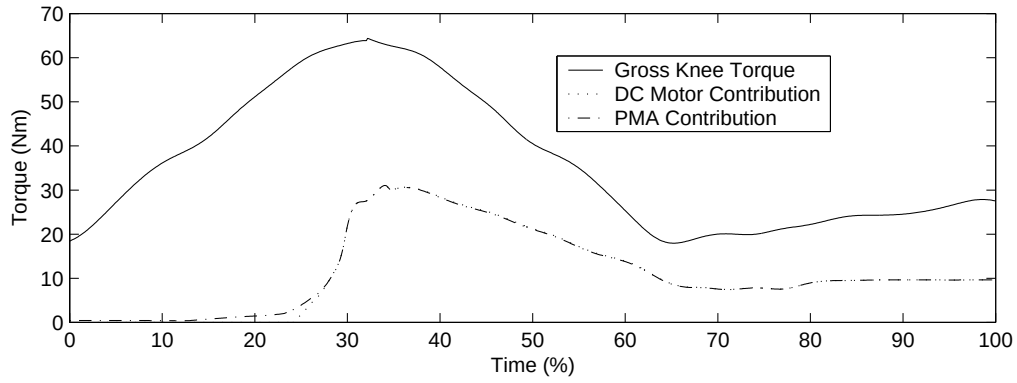

(a) Slow

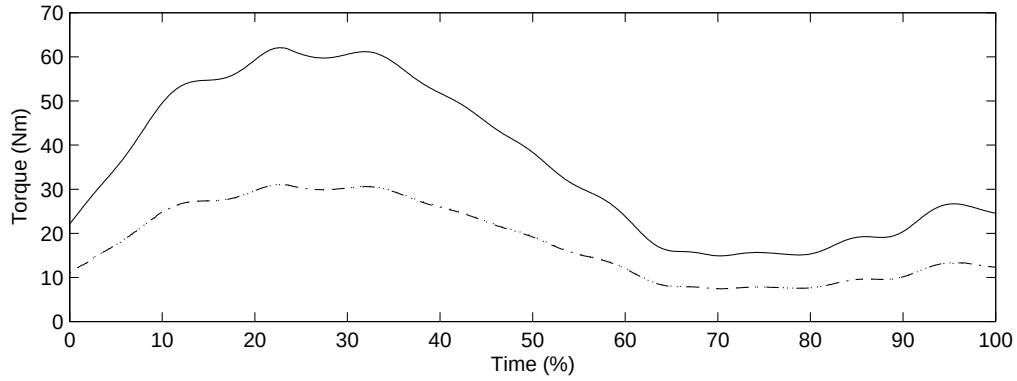

(b) Natural

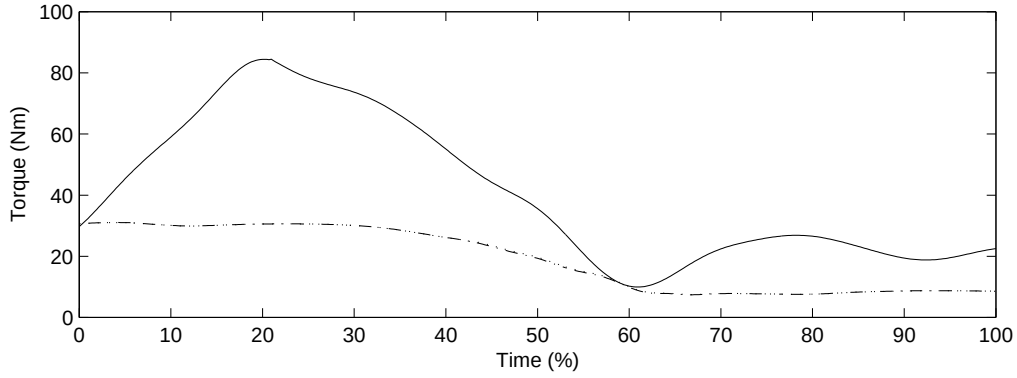

(c) Fast

Figure 6.3: Orthotic torques for (a)Slow, (b)Natural, and (c)Fast STS trials. The control signal is based on an actual STS task, and the torque is provided as soon as STS begins. Here the dynamics are not included in torque output of the actuators.

Figure 6.4 is the same as Figure 6.3, except that it also takes into account the triggering event of the heel. That is, the orthotic in Figure 6.4 is activated when the heel force becomes greater than $75N$, as was previously determined in Section 4.3.1.2. Note that this results in a step change in torque on the user for the natural and fast trials, but that here the dynamics of the actuator are also being ignored. The dynamics of the actuator should reduce the demands placed on the user.

Figure 6.5 extends the results of Figure 6.4 by adding in the actuator dynamics. The influence of the PMA and DC motor actuators is seen primarily in low-pass filtering the step-like change in torque. The resulting torque that the user must exert is largely within the $3Hz$ bandwidth. Any small component above $3Hz$ will be further low-pass filtered by the soft tissue compliance at the orthotic to user interface.

With the heel force being used as a trigger, it can be seen in Figure 6.5 that the orthotic does not do a particularly good job of assisting the STS task by providing 50% of the required torque. Indeed, the orthotic is not even activated until halfway through the peak torque requirements.

Since a heel force trigger has been shown to be ineffective, the results are shown in Figure 6.6 where the dynamics of the actuator are included and the orthotic provides assistance from the beginning of the task. The assistance of the slow task remains virtually identical to that shown in Figure 6.5(a) due to the requested flexor torque. On the other hand, even the fast trial is well assisted, despite the fact that there is no velocity control.

6.3 Discussion

An examination of the results presented in Section 6.2 above reveals important information. The major revelation is that there is no functional difference between the dynamics of the PMA and the dynamics of the DC motor. While the two actuator technologies are quite different, it appears that they are controllable to an extent that the torque assistance provided to the user is similar. Thus, to provide recommendations on actuator selection, implementation and manufacturing considerations must ultimately be used.

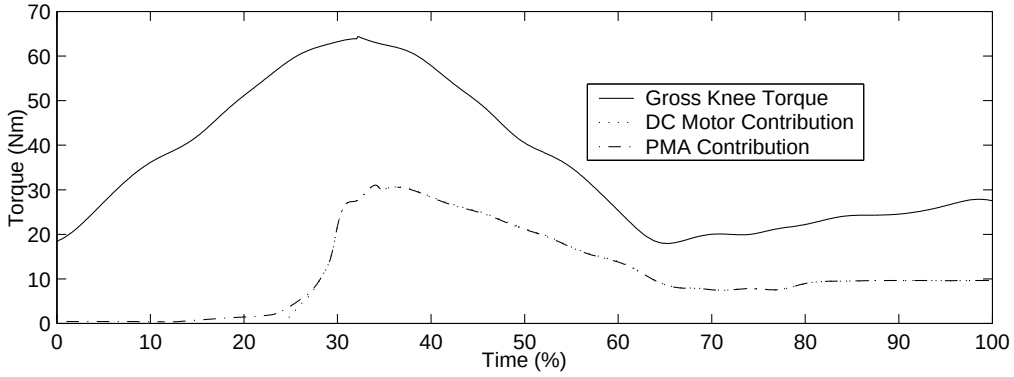

(a) Slow

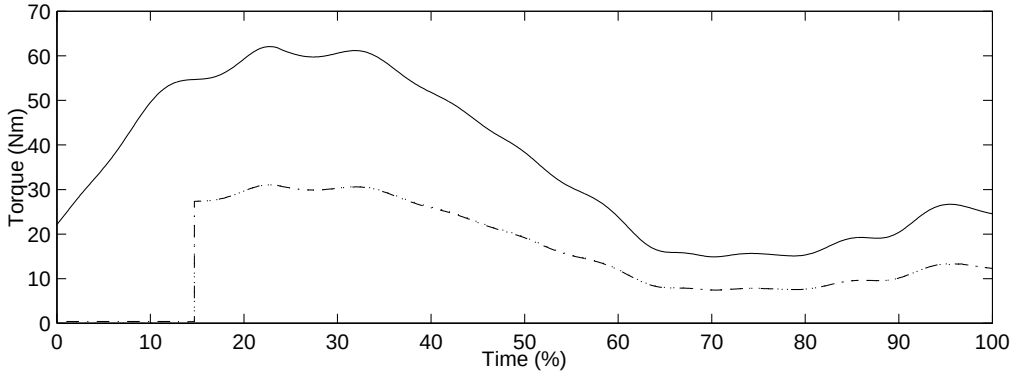

(b) Natural

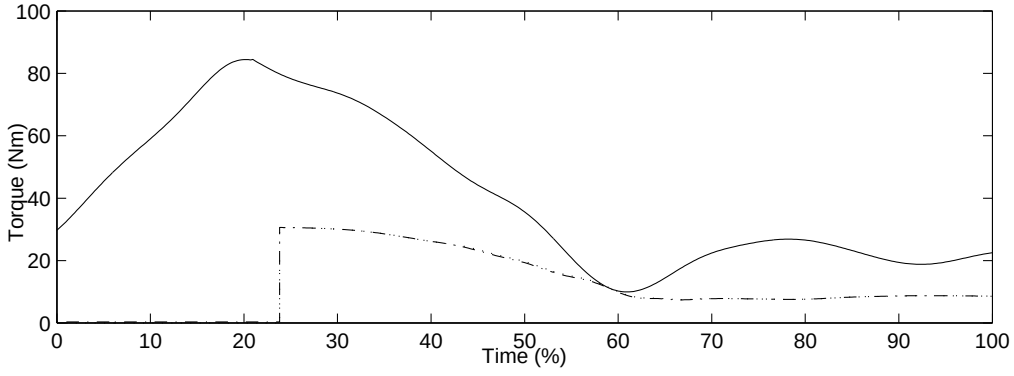

(c) Fast

Figure 6.4: Orthotic torques for (a)Slow, (b)Natural, and (c)Fast STS trials. The control signal is based on an actual STS task, and is triggered by the heel force. Here the dynamics are not included in torque output of the actuators.

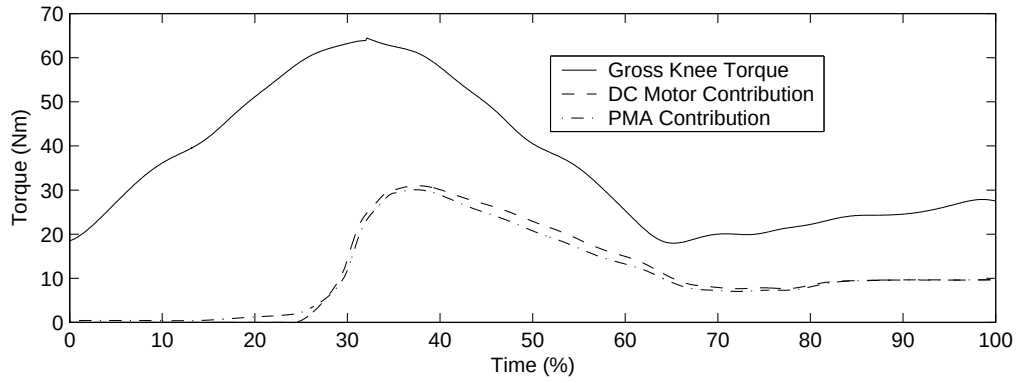

(a) Slow

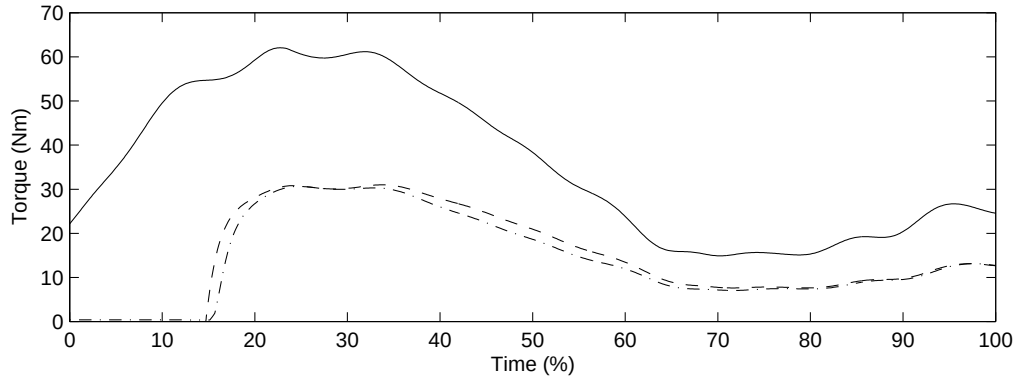

(b) Natural

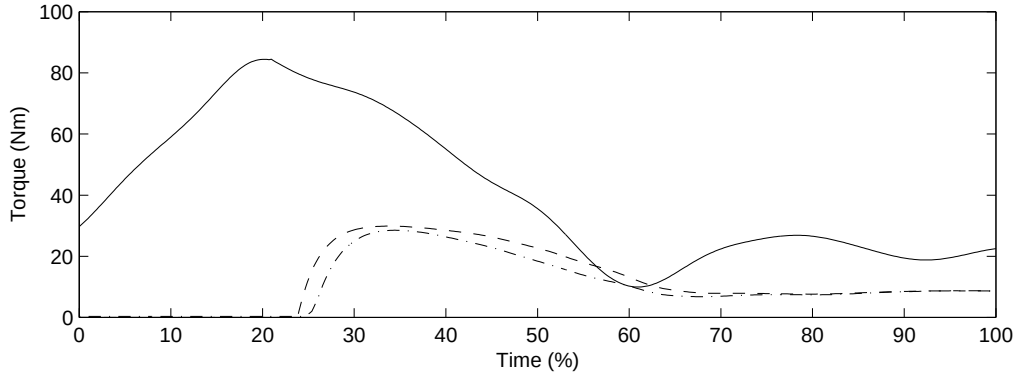

(c) Fast

Figure 6.5: Orthotic torques for (a)Slow, (b)Natural, and (c)Fast STS trials. The control signal is based on an actual STS task, and is triggered by the heel force. The dynamics are included in the torque output of the actuators.

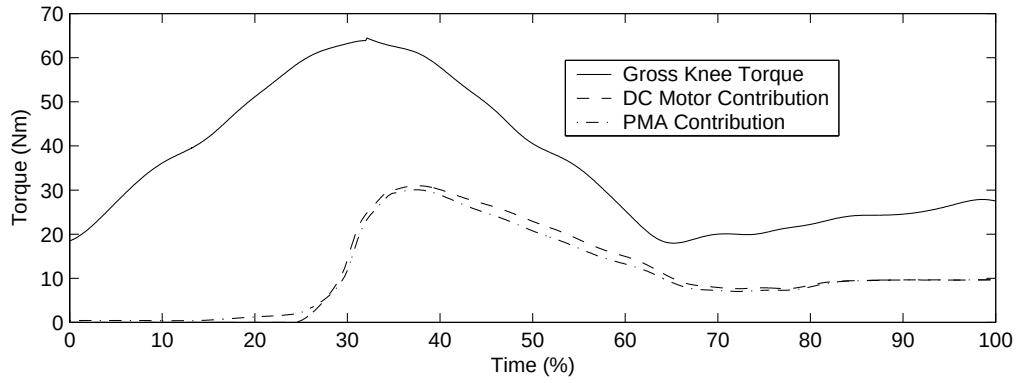

(a) Slow

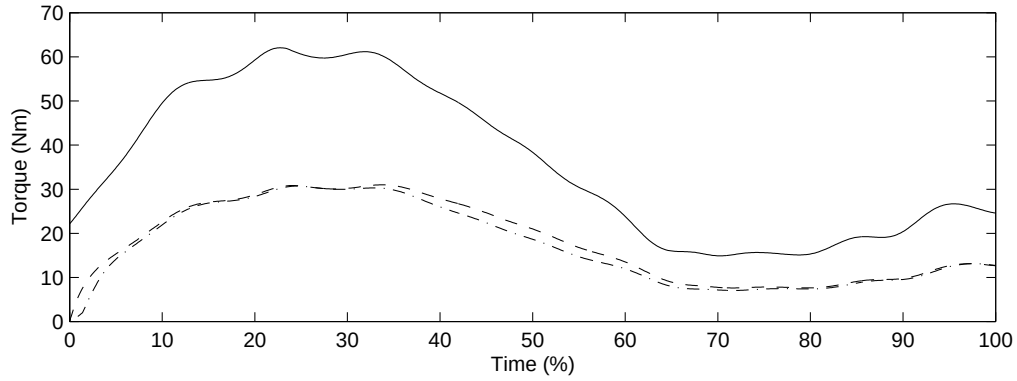

(b) Natural

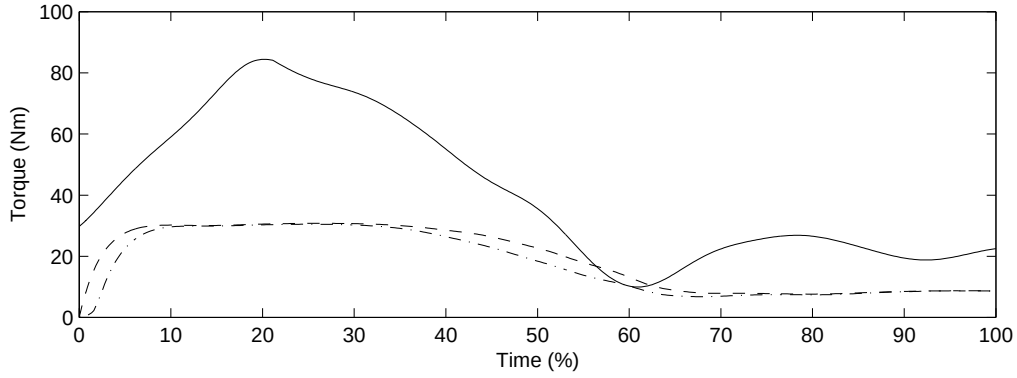

(c) Fast

Figure 6.6: Orthotic torques for (a)Slow, (b)Natural, and (c)Fast STS trials. The control signal is based on an actual STS task, and the torque is provided as soon as STS begins. The dynamics are included in the torque output of the actuators.

The results also provide useful insight into the human-machine interface and the Human-in-Loop controller. It is apparent, from Figure 6.5, that a heel trigger is not a good indicator of STS initiation, as the trigger occurs near peak torque requirements, which is too late to allow the orthotic to provide sufficient assistance. However, if STS onset can be determined, it appears as though a speed-invariant human-in-loop controller can be used with success.

The use of a torque versus knee position curve, based on the natural paced STS, allows the orthotic to provide good assistance to the user despite the fact that the controller is speed invariant. This was illustrated in the natural and fast paced rises. The poor performance of the controller in estimating the torque requirements for the slow paced rise does not indicate a deficiency in the controller. Rather, the need for the user to regulate the rise is shown.

The torque versus knee position curve for the slow paced STS is basically shifted by a few degrees from that of the natural paced STS. The steep slope of the curves from sitting until after seat-off means that the position of the knee has a great impact on the torque output of the knee. However, since the knee angle is only shifted by a few degrees, it is not unreasonable to expect the user to interact with the orthotic by regulating the initial knee angle.

Finally the fast trial was assisted with about 1/3 of the required torque. This was expected since the fast paced trial requires a disproportionately greater knee extensor torque [77] and because a speed-insensitive controller was used. However, it again seems reasonable to expect the user to regulate their ascent. If a greater speed of ascent is required, then the user must exert a greater knee extensor torque. Regardless, the orthotic can be counted on to provide a given torque at a given knee position. That predictability may well outweigh the any minor gains in torque output that could be achieved with the use of a speed-sensitive controller.

Chapter 7

Conclusions and Future Work

In this chapter, conclusions are given about the suitability of the model, the efficacy of the controller, and the best actuator technology. Areas of future work, which include examining larger PMAs, user testing, and the challenges of offering complete STS assistance, are also presented.

7.1 Conclusions

This section presents some conclusions that are drawn from the work presented in this thesis. In this section the suitability of the model components is examined, the effectiveness of the control strategy is considered, and thoughts on actuator selection are put forth.

7.1.1 Model Suitability

The assisted STS model is composed of a three-link planar STS model and the orthotic model, which includes the brace kinematics and the actuator dynamics. The suitability of the model was previously discussed, but is reiterated here for the sake of completeness.

It was found that the STS inverse dynamics model produced torques consistent with those of published literature. A better method to estimate the chair support force is, however, required. The chair support force in the work to date was estimated by fixing the torque at the knee from STS initiation to seat-off. While the results

were congruent, a stronger case could be made for the model by equipping the chair with force sensors, and using those measurements in calculating the chair support force.

It may also be prudent to eventually model STS with arm support. Since the orthotic is being investigated for use as a mobility-assist device, it would be reasonable to expect the user to utilize arm support during STS. The most likely effect would be a reduced torque at the knee and a reduced risk of sit-back failure. The use of arm support, however, secondary to the goal of the project, which was to examine the feasibility of using an orthotic as a mobility-assist device.

As the STS model produces torques that are consistent with published literature, the PMA model used is also consistent with published literature. The major deficiency of the PMA model is that it is only valid for a single configuration. That is, the model is dependent on the valve, on the piping, and on the PMA itself, which includes both the diameter and length of the PMA.

The DC Motor model is based on a well established model and the model parameters are from the published data for a Kollmorgen Direct Drive Rotary DC motor. It was found, however, that the motor was much more controllable with increased mechanical damping and increased electrical damping. These parameters could be increased in an actual implementation, and they are therefore considered reasonable.

The components of the assisted STS model are consistent with the relevant literature. Furthermore, the simulations performed using the model provided results that are consistent with what was expected. The model for assisted STS is therefore considered suitable for examining the feasibility of a powered lower-limb orthotic.

7.1.2 Control Strategy Efficacy

Simulation of assisted STS has provided insight into the efficacy of the orthotic control strategy. Recall that the strategy has both a user interface component and an actuator controller.

It was found that the state-space controllers for the PMA and the DC motor provided good control over the actuator dynamics. The actuator response to input is fast enough to match the human bandwidth. The actuator controllers also overdamp the system, which ensures that user need not adjust for overshoot or oscillations in

the torque assistance.

Analysis of the user interface component of the controller yielded somewhat more ambiguous results. The heel trigger performed poorly at best. Unfortunately, too much of the STS task occurs before the heel force crosses the $75N$ threshold. While the threshold could be lowered, in the trials examined the force rose monotonically from the $75N$ threshold crossing until after seat-off. Whether the monotonic trend is needed to reliably predict STS is a question that would better be answered through user trials. It may well be that a lower threshold could still accurately indicate the onset of STS. A switch is another option that could be used as a trigger to indicate onset of STS. Other than that, it seems unlikely that there is other measurable information with enough content to reliably and uniquely indicate the onset of STS.

While the linear relationship between knee position and desired torque did not produce acceptable results, the use of the natural-paced STS knee position versus desired torque curve did produce good results. It appears as though a velocity-invariant user interface is reasonable, with two caveats. First, user training will be required to ensure that the user does not move ahead of the orthotic, but rather allows the orthotic to assist the task. The second is that a velocity-invariant strategy cannot provide the full goal of 50% torque assistance for the fastest of rises. It was found, though, that the fast paced rise was assisted by 1/3. The strategy, which places the user in the control feedback loop, is able to provide good assistance in STS. It does, however, place responsibility on the user to ensure that they receive the full benefit of the powered lower-limb orthotic.

7.1.3 Actuator Selection

It was found that both the PMA and the DC motor are feasible actuator options. Both actuators were capable of assisting 50% of the knee torque during STS, within the limits of the user interface. Both actuators also placed reasonable frequency requirements on the user. Therefore, other factors must be used in the actuator selection process.

Weight, cost, and convenience are factors that could be considered in actuator selection. The difference in weight between the PMA and the motor is not significant. The cost of the DC motor is also comparable to the cost of pneumatic valve and pneumatic actuators. With the addition of extra pneumatic valves, with an

associated increase in weight and cost, it is possible to speed the dynamics of the PMA. It is an advantage not afforded to the motor-based orthotic. On the other hand, the PMA requires a compressed air supply while the motor requires a more readily available DC source. The weight and operating time of the power supply is also a consideration, though it is expected that there would be no clear advantage between a compressed air supply and a DC supply.

Actuator selection, then, should be based on ability to scale. While the requirements for this feasibility study called for a torque assistance of 50%, one eventual goal may be scale up the actuator and modify the control strategy to offer complete assistance. This would require that the torque producing ability of the actuator scale up 100%. With the PMA it is easy to both add actuators in parallel and to use larger diameter actuators that are able to produce substantially more force. Due to limited space, it would be difficult to mount more than two DC motors per leg. It would also be difficult to find another reasonably sized motor that could output more torque. The PMA, therefore, is a more suitable choice as an actuator for a powered lower-limb orthotic.

7.2 Future Work

In this future work section, areas of research that require further investigation or have yet to be investigated thoroughly are discussed. While it appears as though the implementation of the powered lower-limb orthotic is feasible, further research remains.

7.2.1 Use of Larger PMA

As was previously suggested, gains in performance may be achieved with the use of a larger diameter PMA. The $10mm$ diameter PMA examined can produce a maximum force of $400N$. In contrast, the $20mm$ diameter PMA can produce a force of $1200N$ and the $40mm$ diameter PMA can produce a force of $4000N$. The larger diameter muscles represent a clear advantage in force producing capability.

While the larger muscles are capable of producing a larger force, it is expected that there will be loss in the dynamic response. Given the same compressed air source, pneumatic valve, and piping, the dynamic response of the larger PMAs is

expected to be slower due to the increased filling and emptying time. The dynamics of the larger PMAs should be modelled and their effects examined through simulation.

If it is found that the dynamic response slows considerably for a larger diameter PMA, options exist that could improve the response. The ability of the actuator to vary the force output is related to the rate at which the internal pressure of the PMA can be changed. Therefore, to increase the response time of the PMA, either the flow rate of air entering the muscle must increase or the volume to fill must decrease.

It may be possible to increase the flow rate in two ways. First, it has been found that there is a significant constriction between the valve and the PMA at the inlet port of the PMA. This port could be drilled out to improve air flow. Second, the configuration examined had a valve at one end, and the other end was closed. Therefore another approach to improving the air flow into the PMA would be to use a valve at each end of the PMA.

It is also possible to reduce the internal volume of the PMA with the use of a filler material. Even when discharged, the PMA has a significant internal volume. Using an incompressible filler material to displace the dead air has a twofold benefit of increasing bandwidth and reducing consumption of compressed air. In fact, it has been speculated that bandwidth could be improved 1000% with some filler configurations. Meanwhile, it was also noted that savings of up to 90% could be achieved in air consumption, though the savings are heavily dependent on the PMA configuration [88].

Further modelling should be performed using larger diameter PMAs so that the advantage of increased force output can be compared with the possible reduction in dynamic performance of the PMA. Once the most appropriate PMA has been selected, and configured according to the necessary dynamic response, the next phase of development is the construction of a prototype and user testing.

7.2.2 User Testing

Once a prototype of the powered lower-limb orthotic has been developed, it will be possible to perform some small scale user tests. User testing should answer two questions. One: Does the brace assist STS as expected, and how can it be improved?

Two: Is the brace wearable, and how can wearability be improved?

The first question can be addressed informally with general user feedback. Does the user believe the orthotic was an aid? Did using the orthotic present any issues with postural stability? The questions can also be addressed more formally with the use of EMG or other physiological measurements to determine the assistance provided to the user.

Answering the second question actually involves much more than simply gauging the comfort of the brace. It involves determining if the brace only activates when the user is actually trying to rise. A false triggering of the orthotic could be, depending on the circumstance, quite dangerous. Also, even if the brace activates properly, does the brace allow for unincumbered movement in other tasks? If not, then the brace would not be considered particularly wearable.

A concern raised by Dr. Patrick Cawley, of passive orthotic manufacturer Breg Inc., is that of ischemic implication in axial soft tissue. Essentially, the concern is that the pressure of the brace on the soft tissue of the leg would reduce flow of blood to the underlying and distal tissue, causing circulation-related problems. The concern is valid, though it is believed that it is less important for the partially assisted STS task. It may also be possible to distribute the force of the brace across a greater portion on the limb, reducing the pressure. User testing will be useful in determining the degree to which ischemic implication is cause for concern.

7.2.3 Challenges of Complete Assistance

There are numerous challenges in offering complete torque assistance in the STS task. For example, as was noted above, ischemic implication may be a greater concern when dealing with the larger forces required to completely assist the STS task. Another issue would be to ensure that the actuators are capable of exerting the required forces. These issues, however, are a matter of scale and do not present a new problem.

On the other hand, with complete assistance, as would be necessary for paraplegic or quadriplegic users, the need for a new user interface in the control strategy becomes apparent. Control of the STS task is complex, involving both feedforward trajectory planning and feedback balance control. With partially assisted task, the user remained a part of the control loop by positioning the brace.

While it is beyond the scope of this thesis, alternate user interfaces must be explored in order to offer complete assistance. The finger walking interface of [27] maps finger position to lower-limb position, and is quite promising. It allows the user to participate directly in trajectory planning. It does, however, fail to provide adequate balance control. In the case of the paraplegic user, balance could be achieved with the use of a cane or a walker. For the quadriplegic user, balance will be much more difficult to achieve. It would likely require the interaction of some user controlled feedforward mechanism and an artificial proprioceptive feedback mechanism.

More work will be required to fully allow complete assistance of the STS task. While actuator technologies are sufficiently advanced, user interface research has yet to produce a sufficiently complex interface. Despite the challenges, the goal of providing complete assistance to the mobility-impaired user remains worthwhile.

7.3 Closing Remarks

The work of this thesis has shown that the technology exists to develop a powered knee orthotic capable of assisting the sit-to-stand task by 50%. It appears that the largest difficulty is in designing a robust user interface and control strategy. Clearly current control strategies are not nearly so complex or powerful as the human central and peripheral nervous system. However, significant inroads have been laid, which will allow a starting point on which to base an implemented orthotic.

While there are challenges in developing a powered lower-limb orthotic, the goal of offering assistance to the mobility-impaired user is worthwhile. An assistive device that can provide the user with improved mobility can help to mitigate the severe emotional and financial costs of injury or degeneration. Throughout the long development process, it will be important to remember that the powered lower-limb orthotic may provide an increased sense of freedom, speed the ability of the user to return to work, and lessen the emotional strain placed on the injured person and his or her family.

Appendix A

Definition of Segment Parameter Values for STS Model

Based on the anthropometric data provided in [29], the following values are used in the three-link planar model of the sit-to-stand task:

$$\begin{aligned} m_1 &= 0.0930m \\ m_2 &= 0.200m \\ m_3 &= 0.678m \\ l_1 &= 0.246l \\ l_2 &= 0.245l \\ l_3 &= 0.288l \\ l_{c1} &= 0.567l_1 \\ l_{c2} &= 0.567l_2 \\ l_{c3} &= 0.626l_3 \\ I_1 &= m_1(l_1 \times 0.302)^2 \\ I_2 &= m_2(l_2 \times 0.323)^2 \\ I_3 &= m_3(l_3 \times 0.496)^2 \end{aligned} \tag{A.1}$$

where subscript 1 represents the shank, 2 represents the thigh, and 3 represents the HAT. The total body mass is given by m, and l is the height of the subject. m_x is

the segment mass, l_x is the segment length, l_{cx} is the distance to the center of mass from the x-th joint, and I_{cx} is the inertia of the segment about the center of mass.

References

[1] L. Cossette and E. Duclos, *A profile of disability in Canada, 2001*, catalogue no. 89-577-xwe ed., Statistics Canada, Dec. 2003.

[2] (2004, Nov.) Effects of rehabilitation on the family. The University of Chicago Hospitals. [Online]. Available: www.uchospitals.edu/online-library/library.php?content=P01157

[3] C. N. Mock, S. Gloyd, S. Adjei, F. Acheampong, and O. Gisch, "Economic consequences of injury and resulting family coping strategies in Ghana," *Accident Analysis & Prevention*, vol. 35, no. 1, pp. 81–90, Jan. 2003.

[4] L. Gilchrist and D. Winter, "A two-part viscoelastic foot model for use in gait simulations," *Journal of Biomechanics*, vol. 29, no. 6, pp. 795–798, 1996.

[5] M. S. Redfern and T. Schumann, "A model of foot placement during gait," *Journal of Biomechanics*, vol. 27, no. 11, pp. 1339–1346, 1994.

[6] P. O. Riley, R. W. Mann, and W. A. Hodge, "Modelling of the biomechanics of posture and balance," *Journal of Biomechanics*, vol. 23, no. 5, pp. 503–506, 1990.

[7] C. E. Bauby and A. D. Kuo, "Active control of lateral balance in human walking," *Journal of Biomechanics*, vol. 33, no. 11, pp. 1433–1440, 2000.

[8] A. Schultz, N. Alexander, and J. Ashton-Miller, "Biomechanical analyses of rising from a chair," *Journal of Biomechanics*, vol. 25, no. 2, pp. 1383–1391, 1992.

[9] D. L. Wight, "Control of a pneumatically powered orthosis," Master's thesis, University of Waterloo, Waterloo, ON, Canada, 2003.

[10] P. Jansen-Osmann, S. Richter, J. Konczak, and K. T. Kalveram, "Force adaptation transfers to untrained workspace regions in children: Evidence for developing inverse dynamic motor models," *Experimental Brain Research*, vol. 143, no. 2, pp. 212–220, Jan. 2002. [Online]. Available: http://education.umn.edu/kls/research/motorlab/PDF/jansen-etal-02.pdf

[11] G. Loeb and F. Richmond, *Neural Prostheses for Restoration of Sensor and Motor Function*. Boca Raton, FL, USA: CRC Press, 2000, ch. BION Implants for Therapeutic and Functional Electrical Stimulation. [Online]. Available: http://ami.usc.edu/Projects/Bion/docs/bionchfn.pdf

[12] (2004, Mar.) Contraction of motor units. Mr. Verdecchia's Science Corner. Fayette, KY, USA. [Online]. Available: http://staff.fcps.net/cverdecc/index.htm

[13] R. Kamnik, T. Bajd, and A. Kralj, "Functional electrical stimulation and arm supported sit-to-stand transfer after paraplegia: A study of kinetic parameters," *Artificial Organs*, vol. 23, no. 5, pp. 413–417, May 1999.

[14] M. M. Mirbagheri, M. Ladouceur, H. Barbeau, and R. E. Kearney, "The effects of long-term FES-assisted walking on intrinsic and reflex dynamic stiffness in spastic spinal-cord-injured subjects," *IEEE Transactions on Neural Systems and Rehabilitation Engineering*, vol. 10, no. 4, pp. 280–289, Dec. 2002.

[15] M. Weber and F. Pfeiffer, "Therapy of hemiparetic walking by FES," in *Proc. of the 2003 IEEE International Conference on Robotics & Automation*, vol. 3, Taipei, Taiwan, Sept. 2003, pp. 4002–4007.

[16] K. M. Bogie and R. J. Triolo, "Effects of regular use of neuromuscular electrical stimulation on tissue health," *Journal of Rehabilitation Research and Development*, vol. 40, no. 6, pp. 469–476, Nov./Dec. 2003.

[17] D. U. Silverthorn, *Human Physiology: An integrated approach*, 2nd ed. Toronto, ON, Canada: Prentice Hall, 2001.

[18] B. Andrews, "Control of paraplegic locomotion using hybrid FES systems," in *Annals of Biomedical Engineering*, vol. 19, no. 5, Charlottesville, VA, USA, Oct. 1991, pp. 626–627.

[19] Z. Z. Karu, W. K. Durfee, and A. M. Barzilai, "Reducing muscle fatigue in FES applications by stimulating with N-Let pulse trains," *IEEE Transactions on Biomedical Engineering*, vol. 42, no. 8, pp. 809–817, Aug. 1995.

[20] R. P. Patterson and J. S. Lockwood, "The influence of electrode size and type on surface stimulation of the quadriceps," *IEEE Transactions on Rehabilitation Engineering*, vol. 1, no. 1, pp. 59–62, Mar. 1993.

[21] J. Chae and R. Hart, "Comparison of discomfort associated with surface and percutaneous intramuscular electrical stimulation for persons with chronic hemiplegia," *American Journal of Physical Medicine & Rehabilitation*, vol. 77, no. 6, pp. 516–522, Nov./Dec. 1998.

[22] J. Rosen, M. Brand, M. B. Fuchs, and M. Arcan, "A myosignal-based powered exoskeleton system," *IEEE Transactions on Systems, Man, and Cybernetics—Part A: Systems and Humans*, vol. 31, no. 3, pp. 210–222, May 2001.

[23] Y. Umetami, Y. Yamada, T. Morizono, T. Yoshida, and S. Aoki, "'skil mate', wearable exoskeleton robot," in *Proc. of the IEEE International Conference on Systems, Man and Cybernetics*, vol. 4, Tokyo, Japan, Oct. 1999, pp. 984–988.

[24] K. Yamamoto, K. Kyodo, M. Ishii, T. Matsuo, and K. Sawada, "Power assisting suit utilizing muscle hardness sensor using load cell and rotary actuator using pressure cuff," in *Proc. of the sixth triennial International Symposium on Fluid Control, Measurement, and Visualization*, Sherbrooke, QC, Canada, Aug. 2000.

[25] (2004, Jan.) Exoskeletons for human performance augmentation. Defense Advanced Research Projects Agency. Arlington, VA, USA. [Online]. Available: http://www.darpa.mil/dso/thrust/matdev/ehpa.htm

[26] D. P. Ferris, J. M. Czerniecki, and B. Hannaford, "An ankle-foot orthosis powered by artificial muscles," unpublished. [Online]. Available: http://asb-biomech.org/onlineabs/abstracts2001/pdf/047.pdf

[27] D. C. Johnson, D. W. Repperger, and G. Thompson, "Development of a mobility assist for the paralyzed, amputee, and spastic patient," in *Proc. of the 1996 fifteenth Southern Biomedical Engineering Conference*, Dayton, OH, USA, Mar. 1996, pp. 67–70.

[28] (2004, Jan.) Powered prosthetics and orthotics. Yobotics, Inc. Cincinnati, OH, USA. [Online]. Available: http://www.yobotics.com/robowalker/robowalker.html

[29] D. A. Winter, *Biomechanics of Human Movement*. Toronto, ON, Canada: John Wiley & Sons, 1979.

[30] ——, *Biomechanics and Motor Control of Human Gait: Normal, Elderly, and Pathological*, 2nd ed. Waterloo, ON, Canada: University of Waterloo Press, 1991.

[31] S. McGill and R. Norman, "Partitioning of the L4-L5 dynamic moment into disc, ligamentous, and muscular components during lifting," *Spine*, vol. 11, no. 7, pp. 666–678, 1986.

[32] S. J. Olney and D. A. Winter, "Predictions of knee and ankle moments of force in walking from emg and kinematic data," *Journal of Biomechanics*, vol. 18, no. 1, pp. 9–20, 1985.

[33] P. Komi, "Relationship between muscle tension, EMG, and velocity of contraction under concentric and eccentric work," *New Developments in Electromyography and Clinical Neurophysiology*, vol. 1, pp. 596–606, 1973.

[34] P. G. Bedewi and N. E. Bedewi, "Modeling of occupant biomechanics with emphasis on the analysis of lower extremity injuries," *International Journal of Crashworthiness*, vol. 1, no. 1, 1996. [Online]. Available: http://www.ncac.gwu.edu/archives/papers/lower/lower.html

[35] K. Manal and T. S. Buchanan, "A one-parameter neural activation to muscle activation model: estimating isometric joint moments from electromyograms," *Journal of Biomechanics*, vol. 36, no. 8, pp. 1197–1202, 2003.

[36] B. A. Alkner, P. A. Tesch, and H. E. Berg, "Quadriceps EMG/force relationship in knee extension and leg press," *Medicine & Science in Sports & Exercise*, vol. 32, no. 2, pp. 459–463, 2000.

[37] C. J. De Luca, "The use of surface electromyography in biomechanics," *Journal of Applied Biomechanics*, vol. 13, pp. 135–163, 1997.

[38] H. Kawamoto and Y. Sankai, "Power assist system HAL-3 for gait disorder person," in *Proceedings of the 8th International Conference on Computers Helping People with Special Needs*, July 2002, pp. 196–203.

[39] D. Repperger and C. Phillips, "Developing intelligent control from a biological perspective to examine paradigms for activation utilizing pneumatic muscle actuators," in *Proceedings of the 15th IEEE International Symposium on Intelligent Control*, Rio Patras, Greece, July 2000, pp. 205–210.

[40] T. Hesselroth, K. Sarkar, and K. S. Patrik van der Smagt, "Neural network control of a pneumatic robot arm," *IEEE Transactions on Systems, Man, and Cybernetics*, vol. 24, no. 1, pp. 28–38, Jan. 1994.

[41] R. T. Pack, J. L. Christopher Jr, and K. Kawamura, "A rubbertuator-based structure-climbing inspection robot," in *Proceedings of the 1997 IEEE International Conference on Robotics and Automation*, Albuquerque, NM, USA, Apr. 1997, pp. 1869–1874.

[42] M. Birch, R. Quinn, G. Hahm, S. Phillips, B. Drennan, R. Beer, Y. Xinyu, S. Garverick, S. Laksanacharoen, A. Pollack, and R. Ritzmann, "A miniature hybrid robot propelled by legs," in *Proceedings of the 2001 IEEE/RSJ International Conference onIntelligent Robots and Systems*, vol. 2, Maui, HI, USA, Oct. 2001, pp. 845–851.

[43] D. Caldwell, N. Tsagarakis, P. Artrit, J. Canderle, S. Davis, and G. Medrano-Cerda, "Biomimetic and smart technology principles of humanoid design," in *Proceedings of the 2001 IEEE/ASME International Conference on Advanced Intelligent Mechatronics*, vol. 2, Como, Italy, July 2001, pp. 965–970.

[44] D. Caldwell, N. Tsagarakis, G. Medrano-Cerda, J. Schofield, and S. Brown, "Development of a pneumatic muscle actuator driven manipulator rig for nuclear waste retrieval operations," in *Proceedings of the 1999 IEEE International Conference on Robotics and Automation*, vol. 1, Detroit, MI, USA, May 1999, pp. 525–530.

[45] N. Tsagarakis, D. Caldwell, and G. Medrano-Cerda, "A 7 dof pneumatic muscle actuator (pMA) powered exoskeleton," in *8th IEEE International Workshop Robot and Human Interaction*, Pisa, Italy, Sept. 1999, pp. 327–333.

[46] D. Caldwell, N. Tsagarakis, D. Badihi, and G. Medrano-Cerda, "Pneumatic muscle actuator technology: a light weight power system for a humanoid robot," in *Proceedings of the 1998 IEEE International Conference on Robotics and Automation*, vol. 4, Leuven, Belgium, May 1998, pp. 3053–3058.

[47] D. Caldwell, G. Medrano-Cerda, and M. Goodwin, "Braided pneumatic actuator control of a multi-jointed manipulator," in *Proceedings of the 1993 International Conference on Systems, Man, and Cybernetics*, vol. 1, Oct. 1993, pp. 423–428.

[48] R. Colbrunn, G. Nelson, and R. Quinn, "Design and control of a robotic leg with braided pneumatic actuators," in *Proceedings of the 2001 IEEE/RSJ International Conference onIntelligent Robots and Systems*, vol. 2, Maui, HI, USA, Oct. 2001, pp. 992–998.

[49] T. Noritsugu and T. Tanaka, "Application of rubber artificial muscle manipulator as a rehabilitation robot," *IEEE/ASME Transactions on Mechatronics*, vol. 2, no. 4, pp. 259–267, Dec. 1997.

[50] T. Noritsugu, D. Sasaki, and M. Takaiwa, "Application of artificial pneumatic rubber muscles to a human friendly robot," in *Proceedings of the 2003 IEEE International Conference on Robotics and Automation*, vol. 2, Taipei, Taiwan, Sept. 2003, pp. 2188–2193.

[51] Y. Jeong, D. Lee, K. Kim, and J. O. Park, "A wearable robotic arm with high force-reflection capability," in *Proceedings of the 9th IEEE International*

Workshop on Robot and Human Interactive Communication, Taipai, Taiwan, Sept. 2000, pp. 411–416.

[52] S. Prior and P. Warner, "A new development in low cost pneumatic actuators," in *Fifth International Conference on Advanced Robotics*, vol. 2, June 1991, pp. 1590–1593.

[53] (2004) Fluidic muscle MAS data sheet. Festo Corporation. [Online]. Available: www.festo.com

[54] G. Medrano-Cerda, C. Bowler, and D. Caldwell, "Adaptive position control of antagonistic pneumatic muscle actuators," in *IEEE/RSJ International Conference on Intelligent Robots and Systems*, vol. 1, Aug. 1995, pp. 378–383.

[55] B. Tondu and P. Lopez, "Modeling and control of McKibben artificial muscle robot actuators," *IEEE Control Systems Magazine*, vol. 20, no. 2, pp. 15–38, Apr. 2000.

[56] P. Carbonell, Z. Jiang, and D. Repperger, "Nonlinear control of a pneumatic muscle actuator: backstepping vs. sliding-mode," in *Proceedings of the 2001 IEEE International Conference on Control Applications*, Mexico City, Mexico, Sept. 2001, pp. 167–172.

[57] D. G. Caldwell, G. A. Medrano-Cerda, and M. Goodwin, "Characteristics and adaptive control of pneumatic muscle actuators for a robotic elbow," in *Proceedings of the 1994 IEEE International Conference on Robotics and Automation*, vol. 4, May 1994, pp. 3558–3563.

[58] E. Papa and A. Cappozzo, "A telescopic inverted-pendulum model of the musculo-skeletal system and its use for the analysis of the sit-to-stand motor task," *Journal of Biomechanics*, vol. 32, no. 11, pp. 1205–1212, Nov. 1999.

[59] ——, "Sit-to-stand motor strategies investigated in able-bodied young and elderly subjects," *Journal of Biomechanics*, vol. 33, no. 9, pp. 1113–1122, Sept. 2000.

[60] E. R. Ikeda, M. L. Schenkman, P. O. Riley, and W. A. Hodge, "Influence of age on dynamics of rising from a chair," *Physical Therapy*, vol. 71, no. 6, pp. 473–481, June 1991.

[61] E. Hutchinson, P. O. Riley, and D. Krebs, "A dynamic analysis of the joint forces and torques during rising from a chair," *IEEE Transactions on Rehabilitation Engineering*, vol. 2, no. 2, pp. 49–56, June 1994.

[62] H. Hemami and V. Jaswa, "On a three-link model of the dynamics of standing up and sitting down," *IEEE Transactions on Systems, Man, and Cybernetics*, vol. 8, no. 2, pp. 115–120, Feb. 1978.

[63] Y. Pai and M. Rogers, "Segmental contributions to total body momentum in sit-to-stand," *Medicine and Science in Sports and Exercise*, vol. 23, no. 2, pp. 225–230, 1991.

[64] M. Miller, A. Schultz, N. Alexander, D. Warwick, and J. Ashton-Miller, "Dynamics of rising from a chair: Experimental data collection," in *ASME 1989 Biomechanics Symposium*, vol. 89, 1989, pp. 329–332.

[65] T. Lundin, M. Grabiner, and D. Jahnigen, "On the assumption of bilateral lower extremity joint moment symmetry during the sit-to-stand task," *Journal of Biomechanics*, vol. 28, no. 1, pp. 109–112, Jan. 1995.

[66] N. Alexander, A. Schultz, and D. Warwick, "Rising from a chair: effects of age and functional ability on performance biomechanics," *Journal of Gerontology: Medical Sciences*, vol. 46, pp. M91–98, 1991.

[67] K. Gruber, H. Ruder, J. Denoth, and K. Schneider, "A comparative study of impact dynamics: wobbling mass model versus rigid body models," *Journal of Biomechanics*, vol. 31, no. 5, pp. 439–444, May 1998.

[68] M. Spong and M. Vidyasagar, *Robot Dynamics and Control*. Toronto, ON: John Wiley & Sons, 1989.

[69] W. R. Eby, "Analysis of a three-link planar robot model for the self-supporting phases of sit-to-stand," University of Waterloo, Tech. Rep., 2002.

[70] V. M. Zatsiorsky, *Kinetics of Human Motion*. Windsor, ON, Canada: Human Kinetics, 2002.

[71] J. Reid and R. Jensen, "Human body segment inertia parameters: A survey and status report," *Exercise and Sport Sciences Review*, vol. 18, pp. 225–241, 1990.

[72] M. Yeadon and M. Morlock, "The appropriate use of regression equations for the estimation of segmental inertia parameters," *Journal of Biomechanics*, vol. 22, no. 6-7, pp. 683–689, 1989.

[73] (2004, Mar.) Modified hanavan model. Boston, MA, USA. [Online]. Available: http://www.kwon3d.com/theory/bspeq/hanavan.html

[74] C.-P. Chou and B. Hannaford, "Measurement and modeling of McKibben pnuematic artificial muscles," *IEEE Transactions on Robotics and Automation*, vol. 12, no. 1, pp. 90–102, Feb. 1996.

[75] B. Tondu, V. Boitier, and P. Lopez, "Naturally compliant robot-arms actuated by McKibben artificial muscles," in *Proceedings of the 1994 IEEE International Conference on Systems, Man, and Cybernetics*, vol. 3, San Antonio, TX, USA, Oct. 1994, pp. 2635–2640.

[76] R. W. Colbrunn, G. M. Nelson, and R. D. Quinn, "Modeling of braided pneumatic actuators for robotic control," in *Proceedings of the 2001 IEEE/RSJ International Conference on Intelligent Robots and Systems*, vol. 4, Maui, HI, USA, Oct./Nov. 2001, pp. 1964–1970.

[77] Y. Pai and M. Rogers, "Speed variation and resultant joint torques during sit-to-stand," *Archives of Physical Medicine and Rehabilitation*, vol. 72, pp. 881–885, Oct. 1991.

[78] D. A. Winter, *Biomechanics and Motor Control of Human Movement*, 2nd ed. Toronto, ON, Canada: John Wiley & Sons, 1990.

[79] J. Pezzack, R. Norman, and D. Winter, "An assessment of derivative determining techniques used for motion analysis," *Journal of Biomechanics*, vol. 10, pp. 377–382, 1977.

[80] D. G. E. Robertson and J. J. Dowling, "Design and responses of Butterworth and critically damped digital filters," *Journal of Electromyography and Kinesiology*, vol. 13, pp. 569–573, 2003.

[81] N. S. Nise, *Control Systems Engineering*, 3rd ed. Toronto: John Wiley & Sons, 2000.

[82] J. Zhang, C. R. Knospe, and P. Tsiotras, "New results for the analysis of linear systems with time-invariant delays," *International Journal of Robust and Nonlinear Control*, vol. 13, no. 12, pp. 1149–1175, Oct. 2003.

[83] P. Dostal, V. Bobal, and M. Sysel, "Design of controllers for integrating and unstable time delay systems using polynomial method," in *Proceedings of the American Control Conference*, Anchorage, AK, May 2002, pp. 2773–2778.

[84] B. Messner and D. Tilbury. (2005, Jan.) Controls tutorial for matlab. Carnegie Mellon and University of Michigan. Ann Arbor, MI, USA. [Online]. Available: http://www.engin.umich.edu/group/ctm/examples/motor/motor.html

[85] J. R. Dormand and P. J. Prince, "A family of embedded Runge-Kutta formulae," *Journal of Computational and Applied Mathematics*, vol. 6, no. 1, pp. 19–26, Mar. 1980.

[86] *MATLAB Function Reference - ode45, ode23, ode113, ode15s, ode23s, ode23t, ode23tb*, The Mathworks, Inc. [Online]. Available: http://www.mathworks.com/access/helpdesk/help/techdoc/ref/ode45.html

[87] L. F. Shampine, *Numerical Solution of Ordinary Differential Equations.* Chapman & Hall Mathematics, 1994.

[88] S. Davis, J. Canderle, P. Artrit, N. Tsagarakis, and D. G. Caldwell, "Enhanced dynamic performance in pneumatic muscle actuators," in *Proceedings of the 2002 IEEE International Conference on Robotics & Automation*, vol. 3, Washington, DC, May 2002, pp. 2836–2841.

Glossary of Terms

Air Muscle See Fluidic Muscle.

Dorsiflexion Bending about the ankle such that the angle between the foot and shank decreases. e.g. Pulling the foot up.

Electromyography (EMG) The measurement of the electrical signals associated with muscular contraction.

Extension Bending about the joint such that the angle between the adjacent bones is increased.

Flexion Bending about the joint such that the angle between the adjacent bones is decreased.

Fluidic Muscle A pneumatically-driven actuator technology. Essentially an inner-tube surrounded by a rhomboidal mesh.

Functional Electrical Stimulation (FES) Purposeful contraction of biological muscle using an externally applied voltage.

Hemiplegia Paralysis of one side of the body due to a brain injury.

Human Performance Augmentation Providing aid to a user to improve their performance beyond normal human levels. Contrast with Mobility Assist.

Isometric Fixed length muscular contraction.

Isotonic Fixed tension muscular contraction.

Mobility Assist Providing aid to the impaired user to improve their performance to normal functional levels. Contrast with Human Performance Augmentation.

Myosignal The electrical signals associated with muscular contraction.

Neuropathology A degradation of the nervous system.

Orthotic A device, such as a crutch or brace, used to support a weak joint or muscle.

Plantarflexion Bending about the ankle such that the angle between the foot and shank increases. e.g. Extending the foot down.

Pneumatic Muscle Actuator (PMA) See Fluidic Muscle.

Prismatic Joint A joint with one translational degree of freedom.

Prosthetic A device used to replace a part of the body.

Revolute Joint A joint with one rotational degree of freedom.

Seat-Off Event The point in the sit-to-stand task when the subject looses contact with the chair.

Spinal-Cord Injury (SCI) A disruption of the efferent (motor) neural pathways and/or afferent (sensory) neural pathways in the spinal cord. Often results in paralysis below the level of the lesion.